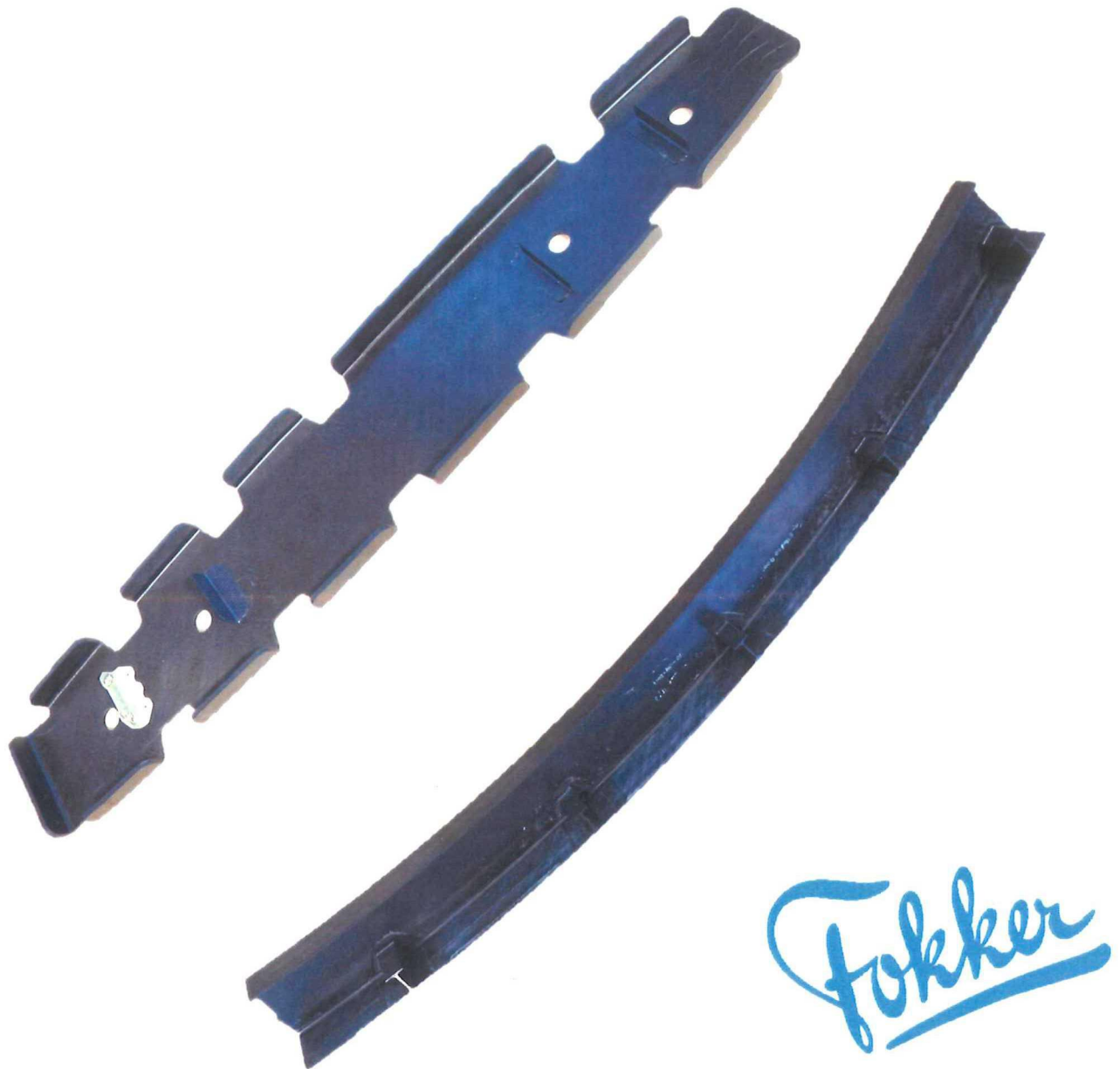


Identifying the Potential and Feasibility of Ultrasonic Welding of Carbon Fiber PEKK Composites

- By Welding System Clips and Fuselage Frames

MSc. Thesis by J.J.E. Renooij

Delft University of Technology
Faculty of Aerospace Engineering



Design and Production of Composite Structures

Identifying the Potential and Feasibility of Ultrasonic Welding of Carbon Fiber PEKK Composites – By Welding System Clips and Fuselage Frames

A first effort to build ultrasonically welded demonstrator products – which push the frontiers of current possibilities – to present the potential and provide an outlook of the large-scale application of ultrasonic welding of continuous fiber-reinforced thermoplastic composites in the aerospace industry.

MASTER OF SCIENCE THESIS

BY

J.J.E. RENOOIJ

In partial fulfillment of the requirements for the degree of Master of Science
in Aerospace Engineering
at Delft University of Technology

TO BE DEFENDED PUBLICLY ON FRIDAY DECEMBER 19TH, 2014 AT 10:00

Chair:	Dr.ir. R.C. Alderliesten	Delft University of Technology
Supervisor:	Dr.ir. I. Fernandez Villegas	Delft University of Technology
	Ing. M. Koetsier	Fokker Aerostructures B.V.
	Dr.ir. W.J.C. Verhagen	Delft University of Technology

Delft University of Technology – Faculty of Aerospace Engineering
Design and Production of Composite Structures

DELFT UNIVERSITY OF TECHNOLOGY
DEPARTMENT OF
AEROSPACE STRUCTURES AND MATERIALS
DESIGN AND PRODUCTION OF COMPOSITE STRUCTURES

The undersigned hereby certify that they have read and recommended to the Faculty of Aerospace Engineering for acceptance a thesis entitled **"Identifying the Potential and Feasibility of Ultrasonic Welding of Carbon Fiber PEKK Composites – By Welding System Clips and Fuselage Frames"** by **J.J.E. Renooij** in partial fulfillment of the requirements for the degree of Master of Science.

Dated: December 19th, 2014

Chair:

Dr.ir. R.C. Alderliesten

Supervisor:

Dr.ir. I. Fernandez Villegas

Reader (external, Fokker Aerostructures B.V.):

Ing. M. Koetsier

Reader:

Dr.ir. W.J.C. Verhagen

Abstract

Ultrasonic welding (USW) of thermoplastics has been one of the most popular bonding techniques in the plastics industry since the sixties, because it has proven to be fast, reliable, and easy-to-automate, while only requiring a limited capital investment. However, until now, USW of carbon fiber reinforced thermoplastic composites (CFRTPCs) has not yet been applied to obtain structural bonds in an industrial setting. Now that the popularity of CFRTPCs is rapidly increasing (e.g. initiation of TAPAS 1 & 2 program) and associated assembly techniques have to be developed, it is time to upscale the USW process. Therefore, the main objective of this research project is to identify the potential and feasibility of USW of CFRTPCs (CF/ PEKK in particular) in an industrial setup by welding demonstrator products. Two have been welded: 1) system clips to a rib of the horizontal stabilizer of the G650, and 2) a fuselage frame to a stiffener of a skin panel.

First, system clips were welded. The following results were derived from welding system clips in an experimental setup: a) a new tooling concept – in which the clips were not clamped but merely kept in position by alignment plates – was successfully used to weld sample clips; b) a good energy director (ED) configuration – the use of multiple slender ED strips – was discovered; and c) an ‘optimal’ energy level – to consistently reproduce high quality welds – was found. The first demonstrator was a success, because clips could be consistently welded with a high bond quality. Moreover, a study performed by the cost engineering department of Fokker Aerostructures pointed out that it is 35 [%] cheaper to ultrasonically weld a composite clip (in case the ED is integrated) than to rivet an aluminum equivalent. Because on a large passenger plane there are thousands of small clips (and brackets) to be found, spot welding of small CFRTPC components has a huge potential. It is recommended that efforts to certify USW of small CFRTPC components are made soon.

Next, the fuselage frame was welded. This demonstrator is really pushing the frontiers of current possibilities, because no known CFRTPC components of this size have ever been ultrasonically welded using a sequential approach. Before the second demonstrator was welded, fundamental research was performed on clamping of the upper sample as: a) the fuselage frame had to be clamped to the orthogrid panel, and b) it was believed that a first spot weld basically creates a clamped situation for the consecutive weld. It was observed that successful welds can still be made when the composites are tightly clamped, although the process does indeed become more challenging. Subsequently, a dedicated fixture for the fuselage frame was designed and produced. Using this fixture, the frame was successfully welded to a section of Fokker’s orthogrid panel. Although the joints are far from perfect, the second demonstrator indicates that it is possible to ultrasonically weld CFRTPC structures using a sequential approach. If the sequential USW process is perfected, it stands to have a huge potential for industry wide application. Therefore, it is stressed that the research on sequential USW should be continued.

In addition to welding demonstrator products, an in-depth study of the development of the squeeze flow and weld quality – as a function of the total amount of energy applied – is conducted. Using cross-sectional microscopy, fractography, and non-destructive testing (NDT) techniques, the different stages in the welding process were identified and related to patterns in the welding data. Understanding how patterns in the welding data relate to the weld quality should make it easier to find the optimal welding settings for future applications. Moreover, by understanding these patterns, it should be possible to eventually monitor the quality of the weld ‘in-situ’.

Furthermore, a successful effort was made to integrate triangular EDs into a composite laminate without adding major processing steps. Having integrated EDs are favorable in an industrial setting, as they reduce the number of process steps significantly and are expected to be more consistent. Last, but not least, an outlook for the USW of CFRTPCs in the aerospace industry is presented.

Acknowledgements

It was about a year ago that I had the first contact concerning this research project with dr.ir. Irene Fernandez Villegas and the R&D department from Fokker Aerostructures. They wanted to collaborate more closely in the development and application of ultrasonic welding of continuous fiber-reinforced thermoplastic composites. As such, they were looking for MSc. student who would weld demonstrator products and assess the process' potential to serve the needs of the aerospace industry. I believed, and I still do, that ultrasonic welding is a very promising technique to join thermoplastics and therefore, I decided to make this the topic for my graduation project. Now, one year later, I am finishing my MSc. thesis and I can say that it has indeed been a fantastic experience. Therefore, I would like to take the opportunity to thank a number of people who supported me and made it possible for me to have such a great time.

First, and most of all, I would like to thank my two coordinators: dr.ir. Irene Fernandez Villegas from the TU Delft and Marc Koetsier from Fokker Aerostructures, as they were honestly the best two coaches I could have wished for. Dr.ir. Irene Fernandez Villegas was very involved in the project, and as a result our discussions always managed to bring an invaluable contribution to both my thinking process and general overview of the topic. She constantly pushed me to achieve focus in both thinking and writing, and her advice helped me to significantly improve the structure of my outputs. Marc Koetsier, who was the first to promote the potential of ultrasonic welding of continuous fiber-reinforced thermoplastic composites within Fokker, provided me with numerous new ideas during our frequent brainstorm sessions. Moreover, he facilitated my access to various locations where I could seek inspiration for my project: the Airbus site in Hamburg, the Fokker facilities in Papendrecht, and the KLM Engineering & Maintenance department at Schiphol.

Next, I want to thank Dr. Genevieve Palardy, who supported me during the experiments phase of the research and helped me analyze their results, while also providing me with new ideas of how to approach my research topic.

Moreover, I would also like to thank my colleagues at Fokker. Jaap Willem van Ingen did not only help me formulate high goals – like welding the fuselage frame; but, given his pragmatic mindset, also enabled me to achieve these goals. Furthermore, Michael Wielandt provided me all the resources I needed to weld clips to a rib. John Hoogenboom made a cost comparison analysis between welding a composite clip and riveting an aluminum one. Moreover, Gijs Gijsbertse manufactured all the composite laminates used for this project and Luuk Koster made my work so much easier by sawing the laminates into the samples sizes I needed for the experiments. John Teunissen, Ivo Lippers, and Mark Wesseling often helped me with generating new ideas. Next, the group interns at the R&D department made sure I had plenty of fun at and outside of work.

Furthermore, I would like to thank one of my best friends, Silvia Toma, for being a sounding board to my ideas in terms of structuring and planning my work. I am grateful to have been able to rely on her patience to thoroughly read this document and improve the text's readability.

Last but not least, I want to thank my friends and family for supporting me during the last year.

Table of Contents

Abstract	I
Acknowledgements	III
Table of Contents	V
List of Figures	VIII
List of Tables	XV
List of Abbreviations	XVI
List of Symbols	XVI
I – Research Design	1
1. Introduction	3
1.1. Motivation	3
1.1.1. Potential of ultrasonic welding	3
1.1.2. TAPAS2	3
1.1.3. Demonstrator products	4
1.2. Background information	4
1.2.1. Literature review	4
1.2.2. Research gap	11
1.2.3. Practical observations	11
1.3. Objectives & research questions	15
1.4. Outline	16
2. Experimental Set-up	17
2.1. Materials, manufacturing & preparation	17
2.1.1. Composite samples	17
2.1.2. Energy director	17
2.1.3. Clips	18
2.2. Ultrasonic welding equipment	18
2.2.1. Ultrasonic welding machine	18
2.2.2. Sonotrodes	19
2.2.3. Fixture	19
2.3. Welding configurations	20
2.3.1. Sample clips	20
2.3.2. System clips	20
2.3.3. Single and double-side clamping	21
2.3.4. Fuselage frame	21
2.4. Testing equipment & procedures	22
II – Experiments, Results & Discussion	25

3. Selection of Energy Director Configuration	27
3.1. Flat energy director	27
3.2. New energy director concept: flat strips	29
3.3. Optimizing the ED strip configuration	31
3.4. Conclusions	35
4. Squeeze Flow & Weld Quality Development	37
4.1. Analysis of various stages in the welding process	37
4.1.1. Welding data	37
4.1.2. LSS results	38
4.1.3. Fractography	39
4.1.4. Cross-section microscopy	42
4.1.5. NDT analysis	48
4.1.6. Analysis of welding data	50
4.2. Optimal energy level & validation experiments	52
4.3. Conclusions	54
5. System Clips	55
5.1. System clip design	55
5.2. Energy director configuration	56
5.3. Energy determination	57
5.4. Demonstrator	60
III – New Concepts & Fuselage Frame	63
6. Integrated Triangular Energy Directors	65
6.1. Materials & manufacturing	65
6.2. Welding of sample clips with integrated energy directors	66
6.3. Recommendations	68
7. Clamping & Sequential Welding	69
7.1. Welding of single-side clamped samples	69
7.2. Welding of double-side clamped samples	73
7.3. Recommendations	75
8. Fuselage Frame	77
IV – Conclusions & Recommendations	79
9. Conclusions	81
10. Outlook	83
11. Future Research Recommendations	85
References	87
Appendices	91
Appendix A. Squeeze Flow & Weld Quality Development	92

Appendix B.	CAD Drawings	97
Appendix C.	Materials & Manufacturing	101
Appendix D.	Integrated Triangular Energy Directors	103
Appendix E.	Single-Side Clamping	105
Appendix F.	System Clips.....	111
Appendix G.	Fuselage Frame.....	115
Appendix H.	Outlook.....	119

List of Figures

Figure 1-1: Target applications for thermoplastics as defined in the TAPAS2 project plan (Fokker, 2013).....	3
Figure 1-2: Demonstrator 1 – clips welded to a rib.	4
Figure 1-3: Demonstrator 2 – fuselage frames welded to an orthogrid panel.	4
Figure 1-4: Schematic drawing of ultrasonic welding machine (Yousefpour et al., 2004).....	5
Figure 1-5: Composite welding system and corresponding lumped parameter model (Benatar & Gutowski, 1989).	7
Figure 1-6: Healing of welding interface: a) two distinct components; b) intimate contact between components; and 3) intermolecular diffusion into one component (Prager & Tirrell 1981).	8
Figure 1-7: Typical evolution of the dissipated power and the displacement of the sonotrode (Villegas, 2013a).	9
Figure 1-8: Power and displacement curves for two identical specimens welded with the same peak-to-peak amplitude (86.2 [μm]) and welding force (300 [N]). The time to stage 4 varies considerably, whereas the displacement at stage 4 is constant (Villegas, 2013a).	10
Figure 1-9: Schematic drawing of the ultrasonic welding process using a flat energy director (Levy et al., 2014).	10
Figure 1-10: Conceptual design of tool to sequentially weld fuselage frame (dark blue) to the orthogrid panel (light blue). Clamping of fuselage frame and orthogrid panel not included. An actuator (yellow) is used to clamp the area to be welded between the anvil of the C-frame (orange) and the welding stack (grey).	12
Figure 1-11: Left: welding interface where ED has two free edges (single lap shear sample has four free edges); right: welding interface where ED has no free edges.	13
Figure 1-12: Force (top), displacement (middle) and power (bottom) curves of sample clip USW140911-08 welded with an energy of 2,000 [J], an amplitude of 51.8 [μm], and a welding force of 1,500 [N]. The various stages in the ultrasonic welding process are indicated by the black dashed lines.	13
Figure 2-1: Recommended vacuum bag scheme (Cytec, 2009).	17
Figure 2-2: Dynamic 3000 ultrasonic welding machine with generator ACU (Rinco Ultrasonics AG, 2008).	18
Figure 2-3: The Z51414 fixture designed to both flexible and simple.	19
Figure 2-4: Side-view of the Z51414 fixture. The T-slots make the tool very flexible.	19
Figure 2-5: Fixture Z51414 in the sample clip configuration.	20
Figure 2-6: Fixture Z51414 in the system clip configuration.	20
Figure 2-7: Fixture Z51414 in the single-side clamping configuration.	21
Figure 2-8: Fixture Z51414 in the double-side clamping configuration.	21
Figure 2-9: Fixture Z51414 with the Z51430 expansion especially designed to ultrasonically weld fuselage frames to the orthogrid panel.	22
Figure 2-10: Tensile testing setup schematic.	22
Figure 2-11: Example of A (upper-left), S (upper-right), and C-scan (lower) of a sample clip.	23
Figure 3-1: Power (solid) and displacement (dotted) plots of CF/ PEKK ASTM D1002 samples ultrasonically welded with flat PEKK EDs in the 9109 fixture under the same conditions.	27
Figure 3-2: Flat square 1 [cm ²] ED plunge welded to the lower composite. The plunge weld is indicated by the red arrow. .	28
Figure 3-3: Sample clip USW configuration with a flat square 1 [cm ²] ED.	28
Figure 3-4: Power (solid) and displacement (dotted) plots of sample clips welded with flat square 1 [cm ²] EDs with varying welding settings.	29
Figure 3-5: Three sample clips welded with flat square 1 [cm ²] EDs and a displacement of 0.08 [mm] as the welding driver. All three clips are damaged at the edges, but the damage is visibly reduced for the later samples.	29

Figure 3-6: Slender ED strips are a new ED concept to weld sample clips. Both the ED strips and the alignment plates are fixed with tape.	30
Figure 3-7: Sample clip welded with two ED strips at 2,000 [J].	30
Figure 3-8: Power (solid) and displacement (dotted) plots of five sample clips welded with two ED strips under the same conditions.	31
Figure 3-9: Power (solid) and displacement (dotted) plots of sample clips with single ED strips of varying widths.	32
Figure 3-10: The welded sample clips ordered by the width of the ED strip from 2 [mm] to 8 [mm]. None of the sample clips is damaged.	32
Figure 3-11: Fracture surfaces of sample USW141003-04 (left) with an ED spacing of 3 [mm] and welded with 750 [J] and sample USW141010-07 (right) with an ED spacing of 12.7 [mm] and welded with 1,000 [J]. In case of the left sample, the flow fronts have met.	33
Figure 3-12: Power (solid) and displacement (dotted) plots of samples clamped at both sides with an ED spacing of either 3 [mm] or 12.7 [mm]. The displacement ceiling is similar for both ED configurations.	33
Figure 3-13: Cross-section of the welding interface of a sample clip welded with 300 [J]. The left ED has melted, whereas the second one has not. The gap is 225.8 [μm] on the left side, whereas it is 258.1 [μm] on the right.	34
Figure 4-1: Power (solid) and displacement (dots) plots of five sample clips welded under the same conditions with 2,000 [J]. The black dashed lines indicate the location of the second peak. The location of the second peak of sample clip USW140911-09 is off from the locations of the others.	37
Figure 4-2: The tensile breaking force and associated LSS for sample clips welded with different amounts of energy.	38
Figure 4-3: Fracture surfaces of sample clips in the order of the amount of energy used to weld. The two molten ED strips are merged between 700 [J] and 800 [J] and become one weld.	39
Figure 4-4: The presence of numerous voids at the welding interface indicates that PEKK started to degrade in a sample clip welded at 800 [J].	40
Figure 4-5: Clear signs of burned PEKK and countless voids at the welding interface of a sample clip welded at 2,000 [J]. ...	40
Figure 4-6: Flow fronts almost meeting each other in sample clip welded at 400 [J]. Reflecting light underneath the squeeze flow probably indicates that the ED became amorphous, and possibly that a poor or no bond has formed. The flow fronts light up due to the external cold light sources used.	40
Figure 4-7: The fibers observed in the unaffected substrate seem to continue underneath the squeeze flow of ED. SEM microscopy should confirm that these lines are not fiber imprints in the squeeze flow, though.	40
Figure 4-8: Merging flow fronts in a sample clip welded at 700 [J]. The reflection of light (white section) indicates that there was probably no or a weak bond at the centerline. Flow directions are indicated with the red arrows.	41
Figure 4-9: Merged flow fronts in a sample clip welded at 800 [J]. Flow directions are indicated with the red arrows.	41
Figure 4-10: First ply failure at fracture surface of sample clip welded at 600 [J]. Fibers stick out of broken lamina.	41
Figure 4-11: First ply failure at fracture surface of sample clip welded at 700 [J]. Fibers stick out of broken lamina.	41
Figure 4-12: Two cross-sections are obtained from one sample clip.	42
Figure 4-13: Development of the gap between the composite substrates measured in the cross-section micrographs at the locations of the flow fronts of the squeezed-out ED. The dots represent the average value and the error bars represent the standard deviation. Just one sample has been studied per data point. Four measurements per sample have been done. ...	42
Figure 4-14: Overview of cross-section microscopy panoramas of sample clips' welding interfaces ordered by the amount of energy used during welding. The red solid line indicates the moment after the abrupt increase in displacement and the dashed blue lines indicate the initial size and position of the ED strips.	43
Figure 4-15: Flow front of ED at the welding interface of a sample clip welded with 500 [J]. There are small pieces of PEKK that have not been in a molten state as they retained a rectangular shape.	44

Figure 4-16: Meeting flow fronts of ED at the welding interface of a sample clip welded with 500 [J]. It can be observed that the molten squeeze flow on the left pushes a piece of unmelted ED forward.	44
Figure 4-17: Squeeze flow of ED at the welding interface of a sample clip welded with 1,200 [J]. Even at the higher amounts of energy there are still pieces of PEKK ED which have not been in a molten state.	44
Figure 4-18: Squeeze flow of ED at the welding interface of a sample clip welded with 2,000 [J]. Still pieces of PEKK ED which have not been in a molten state are observed.....	44
Figure 4-19: Squeeze flow of ED at the welding interface of a sample clip welded with 300 [J]. Only the two outer layers of PEKK film have been in a molten state. No bond between the squeezed out ED and the substrate composite has been formed near the flow front.	45
Figure 4-20: Squeeze flow of ED at the welding interface of a sample clip welded with 400 [J]. Only the lower layers of PEKK film have been in a molten state.....	45
Figure 4-21: Cross-section micrograph with UV light of unmelted ED in a sample clip welded at 300 [J]. Separation between 50 [μm] PEKK films, as indicated by red arrows, can be observed.	45
Figure 4-22: SEM scan of fracture surface of unused ED manufactured of 5 layers of 50 [μm] PEKK film. Separation between first and second film can be observed.....	45
Figure 4-23: Cross-section micrograph with UV light of squeeze flow in a sample clip welded at 720 [J]. A piece of ED that has not been in a molten state can be observed. This piece consists of 2 layers of 50 [μm] PEKK film (red arrow indicates boundary). Moreover, there is no bond between the squeeze flow and the substrate composite near the flow front.	46
Figure 4-24: Cross-section micrograph with UV light of squeeze flow in a sample clip welded at 800 [J]. There is no bond between the flow front and bottom the substrate composite.	46
Figure 4-25: Unmelted ED at the welding interface of a sample clip welded with 300 [J]. There are already many voids present in the ED.	47
Figure 4-26: Squeeze flow of ED at the welding interface of a sample clip welded with 400 [J]. At least parts of the ED must have been in a molten state as there is a clear pattern in the squeeze out of the voids as indicated by the red arrows.....	47
Figure 4-27: Welding interface of a sample clip welded with 800 [J]. A few large voids are present in the squeeze flow of ED.	47
Figure 4-28: Welding interface of a sample clip welded with 1,000 [J]. Numerous large voids are present in the squeeze flow of ED.....	47
Figure 4-29: Welding interface (indicated with red arrow) of a sample clip welded with 1,200 [J]. Voids between the first and second ply start to develop, which push the first ply towards the molten ED at the welding interface.	48
Figure 4-30: Welding interface of a sample clip welded with 2,000 [J]. Fibers from the first ply have redistributed through the squeeze flow and a result the exact location of the welding interface can hardly be identified anymore. The red arrow indicates the approximate location, though.....	48
Figure 4-31: PA scan of USW141017-04 which is welded with 600 [J]. The A, S, and C-scan show that the two ED strips have melted and formed two proper welds. However, the flow fronts did not merge yet.	48
Figure 4-32: PA scan of USW140912-10 which is welded with 700 [J]. The A, S, and C-scan show that the two ED strips merged into a proper uniform weld.	48
Figure 4-33: PA Scan of USW140912-02 which is welded with 800 [J]. The A, S, and C- scan show signs of material degradation on the right side of the weld as the signal is lost.	49
Figure 4-34: PA scan of USW140911-08 which is welded with 2,000 [J]. The A, S, and C-scan show that the two ED strips have merged but the weld quality has deteriorated.	49
Figure 4-35: C-scan overview of welded sample clips. An energy of 700 [J] provides the best weld quality. The solid blue lines indicate from which point onwards the samples experienced the squeeze out.	50
Figure 4-36: Power (solid) and travel (dotted) plots of sample clips used for fractography.	51
Figure 4-37: Three examples of force (solid) and travel (dotted) plots of clips used for fractography.	52

Figure 4-38: C-scans of five sample clips welded in the same conditions with 720 [J]. The C-scans validate the consistency of the welding quality using these settings as five good welds are obtained. The average breaking force is 11,374 [N] with a CoV of 4.87 [%] and the average LSS is 36.9 [MPa] with a CoV of 2.63 [%].	53
Figure 4-39: Fracture surfaces of five validation samples welded in the same conditions with 720 [J]. The fracture surfaces are similar in terms of area and failure mode as expected.	53
Figure 4-40: First-ply failure observed at the fracture surface of USW141001-01 which is welded with 720 [J].	53
Figure 4-41: Power (solid) and displacement (dotted) plots of five validation samples welded in the same conditions with 720 [J]. The plots show that the theoretical optimum is approximately reached as the slopes of the power curves approach zero.	54
Figure 5-1: Original position of the aluminum clip on a rib of the horizontal stabilizer of the G650, as indicated by the red ellipse. The clip is fastened by three rivets.	55
Figure 5-2: Original aluminum clip. The three holes at the bottom flange are used to rivet the clip to the rib. Two floating nuts are riveted to the other flange.	55
Figure 5-3: Composite clip based on the dimensions of the original aluminum clip. The clip is welded to the rib. The floating nuts could be integrated in the design or welded as well as there are already thermoplastic floating nuts.	55
Figure 5-4: ED configuration 1 – Four EDs with a spacing of 10 [mm] are placed in the transverse direction.	56
Figure 5-5: ED configuration 2 – Two EDs with a spacing of 3 [mm] are placed in the longitudinal direction.	56
Figure 5-6: A clip welded with ED configuration 1 (left) and a clip welded with ED configuration 2 (right). It can be observed that clip welded with ED configuration 1 is damaged at the sides, and the one welded in configuration 2 is slightly damaged at the lower edge. The damages are indicated with the red ellipses.	56
Figure 5-7: Side-view of configuration 1. The sonotrode cannot fully overlap the area of the ED that is supporting the clip in the area marked by the red circle.	57
Figure 5-8: Power (solid) and displacement (dotted) plots of five clips welded with 2,000 [J]. The plots are similar, however, no clear second peak can be identified.	58
Figure 5-9: PA scan of clip (USW141114-11) welded with 1,000 [J]. The S-scan indicates that the two EDs have not merged yet. The lower ED formed a strong bond, but the upper ED did not as can be seen in the C-scan.	58
Figure 5-10: PA scan of clip (USW141114-12) welded with 1,250 [J]. The weld has improved w.r.t. the previous weld. However, the upper left section of the weld is not optimal as can be seen in the C-scan.	58
Figure 5-11: PA scan of clip (USW141114-09) welded with 1,500 [J]. The A, S, and C-scan confirm that an excellent weld has been obtained, with the exception of a small area at the center of the weld, as can be seen in the C-scan.	59
Figure 5-12: A second PA scan of clip (USW141114-09) welded with 1,500 [J]. The A and S-scan show that the quality of the section at the center is still acceptable as the signal returns from the back of the lower composite.	59
Figure 5-13: PA scan of clip (USW141114-13) welded with 1,750 [J]. The A, S, and C-scan show that the weld is deteriorating at the left side.	59
Figure 5-14: PA scan of clip (USW141114-08) welded with 2,000 [J]. The A and S scan indicate that a strong signal returns from the welding interface, which implies that the material at the welding interface has degraded.	59
Figure 5-15: A clip welded with 1,250 [J] (left) and a clip welded with 1,500 [J] (right). In case of the right clip, fibers are squeezed out.	60
Figure 5-16: Clamping of the rib onto the anvil of the Rinco 3000. The rib is simply clamped with two glue clamps. Wooden sticks are placed in between to prevent damage.	60
Figure 5-17: Positioning plates (transparent orange) and a wooden bar (brown) prevent the clip from moving sideways during the USW process. The plates and the bar are taped to the rib.	60
Figure 5-18: CFRTPC clips ultrasonically welded to a CFRTPC rib. The left-most clip is the original aluminum clip and it is riveted to the rib. The second clip is a CF/ PPS clip and the two right-most clips are CF/ PEKK clips. The CF/ PPS clip is welded with PEKK EDs.	61

Figure 5-19: Power (solid) and displacement (dotted) plots of the clips welded to the rib. The data of one clip from the previous section is provided as a reference.	61
Figure 5-20: PA scan of the first clip welded. The weld is still in an early stage as some sections of the ED strips have not formed a proper bond yet.	62
Figure 5-21: PA scan of the second weld. The squeeze flows of the EDs seem to have merged and formed a proper bond. A delamination has been observed close to the weld as indicated with the red circle in the S-scan.	62
Figure 6-1: Aluminum cover plate with triangular channels.	65
Figure 6-2: The triangular channels are spaced 10 [mm] apart, have a depth of 1 [mm], and have angles of 60 [°].	65
Figure 6-3: Sample clip with integrated triangular ED ribs.	65
Figure 6-4: Integrated triangular ED onto sample clip. Fibers in the laminate are slightly disturbed. Near the ribs, there is excess resin on top of the first ply.	66
Figure 6-5: Power, force and displacement curves of sample USW141117-03 welded at 2,000 [J].	67
Figure 6-6: Power (solid) and displacement (dotted) curves of five samples with integrated triangular ED ribs. The scale of the displacement has been adjusted to study the 'ceiling' (see Figure D-2 for normal scale).	67
Figure 6-7: Sample clip USW141117-03 welded with 2,000 [J]. The triangular EDs are integrated in the upper sample. Squeeze out of ED and fibers is observed.	68
Figure 6-8: PA scan of sample clip USW141117-03 welded with 2,000 [J]. The weld quality is excellent near the upper edge, but poor near the lower edge.	68
Figure 7-1: A schematic drawing of the welding interface of a sequential weld. The section on the left side has not been welded yet, whereas the right section has been. The grey rectangles represent EDs.	69
Figure 7-2: The position of the clamps is varied when welding the single-side clamped ASTM D1002 samples to investigate the effects of the clamping distance on the USW process and weld quality. From left to right: the clamps are placed at a distance of 6 [cm], 3.5 [cm], and 1.5 [cm] w.r.t. the centerline.	69
Figure 7-3: Averages and standard deviations (error bars) of welding data of single-side clamped ASTM D1002 samples clamped at 1.5, 3.5, or 6 [cm] distance from the centerline with rubber pads and a torque of 2.5 [Nm] per bolt. Welding settings: 70.4 [μm]; 500 [N]; 0.11 [mm].	70
Figure 7-4: Averages and standard deviations (error bars) of welding data of single-side clamped ASTM D1002 samples clamped at 1.5, 3.5, or 6 [cm] distance from the centerline with rubber pads and a torque of 7.5 [Nm] per bolt. Welding settings: 70.4 [μm]; 500 [N]; 0.11 [mm].	70
Figure 7-5: The related fracture surfaces of USW140827-05 clamped at 6 [cm] and with a torque of 2.5 [Nm]. There are 1) two resin rich areas in the middle; 2) fiber squeeze-out near the side edges; and 3) voids on one side of the weld.	71
Figure 7-6: The PA scan of USW140827-05 clamped at 6 [cm] and with a torque of 2.5 [Nm]. The left section of the C-scan represents the sample, whereas the right section represents the weld. The middle of the weld has a good joint quality. However, the quality is poor near the edges of the weld.	71
Figure 7-7: The related fracture surfaces of USW140805-06 clamped at 3.5 [cm] and with a torque of 2.5 [Nm]. There are 1) resin rich areas; 2) fiber squeeze-out near the side edges; and 3) voids on one side of the weld.	71
Figure 7-8: The related fracture surfaces of USW140804-20 clamped at 1.5 [cm] and with a torque of 2.5 [Nm]. The sample shows 1) fiber squeeze out, and 2) intense first ply failure.	71
Figure 7-9: The C-scans of samples clamped at 6 [cm] and with a torque of 2.5 [Nm].	72
Figure 7-10: The C-scans of samples clamped at 6 [cm] and with a torque of 7.5 [Nm].	72
Figure 7-11: The C-scans of samples clamped at 1.5 [cm] and with a torque of 2.5 [Nm].	72
Figure 7-12: The C-scans of samples clamped at 1.5 [cm] and with a torque of 7.5 [Nm].	72
Figure 7-13: Power (solid) and displacement (dotted) curves of ASTM D1002 samples with 0.25 [mm] flat EDs, welded using the Z51414 fixture (1-5) and the 'ideal' 9109 jig (6-10) under the same conditions: 70.4 - 72.6 [μm]; 500 [N]; 0.11 [mm].	73

Figure 7-14: The position of the clamps is varied when welding the double-side clamped long lap shear samples to investigate the effects of the clamping distance on the USW process. The clamps are placed at a distance of 6 [cm] (left) and 2.1 [cm] (right) w.r.t. the centerline.	73
Figure 7-15: Averages and standard deviations (error bars) of welding data of double-side clamped long lap shear samples with two ED strips clamped at 2.1 [cm] or 6 [cm] distance from the centerline with rubber pads and a torque of 2.5 [Nm] per bolt. Welding settings: 51.8 [μ m]; 1,500 [N]; 750 [J].....	74
Figure 7-16: Power (solid) and displacement (dotted) curves of double-side clamped long lap shear samples with two ED strips clamped at 6 [cm] (1-5) or 2.1 [cm] (6-10) distance from the centerline with rubber pads and a torque of 2.5 [Nm] per bolt. Welding settings: 51.8 [μ m]; 1,500 [N]; 750 [J].	74
Figure 8-1: Isometric view of the Z51430 fixture to weld the fuselage frame to the orthogrid panel.	77
Figure 8-2: Two ED strips with a thickness of 0.25 [mm] and a width of 2 [mm] per weld are taped to the orthogrid panel.	77
Figure 8-3: The fuselage frame welded to a section of the orthogrid panel. Upper: top-view of the fuselage frame; lower: bottom-view of the fuselage frame. The red numbers indicate the locations and sequence of the spot welds. See Figure G-1 for a larger version of this picture.	78
Figure 8-4: Damage to the fuselage frame as indicated with the red ellipse.	78
Figure A-1: Overview of cross-section microscopy panoramas of sample clips' welding interfaces ordered by the amount of energy used during welding. The red solid line indicates the moment after the abrupt increase in displacement and the dashed blue lines indicate the initial size and position of the ED strips.	92
Figure A-2: Squeeze flow of ED at the welding interface of a sample clip welded with 800 [J]. The deformation of the first ply indicates that the substrate material started to melt.	94
Figure A-3: Power (solid) and displacement (dots) plots of sample clips used for optical microscopy. Welding settings: 51.8 [μ m]; 1,500 [N].	94
Figure A-4: PA Scan of USW141001-01 which is welded with 720 [J].	95
Figure A-5: PA Scan of USW141001-02 which is welded with 720 [J].	95
Figure A-6: PA Scan of USW141001-03 which is welded with 720 [J].	95
Figure A-7: PA Scan of USW141001-04 which is welded with 720 [J].	95
Figure A-8: PA Scan of USW141001-05 which is welded with 720 [J].	95
Figure B-1: Aluminum clip	97
Figure B-2: Composite clip.....	97
Figure B-3: Z51414 Anvil.....	98
Figure B-4: Z51414 Clamp	98
Figure B-5: Z51414 Alignment Block	99
Figure B-6: Z51430 Anvil.....	99
Figure B-7: Z51430 Clamp	100
Figure C-1: Example of autoclave cycle in which the CF/ PEKK laminates are consolidated.	101
Figure C-2: Autoclave cycle in which the PEKK ED is consolidated.	101
Figure C-3: Welding stack of the Rinco Dynamic 3000. A: Piezoelectric converter, B: Booster, and C: Sonotrode.	102
Figure D-1: Ultrasonic welding stages for plastics with integrated triangular EDs (Troughton, 2008)	103
Figure D-2: Power (solid) and displacement (dotted) curves of five samples with integrated triangular ED ribs. Welding settings: 51.8 [μ m]; 1,500 [N]; 2,000 [J].	103

Figure E-1: Power (solid) and displacement (dotted) plots of single-side clamped ASTM D1002 samples clamped at 6 [cm] from the centerline with rubber pads and a torque of 2.5 [Nm] per bolt. Welding settings: 70.4 [μm]; 500 [N]; 0.11 [mm].	105
Figure E-2: Power (solid) and displacement (dotted) plots of single-side clamped ASTM D1002 samples clamped at 3.5 [cm] from the centerline with rubber pads and a torque of 2.5 [Nm] per bolt. Welding settings: 70.4 [μm]; 500 [N]; 0.11 [mm].	105
Figure E-3: Power (solid) and displacement (dotted) plots of single-side clamped ASTM D1002 samples clamped at 1.5 [cm] from the centerline with rubber pads and a torque of 2.5 [Nm] per bolt. Welding settings: 70.4 [μm]; 500 [N]; 0.11 [mm].	106
Figure E-4: Power (solid) and displacement (dotted) plots of single-side clamped ASTM D1002 samples clamped at 6 [cm] from the centerline with rubber pads and a torque of 7.5 [Nm] per bolt. Welding settings: 70.4 [μm]; 500 [N]; 0.11 [mm].	106
Figure E-5: Power (solid) and displacement (dotted) plots of single-side clamped ASTM D1002 samples clamped at 3.5 [cm] from the centerline with rubber pads and a torque of 7.5 [Nm] per bolt. Welding settings: 70.4 [μm]; 500 [N]; 0.11 [mm].	107
Figure E-6: Power (solid) and displacement (dotted) plots of single-side clamped ASTM D1002 samples clamped at 1.5 [cm] from the centerline with rubber pads and a torque of 7.5 [Nm] per bolt. Welding settings: 70.4 [μm]; 500 [N]; 0.11 [mm].	107
Figure E-7: Fracture surfaces of single-side clamped ASTM D1002 samples clamped with rubber pads at the distances: 1.5 [cm], 3.5 [cm], and 6 [cm]. The bolts of the clamp are tightened with 2.5 [Nm]. Welding settings: 70.4 [μm]; 500 [N]; 0.11 [mm]. The third value given is the LSS and the fourth is the CoV of the LSS.	108
Figure E-8: Fracture surfaces of single-side clamped ASTM D1002 samples clamped with rubber pads at the distances: 1.5 [cm], 3.5 [cm], and 6 [cm]. The bolts of the clamp are tightened with 7.5 [Nm]. Welding settings: 70.4 [μm]; 500 [N]; 0.11 [mm]. The third value given is the LSS and the fourth is the CoV of the LSS.	108
Figure E-9: The C-scans of samples clamped at 3.5 [cm] and with a torque of 2.5 [Nm].	109
Figure E-10: The C-scans of samples clamped at 3.5 [cm] and with a torque of 7.5 [Nm].	109
Figure F-1: Horizontal stabilizer of the Gulfstream G650 being assembled at Fokker Aerostructures in Papendrecht. Various clips are riveted on the ribs.	111
Figure F-2: System clip on which the composite clip, welded in this thesis, is based.	111
Figure F-3: Cargo hold of Boeing 737-800 being maintained by KLM Engineering & Maintenance. Numerous system clips can be seen that could possibly be welded in case the load carrying beams of the cargo floor were made of CFRTPCs.	112
Figure F-4: Floor panel of Boeing 737-800 seen from the cargo hold which is being maintained by KLM Engineering & Maintenance. Numerous system clips can be seen that could possibly be welded in case the load carrying beams of the cargo floor were made of CFRTPCs.	112
Figure F-5: Force and displacement curves of system clip welded with 2,000 [J].	113
Figure F-6: Force and displacement curves of system clip welded with 2,000 [J].	113
Figure F-7: Force and displacement curves of system clip welded with 2,000 [J].	113
Figure F-8: Force and displacement curves of system clip welded with 2,000 [J].	114
Figure F-9: Force and displacement curves of system clip welded with 2,000 [J].	114
Figure G-1: A fuselage frame ultrasonically welded to a section of the orthogrid panel. Left: bottom view; right: top view.	115
Figure G-2: Side-view of the Z51430 fixture to weld the fuselage frame to the orthogrid panel.	116
Figure G-3: Front-view of the Z51430 fixture to weld the fuselage frame to the orthogrid panel.	116
Figure G-4: The fuselage frame and the orthogrid panel clamped in the Z51430 fixture.	117

Figure G-5: Power (solid) and displacement (dotted) plots of the fuselage frame welded to the orthogrid panel. Welding settings: 52.8 [μm]; 1,500 [N]. (No data was stored for the first weld). 117

Figure H-1: Schematic drawing of a Cartesian robot. 119

Figure H-2: A350 fuselage panel assembly line. Frames are fastened to clips on the skin panels. The same line can be envisioned for welding of CFRTPC frames and skin panels (van Ingen, 2014). 119

Figure H-3: Automated riveting in preliminary fuselage assembly line using a robot arm on rails (Broetje-Automation, 2014). 120

List of Tables

Table 2-1: Overview of sonotrodes used for the experiments. *Maximum peak-to-peak amplitude is based on a booster with a gain of 1:2. 19

List of Abbreviations

ACU	Advanced control unit
CF	Carbon fiber
CFRTPC	Continuous fiber-reinforced thermoplastic composite
CoV	Coefficient of variation
DTC	Dutch Thermoplastic Components
ED	Energy director
FEM	Finite element method
LSS	Lap shear strength
NDT	Non-destructive testing
PA	Phased array
PEEK	Polyetheretherketone
PEKK	Polyetherketoneketone
PPS	Polyphenylenesulfide
SEM	Scanning electron microscope
TP	Thermoplastic
TS	Thermoset
USW	Ultrasonic welding
UV	Ultraviolet

List of Symbols

ϵ_o	Amplitude of cyclic strain
\dot{Q}_{avg}	Average energy dissipated per unit time
i	Component index
T_c	Crystallization temperature
b	Energy dissipation
ω	Frequency of vibration
T_g	Glass transition temperature
α_h	Hammering factor
E''	Loss modulus
m	Mass
T_m	Melting temperature
k	Stiffness

I – Research Design

1. Introduction

In this chapter, the research project is introduced. First, in section 1.1, the motivation behind this thesis is provided. Subsequently, in section 1.2, background information on ultrasonic welding and the project is provided. Next, in section 1.3, the objectives and research questions are established. Finally, in section 1.4, the outline of the thesis is presented.

1.1. Motivation

In this section, the motivation for this research project is outlined. First of all, in section 1.1.1, the potential of the ultrasonic welding of (USW) process for welding continuous fiber-reinforced thermoplastic composites (CFRTPCs) in the aerospace industry is described. Subsequently, in section 1.1.2, the relevance of this research project for the TAPAS2 project is explained, and finally, in section 1.1.3 the need for demonstrators is expressed.

1.1.1. Potential of ultrasonic welding

Ultrasonic welding of thermoplastics (TPs) has been one of the most popular bonding techniques in the plastics industry since the sixties, because it has proven to be fast, reliable, and easy-to-automate, while only requiring a limited capital investment (Grewell et al., 2003). Moreover, this technique provides the possibility to monitor the quality of the weld 'in-situ' (Villegas, 2013a; Benatar & Gutowski, 1989), which renders labor-intensive inspections unnecessary. Benatar (1987) was the first to use the USW technique to join CFRTPCs. However, until now, USW of CFRTPCs has not yet been applied to obtain structural bonds in an industrial setting. This is, most likely, because the aerospace industry used to prefer thermosets (TSs) over thermoplastics. Now that the popularity of CFRTPCs is rapidly increasing (e.g. initiation of TAPAS 1 & 2 program), production and assembly techniques for CFRTPCs have to be developed. USW is a likely candidate for extensive application in the aerospace industry because of the aforementioned advantages. In this research project, an effort is made to identify the potential of using USW on CFRTPCs. Such effort is, according to the author's assessment, pushing the limits of the existing body of knowledge.

1.1.2. TAPAS2

Airbus stated that the large-scale application of CFRTPCs is seriously being considered for their future aircraft programs. Consequently, the Thermoplastic Affordable Primary Aircraft Structure (TAPAS) project was initiated. Based on the success registered by TAPAS, the follow-up project TAPAS2 was initiated. The goals of TAPAS2 are: 1) to develop thermoplastic related technologies and corresponding demonstrator products to support Airbus in its decision making process; 2) to promote the Dutch thermoplastics industry for future Airbus programs; 3) to address other opportunities for the application of thermoplastics; and 4) to achieve the technology readiness level – TRL6 – that implies that: a) demonstrator products should have been tested, and b) the positive results of these tests help formulate the technology business cases that justify significant investments in the required production equipment. Airbus points to the fuselage, the engine pylons, and the wet torsion boxes (see Figure 1-1), as areas considered for the potential application of thermoplastics (Fokker, 2013).



Figure 1-1: Target applications for thermoplastics as defined in the TAPAS2 project plan (Fokker, 2013).

A core characteristic of thermoplastics is that they can melt. This gives them an advantage over thermosets in terms of manufacturability, because other more efficient (e.g. less production steps, shorter processing times, etc.) production and assembly techniques – such as welding – can be applied. USW is believed to be one of these ‘efficient’ assembly techniques, but so far, its applicability in relation to CFRTPCs has been insufficiently researched. In order to be able to build sound technology business cases in TAPAS2, USW with CFRTPCs should be further investigated and developed. Therefore, ultrasonic welding of CFRTPCs forms the focus of the present study.

1.1.3. Demonstrator products

In the previous section, the need to develop demonstrator products in the TAPAS2 program was already mentioned. Before the use of USW can be considered to assemble ‘real life’ aircraft parts, the feasibility and advantages of the USW process should first be pointed out. Welding demonstrator products specifically to observe and test USW is an effective way to do this. Agricola (2014) already made a first effort by welding load carrying carbon fiber/ polyetheretherketone (CF/ PEEK) brackets to flat CF/ PEEK plates in a lab environment. Now, it is time to weld more progressive and ‘real life’ like demonstrators. Two of such demonstrators are proposed: 1) system clips ultrasonically spot welded to a rib, as illustrated in Figure 1-2, and 2) a fuselage frame ultrasonically sequential welded to an orthogrid panel, as can be seen in Figure 1-3. The first demonstrator is expected to be feasible (and able to reach TRL6) in the short term, whereas the latter demonstrator is pushing the frontiers of current possibilities, and therefore will hopefully prove feasible in the long term. The demonstrators will have to be made of carbon fiber/ polyetheretherketone (CF/ PEKK) as this is the preferred composite material in the TAPAS2 program due to its excellent structural properties and its relative low cost compared to other high-performance composites, such as, CF/ PEEK.

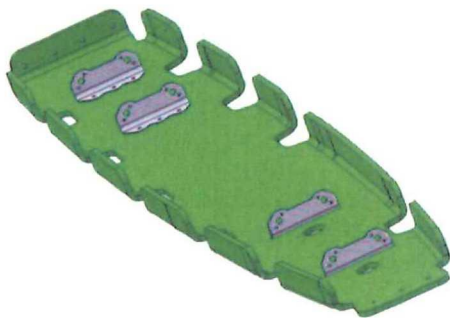


Figure 1-2: Demonstrator 1 – clips welded to a rib.

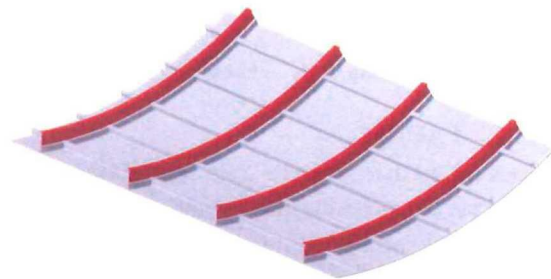


Figure 1-3: Demonstrator 2 – fuselage frames welded to an orthogrid panel.

The goals of this research project regarding the demonstrator products are: 1) to be able to consistently weld clips with a good weld quality in an industrial setting, and 2) to determine the feasibility of welding large components by sequentially placing multiple spot welds next to each other in an industrial setting.

1.2. Background information

In this section, the background information is provided. First, in section 1.2.1, the scientific literature that is most relevant to this research thesis is summarized. Subsequently, in section 1.2.2, the research gap in literature is identified. Finally, in section 1.2.3, the practical observations are described to support the choice of objectives and research questions outlined in the next section (0).

1.2.1. Literature review

This literature review provides a comprehensive up-to-date overview of the knowledge available on USW of CFRTPCs. The first objective of the review is to thoroughly understand the USW process, so that later on the proposed demonstrator products can be successfully welded. Since it is expected that not all aspects of USW required to weld the two demonstrators are covered in the available literature, the second objective is to identify gaps that have to first be investigated before welding the demonstrators.

Introduction to ultrasonic welding

USW has been one of the most popular welding techniques for unreinforced thermoplastics during the last decades. USW of CFRTPCs is less mature, but shows the potential to also become a pervasive method, because of its numerous advantages when compared to other fusion bonding techniques (Villegas et al., 2013): a) USW offers extremely short processing times (less than 5 seconds per weld); b) the process is easy-to-automate and well-suited for mass production; c) USW is reliable as it consistently produces high-strength joints; d) the process is very efficient as it only heats up material near the welding interface; e) there is no need for elaborate ventilation systems; f) the tooling (converter, booster, and sonotrode) can be very compact and can be quickly changed, which makes the process flexible (Villegas & Bersee, 2010; Troughton, 2008); g) USW only requires a small capital investment (Grewell et al., 2003); h) no foreign material has to be added; and last but not least i) the welding data can be used to monitor the quality of the weld 'in-situ', in order to stop or correct the process if required (Villegas, 2013a; Benatar & Gutowski, 1989). As a result of all these advantages, USW is expected to offer higher production rates and lower unit costs than other fusion bonding techniques.

A disadvantage of USW is that, generally, energy directors (EDs) have to be placed at the welding interface. EDs are made unreinforced matrix material and placed in between the substrate composites. They are designed to undergo high cyclic strains during the USW process, so they heat up faster than the substrate composites, and ensure that the dissipation of energy concentrates at the welding interface (Potente, 1984). In contrast to unreinforced and discontinuous fiber-reinforced thermoplastics, where the ED can be integrated during the injection molding process, it is more difficult to introduce EDs on CFRTPCs (Villegas & Bersee, 2010). Another disadvantage of the USW process is that it is currently best suited for spot welding and therefore there are limitations regarding the size of the area that can be welded in one step. Larger welds are still possible – using a sequential approach (Ageorges et al., 2001; Agricola, 2014; Harras et al., 1996), but more research is required before sequential welding can be successfully applied. Another barrier to the application of USW is the need for an anvil and a fixture. Dependent on the application, these additional elements can increase the USW associated complexity and investment (Troughton, 2008).

Ultrasonic welding setup

An USW machine consists of a power supply, a piezoelectric transducer, a booster, a horn, a fixture, and a control unit, as can be seen in Figure 1-4. The transducer, the booster and the horn together are called the welding stack.

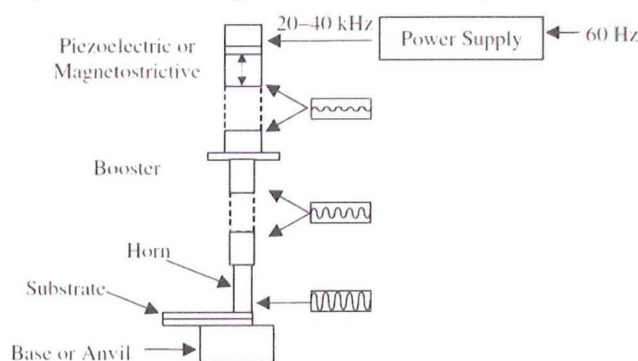


Figure 1-4: Schematic drawing of ultrasonic welding machine (Yousefpour et al., 2004).

The piezoelectric transducer converts high-frequency electrical power, provided by the power supply, into mechanical vibrations. The vibrations are then passed on to the booster, which enlarges the amplitude with a certain gain factor. In addition to amplifying the vibrations, the booster is also used to mount the welding stack to an actuator that controls the displacement and applies a welding force. To be able to fix the welding stack, the booster has a metal ring clamped around its nodal plane, which is used as a mounting point. Next, the

vibrations are passed on to the sonotrode (horn), which further amplifies them with another gain factor. The sonotrode transmits the vibrations in turn to the components being welded. The vibrations that are not dissipated as heat into the components are transmitted to the anvil. The anvil is required to provide a reaction force to the one exerted by the sonotrode, so that the components to be welded are pressed together. Moreover, a fixture is required to align the parts to be welded and to keep them in position during the USW process.

Newer USW machines are often microprocessor-controlled. They offer the possibility to monitor various parameters during the welding process, such as the displacement, velocity and acceleration of the sonotrode, power, and electrical impedance. The collected information can be used to: a) analyze what happened during the process, and b) (eventually) monitor the quality of the weld 'in-situ' (Ling et al., 2006; Villegas, 2013a; Benatar & Gutowski, 1989).

Process description

In order to ultrasonically weld CFRTPCs, the components to be welded are first clamped onto an anvil in a fixture. Subsequently, a sonotrode is transversely pressed onto the upper surface of the composites by the actuator of the USW machine. The actuator gradually applies a force until a preset value for the trigger force level is reached. At this point, the piezoelectric convertor starts vibrating and the sonotrode transmits high-frequency (20 – 40 [kHz]), low-amplitude (10 – 100 [μ m]) mechanical vibrations to the composites. These mechanical vibrations are dissipated in the form of heat at the welding interface of the two composites as a result of interfacial and intermolecular (viscoelastic) friction (Tolunay et al., 1983; Potente, 1984). In order to concentrate the dissipation of energy at the welding interface and speed up the USW process, EDs are generally applied between the parts to be welded (Villegas & Bersee, 2010; Villegas et al., 2014). Since the heating process is highly dependent on the contact pressure between the parts, significant pressures are required to be able to form proper bonds (Potente, 1984). Welding pressures up to 5 [MPa] are not uncommon (Villegas, 2013b).

The vibrations are applied until the ED has melted, been squeezed out, and the substrate composites have united due to intermolecular diffusion of the TP resin in the ED and substrate composites. The moment when the optimal weld is achieved remains to be experimentally determined. Once an optimal weld is observed, it becomes possible to define the 'optimal weld moment' as a specific level of a 'welding driver'. The latter is generally based on time, energy or displacement.

Once the driver value associated with an optimal weld has been reached, the piezoelectric convertor stops the vibrations and the welding pressure is maintained until the molten polymer has completely solidified and formed a proper bond. This phase is called holding or solidification and normally lasts between 4,000 and 9,000 [ms]. The force applied by the actuator during this phase – also called 'holding force' – should be distinguished from the welding force. If pressure is released prematurely, meaning before all material has solidified, the weld acts like a spring and solidifies with many voids at the welding interface.

Process modeling

Benatar and Gutowski (1989) made an effort to model the USW process. According to them, the process can be divided into five distinct yet highly coupled sub-processes:

- 1) Mechanics and vibrations of the parts,
- 2) Intermolecular and interfacial friction,
- 3) Heat transfer,
- 4) Flow and wetting, and
- 5) Intermolecular diffusion.

Going further, they combined these sub-processes and developed one overall model.

Mechanics and vibrations of the parts

The mechanics and vibrations sub-process model describes the strain distribution in the composite parts, the fixture, and the welding equipment. The strain distribution is of interest because it is used to determine the heating rate. The more strain a component experiences, the more energy is dissipated into that component. Therefore, in order to efficiently make a weld, the dissipation of energy has to be focused at the welding line and this is exactly why EDs are used. Benatar and Gutowski (1989) proposed a lumped parameter model, as illustrated in Figure 1-5, to determine the strain distribution. Each mass m_i represents a component of the welding system,

spring constant k_i represents a component's stiffness, and damping coefficient b_i represents the energy dissipation in a component as a result of its strain.

Intermolecular and interfacial friction

Viscoelastic materials, such as the thermoplastics used for USW, dissipate energy into heat when subjected to sinusoidal strain due to intermolecular friction. This phenomenon is called viscoelastic heating. Benatar and Gutowski (1989) identified viscoelastic heating as the main heating mechanism. They used the relation of Tolunay et al. (1983) to estimate the average energy dissipated per time unit (\dot{Q}_{avg}):

$$\dot{Q}_{avg} = \frac{\omega \epsilon_0^2 E''}{2} \quad (1.1)$$

, where ω is the frequency of the vibration, ϵ_0 is the amplitude of the cyclic strain, and E'' is the loss modulus of the thermoplastic material.

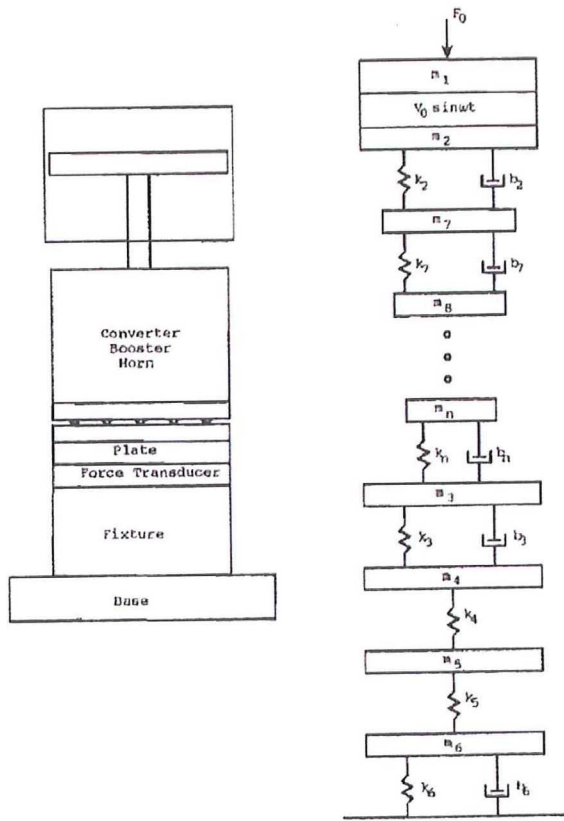


Figure 1-5: Composite welding system and corresponding lumped parameter model (Benatar & Gutowski, 1989).

phenomenon is called the hammering effect. Levy et al. (2014) proposed to incorporate an empirical factor (α_h) into the equation for the average energy dissipation to compensate for this effect. Equation 1.1 becomes:

$$\dot{Q}_{avg} = \frac{\alpha_h^2 \omega \epsilon_0^2 E''}{2} \quad (1.2)$$

Heat transfer

Benatar and Gutowski (1989) also modeled the heat transfer from the welding line to the cooler surrounding material. As the thermoplastic material at the welding line heats up due to the dissipation of vibrational energy, heat is conducted from the welding line to the cooler composite components. The amount of heat conduction is significant because of the large thermal conductivity of carbon fibers. In contrast, heat convection to the air surrounding the weld is relatively small and therefore neglected in the model. Benatar and Gutowski (1989) used

the finite element program FEAP to model the heat flow. They modified the program to include anisotropic conductivity and internal heat generation.

Flow and wetting

When the ED melts, it will start to flow and wet the welding surfaces as a result of the applied welding pressure. When traditional EDs are used – e.g. triangular or rectangular protrusions (Benatar & Gutowski, 1989) – the squeeze flow starts from the moment parts of the ED melt. But when flat EDs are used, the squeeze flow only starts at the moment the complete ED has melted (Villegas, 2013a). When Villegas et al. (2014) made a comparative evaluation of EDs, they could clearly observe this difference in flow behavior in the power/ travel curves of the triangular protrusions versus the flat EDs. The difference is attributed to the fact that flat EDs already cover the whole welding surface.

Benatar and Gutowski (1989) modeled the squeeze flow of triangular EDs. To simplify their model, they analyzed the static force and the dynamic displacement individually and subsequently applied the principle of superposition. Moreover, they assumed an isothermal flow. The model estimates the importance of a) inertia, b) compressibility and c) elasticity. The model shows that, early in the process, both inertial and elastic effects are important, whereas compressibility is negligible. At this point, under static loading, the molten ED behaves like a soft spring in parallel with a soft damper, whereas dynamically it behaves like a moderately hard spring. When the ED melts further and as a result more flow occurs, the spring disappears under the static load, while the impedance of the damper increases. Dynamically, the molten thermoplastic behaves like a stiffer spring. Close to the end of the process, the static behavior is similar to a quasi-steady flow. The dynamic behavior is that of an even stiffer spring. When the melt fronts eventually meet, the static behavior remains similar to a quasi-steady flow, but dynamically compressibility suddenly becomes important and elastic effects start to dominate.

Intermolecular diffusion

An ultrasonic weld acquires its strength from intermolecular diffusion and entanglement of long polymer chains across its interface (Benatar & Gutowski, 1989). The principle of intermolecular diffusion is depicted in Figure 1-6.

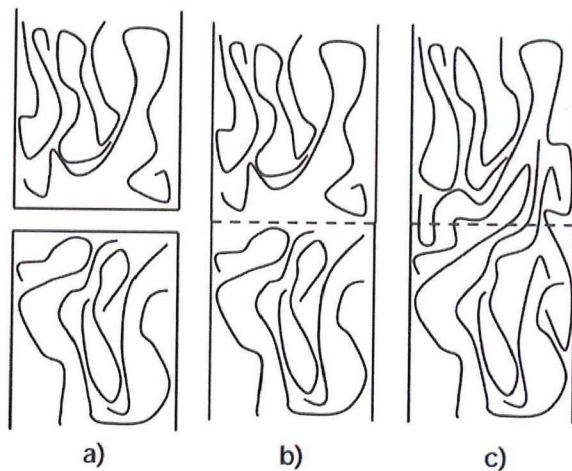


Figure 1-6: Healing of welding interface: a) two distinct components; b) intimate contact between components; and 3) intermolecular diffusion into one component (Prager & Tirrell 1981).

Intermolecular diffusion is initiated above the T_g for amorphous thermoplastics and above the T_m for (semi)-crystalline thermoplastics. Benatar (1987) estimated that the healing time for semi-crystalline thermoplastics is at least six orders of magnitude smaller than the USW time. Because the healing time is negligible, Benatar and Gutowski (1989) did not consider intermolecular diffusion in their model.

In situ process monitoring

Being able to assess the quality of a weld is very important if the wide scale use of welding is to be considered. Non-destructive testing (NDT) methods, such as the A-scan, C-scan and S-scan, are widely applied to inspect the quality of welds. These methods can determine if there are any porosities and/ or contaminations in the welding

interface and/ or the substrate material. Even though the NDT techniques yield valuable information that makes it possible to assess the quality of a joint, they also present a few downsides. First of all, performing NDTs is time consuming. Secondly, NDT is only performed after the components have been welded; taking corrective action during the fusion bonding process is therefore not possible. Repairing a rejected weld is expected to be difficult and labor intensive. Furthermore, the welded components might even have to be scrapped, if they are severely

damaged. Fortunately, Benatar and Gutowski (1989) identified USW's potential for in situ monitoring. Modern microprocessor-controlled USW machines are able to measure every millisecond the welding parameters. By actively monitoring the parameters, irregular behavior can be recognized early in the process and the welding operation can be interrupted and/ or altered before any harm is done to the product.

Benatar and Gutowski (1989) made an effort to monitor joint quality by measuring the mechanical dynamic impedance of the composites during the welding process. They discovered that there is a relation between the impedance and the flow of molten polymer. In the case where triangular EDs are used, the mechanical impedance rises abruptly when the flow fronts of molten polymer meet. At this point a good bond is obtained and the process should move on to the solidification stage. However, dynamic impedance measurements are difficult to perform due to the high frequencies, forces and powers implied by the USW process. Therefore, Benatar and Gutowski (1989) suggested measuring the power and fixture acceleration instead, because – as the authors qualitatively and experimentally confirmed – both of these parameters are related to the impedance .

Villegas (2013a) continued the work on 'in situ' monitoring by investigating the relationships between the events in the power and displacement curves and the transformations at the welding interface when using flat EDs. Villegas (2013a) identified five different stages in the power/ displacement curves of USW as can be seen in Figure 1-7.

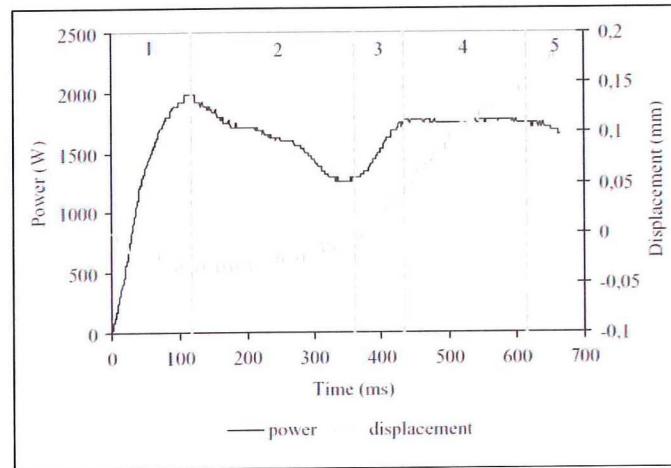


Figure 1-7: Typical evolution of the dissipated power and the displacement of the sonotrode (Villegas, 2013a).

In stage 1, the power ramps up to a maximum and the sonotrode withdraws slightly to accommodate the vibration. Stage 2 starts as soon as the ED melts as a result of nucleation and growth of random hot spots. The power reduces proportionally to the reduction in the solid area of the ED, while the displacement of the sonotrode does not change significantly. Stage 3 starts once the ED has fully melted. The squeeze flow of the molten ED occurs, which can be recognized by a sudden steep increase in the displacement of the sonotrode. In addition, the power also ramps up considerably, because the squeeze flow produces an increase in mechanical impedance, as Benatar and Gutowski (1989) already indicated. Stage 4 starts as soon as the power curve levels out. Note that the weld line thickness is not yet reduced to zero. The power curve levels out because a) the rise in power generated by the increase in mechanical impedance is counteracted by b) a decline in power caused by the melting of the composite substrates. Once the weld line is practically reduced to zero, stage 5 begins. At this point, the dominant factor is the melting of the substrates. This stage is characterized by a reduction in power and a steep rise in displacement.

Ideally, the USW process should stop during stage 4 because this is when the substrate material starts melting. Villegas (2013a) observed that similar specimens welded under identical conditions show a considerable variation in the time taken to reach stage 4, whereas the displacement at stage 4 is as good as constant, as illustrated in Figure 1-8.

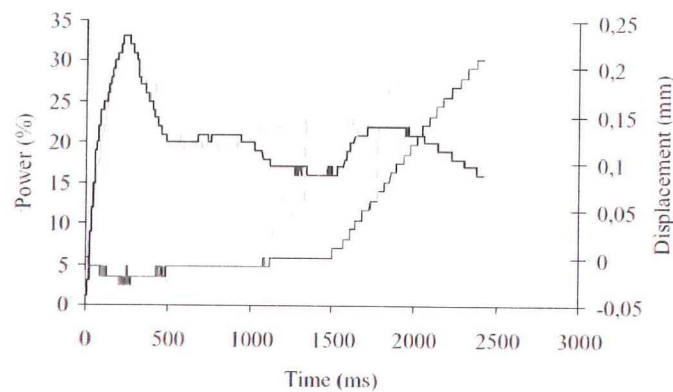


Figure 1-8: Power and displacement curves for two identical specimens welded with the same peak-to-peak amplitude (86.2 [μm]) and welding force (300 [N]). The time to stage 4 varies considerably, whereas the displacement at stage 4 is constant (Villegas, 2013a).

Because the value of the displacement at the beginning of stage 4 is constant, the displacement is a much better driver than the welding time for consistently obtaining a good weld quality.

Villegas (2013a) concluded that, because the power and displacement curves and the relations between them are reproducible, feedback provided by microprocessor-controlled ultrasonic welders can be used to monitor the welding process 'in situ' and, ultimately, to assess the quality of the welds. Patterns, such as the simultaneous rise in power and displacement in stage 3, can be used to identify potential faults. For example, if the power increases without a notable increase in displacement, something unwanted is most likely happening. Moreover, the power and displacement curves can be used to effectively find the optimum set of welding parameters for a new application.

Energy directors

Energy directors are placed in between the substrate composites. They are designed to undergo high cyclic strains during the USW process. Because of this, they heat up faster than the substrate composites, and ensure that the dissipation of energy concentrates at the welding interface (Potente, 1984). EDs are traditionally shaped in the form of matrix resin protrusions, such as rectangular, triangular, or semi-circular polymer ribs (Liu & Chang 2002). Because of the difficulties related to incorporating EDs onto CFRTPCs, Beevers (1991) and Silverman and Griese (1989) investigated the possibility of welding CFRTPCs without EDs. Unfortunately, this made the welding process very troublesome, as the energy dissipation did not concentrate at the welding interface, but instead the composites heated up through-the-thickness. A breakthrough was recently proposed by Villegas (2013a): replace traditionally shaped EDs with a flat polymer film, as illustrated in Figure 1-9. Flat EDs circumvent the difficulties encountered when molding traditional EDs onto CFRTPCs because they do not have to be molded to the substrate composite at all.

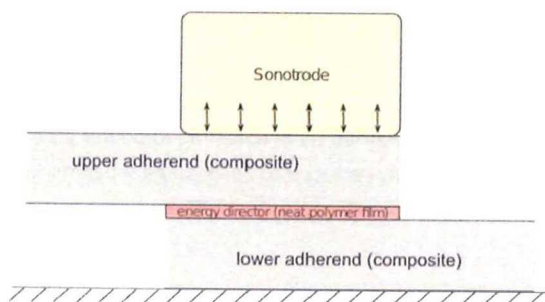


Figure 1-9: Schematic drawing of the ultrasonic welding process using a flat energy director (Levy et al., 2014).

In the case of the traditional EDs, the shape, size and configuration of the EDs strongly affects the strength of the joint, and therefore their design cannot be neglected (Liu, Chang, & Hung, 2001). Chuah et al. (2000) and Liu and Chang (2002) experimentally compared triangular, rectangular, and semicircular EDs and concluded that semi-circular EDs provide the highest joint strength. Villegas and Bersee (2010) experimentally observed that using multiple smaller EDs instead of a single larger one improves the coverage of the overlap area and reduces the disturbance of fibers in the outermost layers of the substrate. Flat EDs already

cover the whole welding interface and therefore their shape, size, and number does not have to be optimized to achieve high-quality welds (Levy et al., 2014). Flat EDs normally have thickness in the range of 0.25 [mm] – 0.40 [mm].

Sequential welding

Lu et al. (1991) succeeded to sequentially weld composite plates using the USW process. Compression molded films with triangular protrusions were used as ED. They noticed that the welding conditions were different for every subsequent plunge weld. For example, in case of the first weld, the top plate is free to vibrate, whereas in case of the second weld, one end of the top plate is already fixed to the bottom plate. The variation in end plate constraint is a challenge as the welding parameters would have to be optimized for every subsequent weld. Moreover, the end plate constraint can result in heating occurring in undesirable places due to vibrations in the top plate. In order to solve these issues Lu et al. (1991) attached rubber dampers to the top plate on either side of the sonotrode. In doing so, the aim was to minimize the zone affected by vibrations. Using this method, they obtained consistent high quality welds throughout the joint.

1.2.2. Research gap

Most research available on USW has been conducted in the lab on lap shear samples in order to optimize various aspects such as the welding parameters and the EDs. However, limited literature is available on the welding of real CFRTPC applications. Aspects such as: a) sonotrode design, b) clamping of composites, c) integration of the EDs on CFRTPCs, and d) tooling design for mobility and accessibility, have been only marginally examined.

Clamping is expected to be of significant importance as the fixture: a) determines the behavior of the vibrations in the composites to be welded, and b) absorbs part of the vibrational energy. However, no literature that investigates the effect of clamping on the USW process is available. Moreover, existing literature focuses mainly on spot welding, whereas many applications might require a sequential or even continuous approach in order for the USW process to be a possible candidate. Furthermore, practical issues such as a) mobility of the tooling, b) accessibility of the tooling when welding applications, and c) the undesirable level of noise created by the USW process, have not yet been investigated. The description and analysis of the effects contamination, such as grease or dust, may have on the quality of the joint are also not covered by existing literature. Moreover, given the speed of the USW process, it is expected that the TP material at the interface becomes amorphous. No literature is available that investigates this phenomenon. It is reasonable to expect that once in a while a poor weld occurs. However, no literature describing if and how corrective action can be taken to repair or improve a weld of poor quality was found. Last but not least, existing literature does not provide any indications regarding if and how curved components can be welded and what effect a) deviation in dimensions of and b) misalignments between the components to be welded have on the welding process.

In this thesis, some of the above mentioned issues will be investigated. Providing answers to practical questions, such as those outlined above, is a prerequisite to any projection about the future that would include the large scale utilization of USW with CFRTPCs.

1.2.3. Practical observations

There are still many challenges that have to be solved before the two proposed demonstrator products can be welded. This section makes an inventory of these challenges, which will subsequently provide the foundation to formulating the objectives and research questions of this thesis. First, the practical challenges of welding clips to a rib are discussed. Next, the challenges associated with welding a fuselage frame to the orthogrid panel are examined. Finally, a new issue observed in practice when welding larger components is explained.

System clips

When designing a setup to weld system clips to a rib, there are a couple of challenges that can be identified. First of all, a fixture has to be designed to keep the clips in place during the USW process. Since the clips are small, and they should preferably be completely overlapped by the sonotrode this can prove to be complicated.

Secondly, an ED configuration has to be chosen. It should be prevented that the molten ED is squeezed out to areas which the sonotrode cannot cover, such as the area right below the flange of the clip, because the ED will solidify and the sonotrode will not be able to melt it again. Finally, the maximum area that can be welded in one spot is unknown.

Fuselage frame

In order to identify the challenges of welding a fuselage frame to Fokker's orthogrid panel, a conceptual design was made in CATIA V5. This design is illustrated in Figure 1-10.

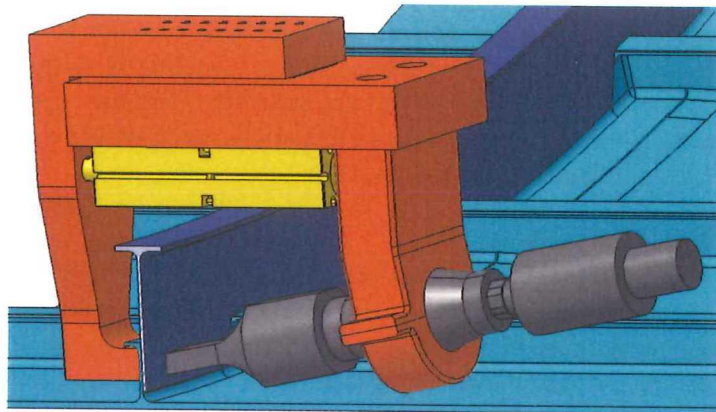


Figure 1-10: Conceptual design of tool to sequentially weld fuselage frame (dark blue) to the orthogrid panel (light blue). Clamping of fuselage frame and orthogrid panel not included. An actuator (yellow) is used to clamp the area to be welded between the anvil of the C-frame (orange) and the welding stack (grey).

First of all, as can be observed in Figure 1-10, accessibility is an issue when welding the frame. Because of this reason, a smaller 35 [kHz] welding stack has been chosen for the conceptual design. However, using smaller tooling is still not sufficient to prevent the welding stack from interfering with the orthogrid panel. Therefore, a chamfered sonotrode (with an angle of 10 [°]) also has to be used. These solutions introduce two challenges: 1) It has to be investigated if CFRTPCs can be welded with the smaller 35 [kHz] USW equipment; and 2) it has to be explored if the USW process works under an angle with a chamfered sonotrode. Moreover, in the proposed conceptual design, welding the frame requires a sequential (or continuous) approach. Therefore, 3) it has to be investigated if USW allows such a process and if it does, how. In addition, 4) it has to be examined what the minimum requirements in terms of stiffness of the frame are as the tooling should also be mobile. Furthermore, 5) research should be conducted on how the two composite components can be clamped together, which might actually become complex as a sequential (or continuous) approach is required. Finally, research should be conducted on 6) which ED configuration best fits USW welding of the frame to the orthogrid panel (in a sequential approach).

Displacement ceiling

In an early stage of the research, various welds were made to determine the possibilities and limitations of the USW process. An issue that kept coming back during the initial experiments was the fact that the steep increase in displacement of the sonotrode, which is expected when the EDs have melted, abruptly came to an end in stage V of Figure 1-12. This abrupt end in the steep increase of displacement – from now on referred to as the displacement ceiling – occurred in every situation where the ED had few free edges, as clarified in Figure 1-11. When welding ASTM D1002 samples, which are often used in USW literature, no displacement ceiling is observed, most likely, because all edges are free and the ED can be squeezed out more easily.

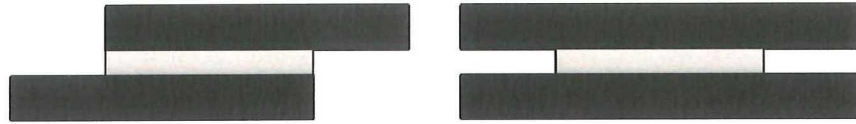


Figure 1-11: Left: welding interface where ED has two free edges (single lap shear sample has four free edges); right: welding interface where ED has no free edges.

The displacement ceiling is found before the second peak in the power curve occurs. Therefore, the displacement cannot be used as the driver anymore, just as Villegas (2013a) suggested. Given that: 1) displacement is expected to be a more reliable driver than either time or energy, 2) the optimal displacement value is independent of geometry, and 3) almost all applications have few or no free edges, it is important to determine the cause of the displacement ceiling. Once the cause is known, efforts can be made to prevent it, so that the methodology proposed by Villegas (2013a) is again applicable.

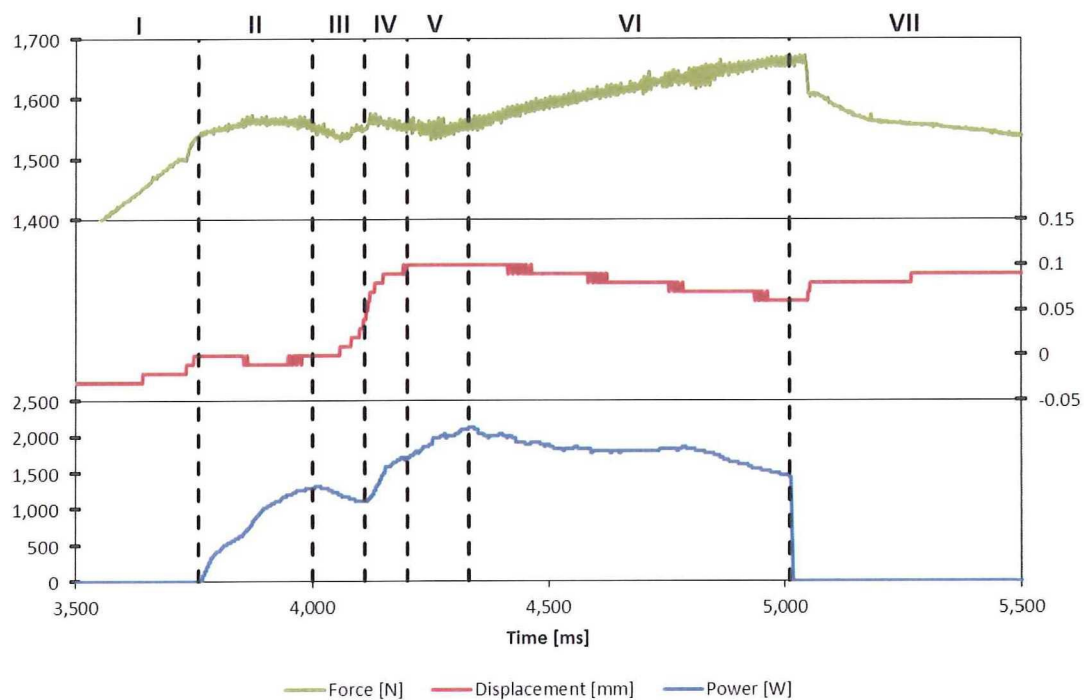


Figure 1-12: Force (top), displacement (middle) and power (bottom) curves of sample clip USW140911-08 welded with an energy of 2,000 [J], an amplitude of 51.8 [μm], and a welding force of 1,500 [N]. The various stages in the ultrasonic welding process are indicated by the black dashed lines.

The welding curves of a sample clip that experienced the displacement ceiling are found in Figure 1-12. Because of the important role welding data plays in this research project, the stages observed in the welding data are once again defined below:

- I) In stage I, the pressure applied by the actuator builds up until the preset trigger force is reached. The USW starts at the end of this stage.
- II) In stage II, the power ramps up until it reaches a maximum: the first peak in the power curve. The displacement slightly reduces to accommodate the vibrations of the sonotrode (Villegas, 2013a). Moreover, because of the vibrations, a slight counterforce is exerted on the sonotrode, which increases the measured force until the actuator of the USW machine corrects for this counterforce and the measured force moves back to the preset trigger value.

- III) Stage III is characterized by a decrease in power until a local minimum in the power curve is reached. This reduction in power is caused by the nucleation and growth of random hot spots in the ED and therefore, the power reduces proportionally to the reduction in solid area of the ED. When the power curve has reached the valley, the ED is completely melted (Villegas, 2013a). At the moment the displacement curve shows the first signs of upward movement (downward displacement of the sonotrode), the force starts to increase.
- IV) At the start of stage IV, the ED has melted and is being squeezed out, as indicated by a sudden steep increase in the displacement of the sonotrode. Moreover, the power considerably ramps up again as the squeeze flow results into an increase in mechanical impedance as explained by Benatar & Gutowski (1989). The displacement increases until it suddenly reaches a ceiling. In this thesis, an effort is made to investigate the cause of this ceiling. At the moment the ED is melted, the force curve shows a short and small sudden movement, which is, most likely, caused by the fact that the sonotrode abruptly accelerates and comes to a stop again. Afterwards, the USW machine slowly reduces the force again until it reaches the preset force value.
- V) Stage V is characterized by a) a further increase in power until the second peak in the power curve is reached, b) the presence of the displacement ceiling, and c) a turn-around in force. According to Benatar & Gutowski (1989), the second peak in the power curve is caused by the melting of the substrate composite. Because of this, (Villegas, 2013a) suggested that USW process should be stopped at the time of the second peak in order to get the best welding quality. It is yet unknown why the force suddenly starts increasing to values much higher than the preset value. However, this phenomenon is expected to be related to the displacement ceiling.
- VI) Stage VI is characterized by: a) the decrease in power due to the melting of the substrate composite, b) a further increase in the welding force, and c) a reduction in displacement. The reduction in displacement and the further increase in force might indicate thermal expansion. Moreover, a hypothesis is established that it also indicates material degradation as voluminous gasses are formed which exert pressure onto the sonotrode and push it upwards. This research project experimentally investigates this hypothesis.
- VII) Stage VII starts as soon as the vibrations of the sonotrode are stopped. At this point no energy is dissipated anymore and the molten thermoplastic is given time to cool down and consolidate, while the welding pressure is maintained. The USW machine gradually changes the applied force to the preset holding force level, and the displacement of the sonotrode increases due to thermal shrinkage until approximately the same level as the one recorded at the moment of the displacement ceiling is reached again.

1.3. Objectives & research questions

The main **objective** is: to identify the potential and feasibility of ultrasonic welding of CF/ PEKK composites in an industrial setup, by welding system clips and fuselage frames.

The objective can be divided into the following **sub-goals**:

1. Design and build appropriate tooling for welding clips
2. Design and build appropriate tooling for welding fuselage frames
3. Be able to weld clips consistently with high-quality welds
4. Make a demonstrator by ultrasonically welding CF/ PEKK clips to a CF/ PEKK rib
5. Make a second demonstrator by ultrasonically welding a CF/ PEKK fuselage frame to a section of Fokker's CF/ PEKK orthogrid panel
6. Present an outlook for ultrasonic welding of CFRTPCs in the aerospace industry

Based on the objective, the literature review and practical observations, the research questions are established. Since more questions have to be answered – in order to be able to weld the fuselage frame to the orthogrid panel – than can be reasonably answered within a MSc. thesis while maintaining the required academic profoundness. Therefore, the larger collection of research questions is divided into two sets: the first one contains the research questions that will be answered at the required academic depth in Section II – Experiments, Results & Discussion, whereas the second one contains the questions that will be answered without fully enlarging upon every detail in Section III – New Concepts & Fuselage Frame. The questions in the second set are introduced to scan the potential of the ultrasonic welding process and also to identify interesting areas for further research.

The **main research question** of the first set is: how can CF/ PEKK clips be ultrasonically welded to a CF/ PEKK rib with consistent high-quality bonds?

This question is divided into the following **sub-questions**:

1. What is causing the displacement ceiling?
2. What is the best method to clamp clips during the ultrasonic welding process?
3. What is a good energy director configuration to ultrasonically spot-weld clips?
4. What is the optimal value of the welding driver – be it energy or displacement – to consistently weld clips with a high-quality bond?

The **main research question** of the second set is: how can CF/ PEKK fuselage frames be ultrasonically welded to Fokker's CF/ PEKK orthogrid panel, and what is the potential of ultrasonic welding in the aerospace industry?

This question is divided into the following **sub-questions**:

1. Is it possible to integrate energy directors into one of the substrate composites?
2. What are the effects of clamping on the ultrasonic welding process?
 - a. What effect do rubber pads placed between the composites and the clamp have?
 - b. What is the effect of the location of the clamps?
 - c. What is the effect of the clamping pressure?
 - d. Does it make a difference if a component is clamped from one side or two sides?
3. How can the fuselage frame be clamped during the ultrasonic welding process?
4. Is a sequential approach feasible for ultrasonic welding?
5. What is the outlook of ultrasonic welding in the aerospace industry?

1.4. Outline

In this section, the outline of the thesis is described. In chapter 2, the experimental set-ups that are used to conduct the experiments are described. Subsequently, in chapter 3, a good ED configuration to weld clips is chosen. Next, in chapter 4, the development of the squeeze flow and the weld quality is studied as a function of the applied energy. Moreover, an effort is made to find the cause of the displacement ceiling. Then, in chapter 5, system clips are welded to a rib. In chapter 6, an effort is made to integrate triangular EDs into a composite laminate. Next, in chapter 7, the effects of clamping are investigated and subsequently, in chapter 8, the fuselage frame is welded. Finally, in chapter 9, 10, and 11, the conclusion, outlook, and recommendations for future research are presented.

2. Experimental Set-up

In this chapter, the experimental set-up is described. First, in section 2.1, it is explained which materials are used, how the samples and EDs are manufactured, and how they are prepared for welding. Subsequently, in section 2.2, the USW equipment is described. Next, in section 2.3, the different welding configurations used are explained. Finally, in section 2.4, the testing equipment and procedures are described.

2.1. Materials, manufacturing & preparation

In this section, it is explained a) which materials have been used and b) how they have been processed to create the products required for the experiments. In section 2.1.1, it is explained how the composite samples are manufactured. Next, in section 2.1.2, it is explained how the EDs are produced. Finally, in section 2.1.3, it is explained how the clips are manufactured.

2.1.1. Composite samples

All composite samples, with the exception of the clips, are made of Cytec APC PEKK-FC with continuous unidirectional carbon fibers. The composite has a typical fiber volume content of 50 [%] to 60 [%]. Moreover, the thermoplastic is semi-crystalline with a T_g of 159 [°C], a T_c of 279 [°C], and a T_m of 337 [°C]. The moisture uptake is less than 0.3 [%] by weight. These are the most relevant material properties for the USW process. Other material properties can be found in Cytec's material data sheet (Cytec, 2009).

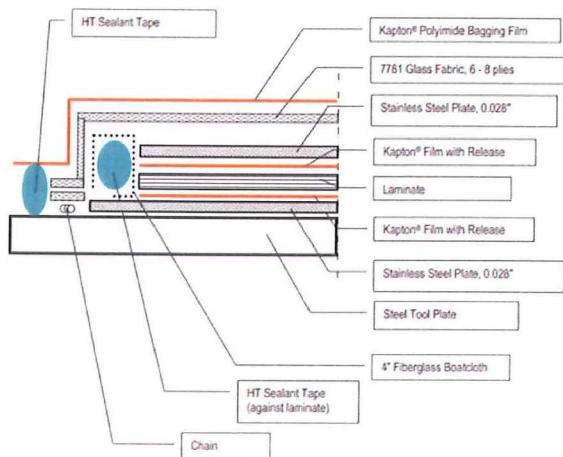


Figure 2-1: Recommended vacuum bag scheme (Cytec, 2009).

The laminate of the composite samples consists of a $[(0/90)_3]_s$ lay-up. Every ply has a thickness of 0.14 [mm], so the total thickness becomes 1.68 [mm]. The plies are manually cut using a cutting table, and manually stacked. In order to keep the plies together during layup, the plies are bonded at the corners with a 35 [kHz] ultrasonic plunge welder.

The laminate is consolidated in an autoclave through vacuum bagging. The vacuum bag scheme is illustrated in Figure 2-1. It should be noted that instead of the two layers of 'Kapton film with release' recommended by Cytec, Upilex 25S film has been used.

The autoclave cycle is as follows: the temperature level increases to 375 [°C] at a rate of 5 [°C/min]. Then the autoclave maintains the temperature level of 375 [°C] for an hour. After that, the autoclave cools down at a rate of 5 [°C/min]. When the laminate has reached room temperature, which is measured with thermocouples at various locations in the laminate, the laminate has consolidated and can be removed from the autoclave. During the whole cycle, the autoclave exercises an overpressure of 6 [bar], while the vacuum bag applies a pressure of 1 [bar]. An example of the autoclave cycle can be seen in Figure C-1.

To saw the samples in the required dimensions, a circular saw with a diamond-coated blade is used. The saw is water cooled. The samples are dried in an oven at 120 [°C] during 6 hours and they are cleaned using PT Technologies' PFQD – Quick Drying Solvent Odorless Degreaser – right before they are welded.

2.1.2. Energy director

The flat ED is made out of 5 layers of 50 [μm] film and therefore it has a thickness of 0.25 [mm]. The ED is manufactured according to the same procedure as the composite laminate, as described in the previous section. However, the autoclave cycle has been changed so that the temperature stays below the melting temperature

of PEKK. This is important to prevent that the thermoplastic polymer becomes liquid and flows away. Since the T_m of PEKK is 337 [°C], the maximum temperature is set to 320 [°C], which the autoclave maintains for 35 [min]. The rate of heating, the rate of cooling, and the pressure remain unchanged. The associated auto clave cycle can be seen in Figure C-2.

Both the flat EDs and the ED strips, used in the experiments, are cut out of the consolidated PEKK using a cutting table. The PEKK ED is also dried for 6 hours in an oven at 120 [°C] and is cleaned using PT Technologies' PFQD – Quick Drying Solvent Odorless Degreaser – right before it is placed between the composites to be welded.

2.1.3. Clips

The clips are made from the same material as the composite samples: Cytec APC PEKK-FC with aligned continuous unidirectional carbon fibers. However, the clips are made out of 8 plies and have a layup of $[45/90/-45/0]_s$. First, a laminate is consolidated in the autoclave, as described in section 2.1.1. Subsequently, the laminate is shear-cut at the edges and press-formed into a Z-profile. The clips are milled out of this profile.

2.2. Ultrasonic welding equipment

In this section, the ultrasonic welding equipment is described. First, in subsection 2.2.1, the ultrasonic welding machine is explained. Then, in section 2.2.2, used sonotrode are presented. Finally, in section 2.2.3, the newly designed fixture is described.

2.2.1. Ultrasonic welding machine

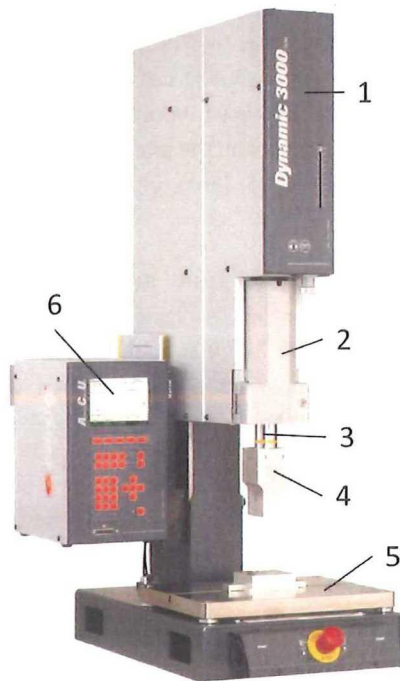


Figure 2-2: Dynamic 3000 ultrasonic welding machine with generator ACU (Rinco Ultrasonics AG, 2008).

All the experiments are conducted with a Rinco Dynamic 3000 (Figure 2-2). The Dynamic 3000 is an ultrasonic welding machine with an Advanced Control Unit (ACU). The machine has an actuator (# 1 in Figure 2-2) that is able to apply a maximum force of 3,000 [N]. Moreover, the converter, which is located in a housing (# 2), offers a maximum peak-to-peak amplitude of 22 [μm]. The amplitude of the converter can be reduced to a minimum of 60 [%]. A booster (# 3) is connected to the converter. The booster amplifies the amplitude with a certain gain factor. The booster used for this research project has a gain factor of 2. The sonotrode (# 4) is connected to the booster. As it will be explained in the next section, three different sonotrodes are used with gain factors ranging between 1.96 and 2.4. The complete welding stack can be seen in Figure C-3. A fixture or anvil can be attached to the clamping table using M6/ M8 T-nuts or T-bolts. The clamping table itself can also be used as an anvil. For this research, a new anvil/ fixture has been designed, as will be explained in section 2.2.3. The power supply (# 6), used in combination with the Dynamic 3000, offers a maximum power of 3,000 [W]. The ACU (also # 6) is the 'brain' of the Dynamic 3000. It controls the welding machine and allows the user to set all the parameters related to the welding process. In order to control the process, the user can select between three welding drivers: 1) energy, 2) displacement, and 3) time. When the user has selected

the welding driver and entered a value, the Dynamic 3000 will automatically stop the vibrations once this driver is reached during the USW process. Furthermore, the ACU records a value for 1) the power, 2) the displacement, 3) the force, and 4) the time every millisecond. This data is processed by the program AcuCapture and stored in a .mdb file. Subsequently, this data can be analyzed using either AcuCapture or the Welding Data Analyzer, which is a Microsoft Access 2010 tool especially build during the course of this research project. More details about the Dynamic 3000 can be found in its operating instructions (Rinco Ultrasonics AG, 2008).

2.2.2. Sonotrodes

For the experiments three different sonotrodes are used. The sonotrodes and their associated properties can be seen in Table 2-1.

Table 2-1: Overview of sonotrodes used for the experiments. *Maximum peak-to-peak amplitude is based on a booster with a gain of 1:2.

				
	Sonotrode 1	Sonotrode 2	Sonotrode 3	Sonotrode 4
Dimensions [mm]	73 x 18	59 x 24	Ø 40	30 x 14.9
Surface area [mm ²]	1,314	1,416	1,257	447
Gain [-]	2.4	2.0	1.96	2.75
Maximum peak-to-peak amplitude [µm]*	105.6	88.0	86.2	120.9

2.2.3. Fixture

For this research project, a new fixture – including an anvil – has been designed and manufactured: the Z51414. The 9109 fixture, used by Villegas (2013a) and Agricola (2014), was designed specifically to weld ASTM D1002 samples and is therefore unsuitable for the experiments in this thesis. The Z51414 fixture, as illustrated in Figure 2-3 and Figure 2-4, is designed to be both simple to use and flexible. The fixture can be used in many different configurations, as will be explained in section 2.3. Moreover, it allows different components to be installed, as will be explained in section 2.3.4, and demonstrated in chapter 0, when an effort is made to weld the fuselage frame. Moreover, the tool is designed to fit both a 35 [kHz] Rinco Standard 745 and a 20 [kHz] Rinco Dynamic 3000 ultrasonic welder.

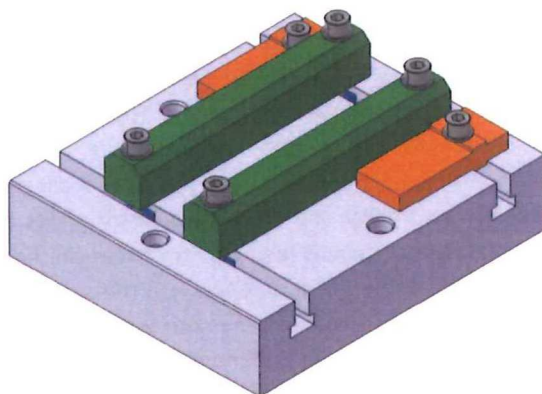


Figure 2-3: The Z51414 fixture designed to both flexible and simple.

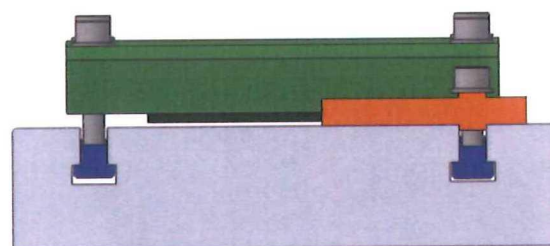


Figure 2-4: Side-view of the Z51414 fixture. The T-slots make the tool very flexible.

The grey block with the two T-slots is the anvil. It can be fixed to the T-slots of the Rinco USW machines using M6 bolts. If required, the anvil can be rotated by 90 [°], since it has counter-bored M6 holes on all four edges. The two green components are the clamps and they can be fixed with M8 bolts to the M8 T-nuts (blue) in the T-slots of the anvil. Teflon coated rubber pads (black), from the Mosites Rubber Company, can be attached to the

clamps if needed. The clamping force can be determined by tightening the M8 bolts with a torque wrench. The orange parts are alignment blocks that can be used to position the composite samples. The anvil, clamps, and alignment blocks are all made from aluminum. The dimensions of the components can be seen in the production drawings in 0.

2.3. Welding configurations

In this section, the welding configurations for the sample clips, the system clips, the single and double-side clamped samples, and the fuselage frame are described in section 2.3.1, 2.3.2, 2.3.3, and 2.3.4, respectively.

2.3.1. Sample clips

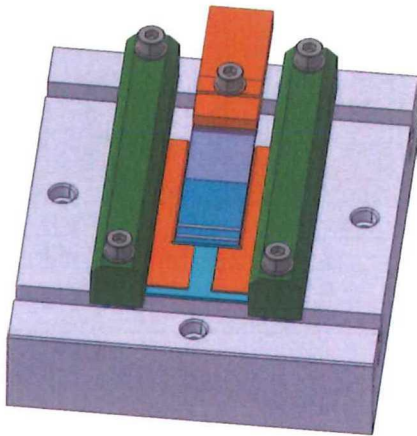


Figure 2-5: Fixture Z51414 in the sample clip configuration.

Sample clips are welded with fixture Z51414 in the configuration presented in Figure 2-5. It can be observed that the upper sample (transparent dark blue) – from now on referred to as the sample clip – is not clamped at all, but merely kept in position by an alignment block and two 1 [mm] thick steel plates (orange) – from now on referred to as the alignment plates. The alignment plates need to be thinner than the thickness of the sample clip to prevent interference with the sonotrode. The sample clip is given approximately 0.5 [mm] spacing with respect to each alignment plate/ block to prevent friction during the USW process. The alignment block is fixed using an M8 bolt, whereas the alignment plates together with the lower composite (light blue) are clamped using the clamps with the Teflon-coated rubber pads installed. The M8 bolts of the clamps are tightened with 2.5 [Nm].

The sample clip is 30 [mm] in width and 80 [mm] in length. The lower composite is 92 [mm] in width and also 80 [mm] in length. The sample clip is sticking out with respect to the lower composite, so that lap shear test can easily be performed. The ED is not described as its configuration varies between the different experiments. Sonotrode 3 is used and it will be positioned at the edge of the sample clip where the ED strips (light yellow strips) are located. It is important the sonotrode overlaps the corners of the sample clip to prevent damage.

2.3.2. System clips

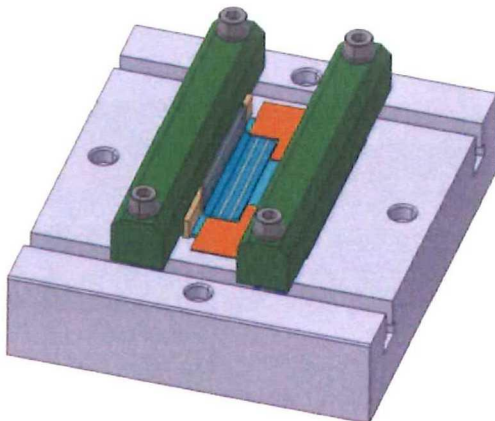


Figure 2-6: Fixture Z51414 in the system clip configuration.

Clips are welded with fixture Z51414 in the configuration illustrated in Figure 2-6. It can be seen that this setup is similar to the one presented in Figure 2-5. The difference is that the sample clip is now replaced by a real clip (transparent dark blue). Since the real clip has a different geometry, two smaller and thinner alignment plates are used. The alignment plates (orange) now have a thickness of 0.7 [mm] to prevent interference with the sonotrode. The alignment block is not used anymore and its function is taken over by one of the aluminum clamps (green). To prevent interaction between the clip and the aluminum clamp, which might damage the clip, a wooden stick (brown) is placed in between.

Sonotrode 1 is used as it completely overlaps the bottom surface of the clip, which is 16 [mm] by 65 [mm]. All dimensions of the clip can be seen in Figure B-2. The lower composite (light blue) is the same as the one used for welding the sample clip, thus with dimensions of 92 [mm]

by 80 [mm]. Moreover, the clamps (green) fastens again both the alignment plates and the lower substrate and the M8 bolts of the clamps are tightened with 2.5 [Nm].

2.3.3. Single and double-side clamping

The Z51414 fixture is also used to weld single lap shear samples. Two different types of lap shear samples have been used for the experiments: 1) single-side clamped samples following the ASTM D1002 standard, with dimensions of: 25.4 [mm] by 101.6 [mm]; and 2) double-side clamped samples, with dimensions of: 25.4 [mm] by 203.2 [mm]. As the names already indicate, the first samples are clamped at only one side (see Figure 2-7), whereas the latter samples are clamped at two sides (see Figure 2-8). These samples are used to investigate the effects of clamping on the USW process. For this purpose, the following elements can be adjusted to the configuration of the welding fixture: a) the Teflon-coated rubber pads can be removed; b) the clamping force can be controlled and adjusted using a torque wrench; and c) the location of the two clamps can be varied parallel to the T-slots of the anvil. In case of the single-side clamping configuration, a third sample or plate with a similar thickness should be placed between the upper sample and the anvil to prevent excessive bending of the sample.

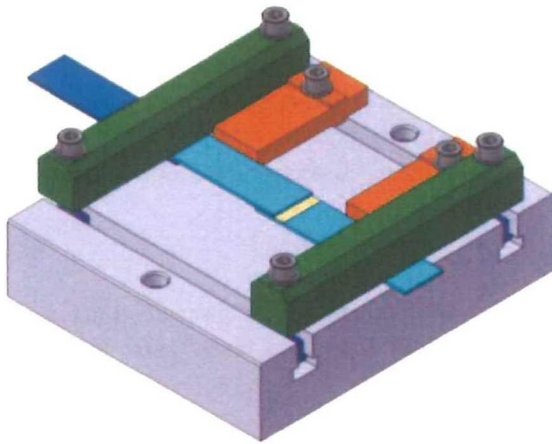


Figure 2-7: Fixture Z51414 in the single-side clamping configuration.

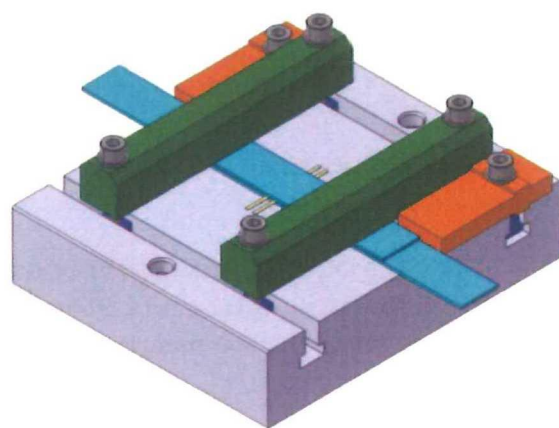


Figure 2-8: Fixture Z51414 in the double-side clamping configuration.

2.3.4. Fuselage frame

In order to weld the fuselage frame in Chapter 0, a new fixture has to be designed particularly for this purpose due to the frame's complexity. Since the inclusion of the T-slot concept in the Z51414 fixture design allows for flexibility, the fixture can easily be expanded by introducing new clamps (green) and a special anvil (yellow). From now on, this new configuration, as can be seen in Figure 2-9, is referred to as the Z51430 fixture.

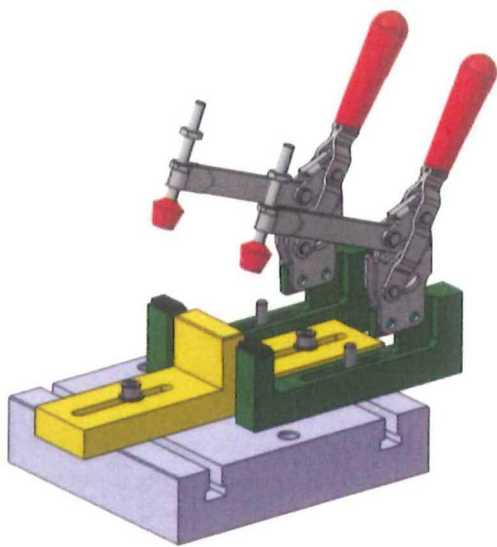


Figure 2-9: Fixture Z51414 with the Z51430 expansion especially designed to ultrasonically weld fuselage frames to the orthogrid panel.

Both the clamps and the anvil stick out so that the bottom of the stringers on the orthogrid panel can be reached. Each clamp has a Destaco 207-LB toggle clamp with a maximum holding capacity of 2,220 [N]. The specifications of this toggle clamp model can be found in Destaco's product overview (Destaco 2014). Toggle clamps are used to make clamping convenient and fast. In addition, Teflon-coated rubber from Mosites is used again to prevent interaction between the composite components and the clamps. Furthermore, the clamps have slots. Both clamps are connected with a single M8 T-bolt and a nut to one of the T-slots of the Z51414's anvil. Because of this construction, the in-plane location of the clamps can be changed. Moreover, the clamps can be rotated around the longitudinal axis of the T-bolts. The anvil also contains slots – one at each side. The anvil is connected to the T-slots with M8 bolts and T-nuts. Because of the similar construction, the in-plane location and the angle of the anvil can also be changed. Due to the adjustability of Z51430, the tool can

hopefully be used in the future to also weld more components than just the fuselage frame. Both the clamps and the anvil are made of steel.

2.4. Testing equipment & procedures

In this section, the testing equipment and procedures used to study the welds, are explained in the following order: 1) tensile testing, 2) optical microscopy, 3) scanning electron microscopy, and 4) non-destructive testing.

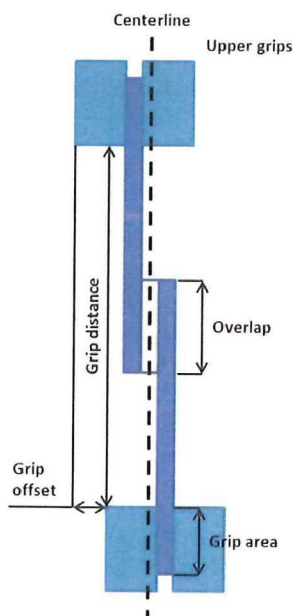


Figure 2-10: Tensile testing setup schematic.

Tensile testing

To perform single lap shear tests, a Zwick/Roell 100 [kN] universal testing machine, available at Fokker Aerostructures in Hooerveen, is used. A schematic drawing of the setup is presented in Figure 2-10. The overlap of the samples and the grip distance depends on the sample tested. However, all samples are clamped with a grip area of 25.4 [mm²] per [mm] width of the sample. The grip distance is simply calculated by subtracting the overlap and two times the grip area from the total length of the samples. Single lap shear samples are not symmetric around the centerline. Therefore, they experience eccentric loading. To minimize this, the lower grip is given an offset (sample + ED thickness).

Optical microscopy

Optical microscopy is performed, using an Olympus BH microscope, an Olympus U-PMTVC camera adapter, and a ColorView I digital camera, which are available at Fokker Aerostructures in Hooerveen. Both fracture surfaces and cross-sections of casted samples are examined using optical microscopy. To analyze the fracture surfaces, cold light is used in addition to the optical microscopy's own light source, a technique that reveals more details. To analyze the cross-sections either a 'normal' or a ultraviolet (UV) light source is used. The UV light source is used to reveal small cracks and the transition between layers in the material. Before the cross-sections can be studied, samples are first casted, sanded, and polished according to Fokker's operating instruction FSP/99-100-02. The samples are casted with Struers EpoFix resin, EpoFix hardener, and EpoDye powder. After the samples have been casted, a vacuum is applied to remove air before curing. The

samples are sanded for 2 minutes at roughness: 180, 220, 500, 800, 1,200 and 4,000; and polished for 3 minutes at roughness: 3 [μm], 1 [μm], and 0.25 [μm].

Scanning electron microscopy

Scanning electron microscope (SEM) microscopy is performed using a JEOL JSM-7500F Field Emission Scanning Electron Microscope, which is available at the Aerospace Engineering faculty of the TU Delft. The specimens are sputtered with gold particles before they are analyzed.

Non-destructive testing

Non-destructive tests (NDTs) are performed with the Olympus Omniscan MX, which uses phased array (PA) technology. The Omniscan is a mobile tool, and therefore can be used in the field. This allows the user to immediately check the quality of a weld right after two components have been welded.

The PA technology works as follows: the PA probe sends ultrasonic signals through the composite, and then measures a) how strong the returning signals are and b) from which distance the signals return. If the signal returns from the back of the upper composite, it can be concluded that there is no joint. When the signal returns from the back of the lower composite, the signal went right through the welding interface, which leads to the conclusion that there is a bond. In case the signal does not return, it is considered that the signal most likely scattered. This can be caused by, for instance, the presence of voids at the welding interface or in the composites themselves. When the signal returns from within a composite, it can be concluded that the composite has delaminated at the location from where the signal returns.

In order to make a PA scan, the surface of the composite has to be moistened and subsequently, the probe of the Omniscan has to be scrolled over the section of the composite that is of interest. While scrolling, the Omniscan makes a collection of A (upper-left) and S-scans (upper-right) and one large C-scan (lower), as can be seen in Figure 2-11. The screen presents the A-scan of the point where the two blue lines in the C-scan intersect. Moreover, it presents the S-scan of the vertical blue line in the C-scan. By moving the two blue lines in the C-scan, other A and S-scans can be seen.

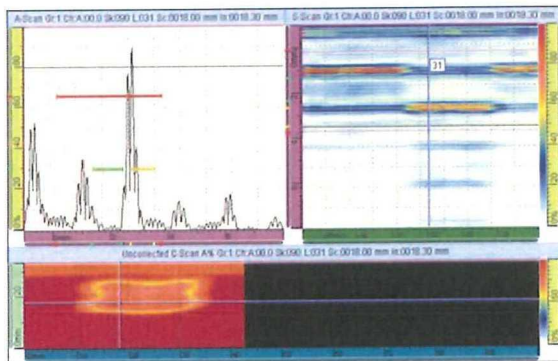


Figure 2-11: Example of A (upper-left), S (upper-right), and C-scan (lower) of a sample clip.

The C-scan shows a map of the signal strength throughout the scanned section. Red indicates that the returning signal is strong; blue indicates the returning signal is weak; and white indicates that the returning signal is completely lost. In the C-scan it can be observed that there is a spot where the signal is slightly less strong: it represents the welded area. However, in order to derive information about the quality of the weld, the A and S-scan have to be assessed. The A-scan is observed first. The first peak from the left in the A-scan represents the input signal, the second peak shows that a poor signal

returns from the welding interface and the third points out that a strong signal returns from the back of the lower composite. Because the third peak is strong and significantly higher than the second peak, it can be concluded that there is a proper bond at the location of the A-scan. The red line in the A-scan determines which range of returning signals is used to make the S and C-scan. The green and yellow line can be ignored. The S-scan should be interpreted as follows. The first horizontal line from the top in the S-scan represents the input signal. The second line from the top represents the back of the upper composite and thus the welding interface. The signal in this line is interrupted at the location of the weld. Since the signal is strong in the third line, which represents the locations in the back of the lower composite where the signal is illustrated as weak in the second line, it can be concluded that a good bond was achieved.

II – Experiments, Results & Discussion

3. Selection of Energy Director Configuration

In this chapter, the ED configuration for the clips is selected. In section 3.1, Villegas' flat ED (2013a) is used to weld ASTM D1002 samples and sample clips. Subsequently, in section 3.2, a new ED concept – slender ED strips – is introduced as a possible solution to the shortcomings of the flat ED. Next, in section 3.3, the configuration of ED strips is optimized, and finally, in section 3.4, the conclusions are provided.

3.1. Flat energy director

Villegas introduced the flat ED, which is simply a loose matrix resin film placed at the welding interface. In several publications, Villegas pointed out that these flat EDs provide a good alternative to the traditional ribs that are generally used in the plastics industry, when welding thermoplastic composites (Romero et al., 2012; Villegas, 2013a; Villegas, 2013b; Levy et al., 2014; Villegas et al., 2014). For this reason, the use of flat EDs is investigated first.

Before clips are welded with the flat EDs, ASTM D1002 samples are welded in the 9109 fixture, as used by Villegas, to provide a baseline and to prove that this type of ED also works with PEKK. A detailed description of the 9109 fixture can be found in an article published by Villegas (2013a) or the MSc. thesis of Agricola (2014). The ED has a thickness of 0.25 [mm] and an effective surface area equal to the overlap of the ASTM D1002 samples, which is $25.4 \times 12.7 = 322.6$ [mm²]. The samples are welded using sonotrode 4 with a peak-to-peak amplitude of 72.6 [μm], a welding force of 500 [N] (equivalent to a welding pressure of 1.55 [MPa]), and a displacement of 0.11 [mm] as the welding driver. The value of the welding driver was determined by applying the methodology proposed by Villegas (2013a), which suggests to use the displacement value at which the second peak in the power curve occurs in order to achieve the optimum weld quality. The resulting power and displacement curves of ten samples, welded under the same conditions, can be seen in Figure 3-1.

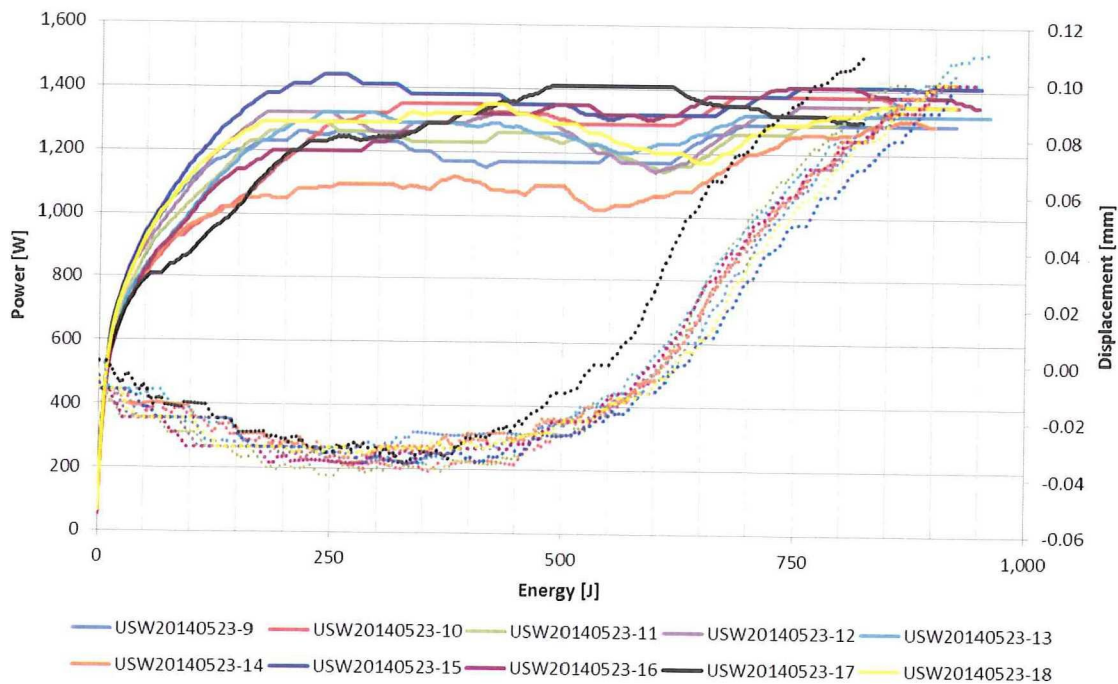


Figure 3-1: Power (solid) and displacement (dotted) plots of CF/ PEKK ASTM D1002 samples ultrasonically welded with flat PEKK EDs in the 9109 fixture under the same conditions.

It can be observed that the power and displacement plots of the ten welds are very similar and show the same pattern as described by Villegas (2013a). Moreover, it can be seen that the USW process nicely stops at approximately the second peak in the power curve. Single lap shear tests, of which the procedure is described in section 2.4, have been performed on all ten samples, and provided an average lap shear strength (LSS) of 47.0

[MPa] with a coefficient of variation (CoV) of 5.76 [%]. These results are promising and confirm that the methodology of Villegas (2013a) can also be applied to the ultrasonic welding of CF/ PEKK composites.

The next step is to weld sample clips using flat EDs. These sample clips are 30 [mm] by 80 [mm] and are welded with the Z51414 fixture in the configuration presented in section 2.3.1 and illustrated in Figure 3-3. Moreover, sonotrode 3 is used. The flat EDs are welded on one side using an ultrasonic plunge welder (Figure 3-2). Unfortunately, it requires a bit of experience to plunge weld the EDs to the lower composite, as both the plunge welder and the square ED tend to slide away due to the vibrations. In order to prevent the ED from moving, the three edges that are not welded are taped to the composite.

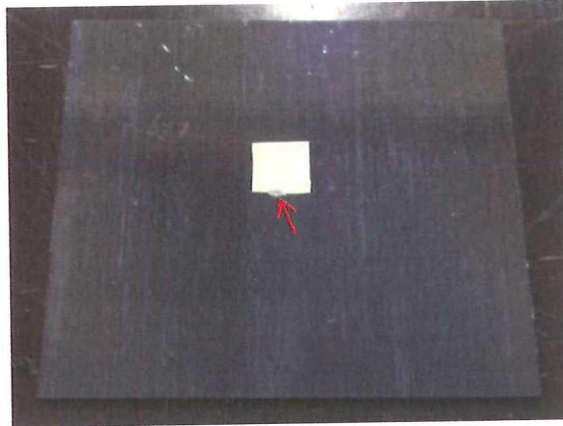


Figure 3-2: Flat square 1 [cm²] ED plunge welded to the lower composite. The plunge weld is indicated by the red arrow.

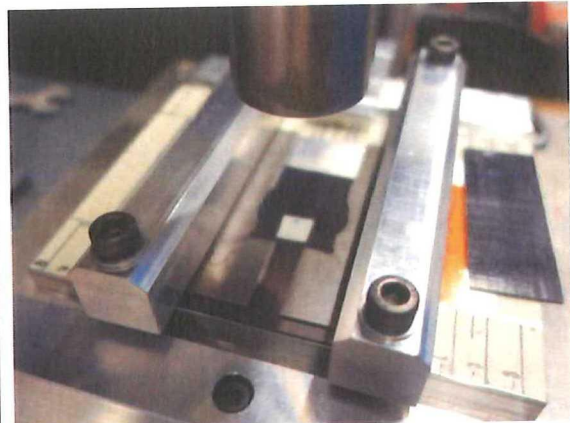


Figure 3-3: Sample clip USW configuration with a flat square 1 [cm²] ED.

The first experiment was conducted with a square 4 [cm²] ED that has a thickness of 0.25 [mm], a peak-to-peak amplitude of 73.4 [μm], a welding force of 500 [N] (equivalent to a welding pressure of 1.25 [MPa]), and a displacement of 0.11 [mm]. However, the displacement of 0.11 [mm] was never obtained and the USW process had to be stopped manually with the emergency stop. As a result, no welding data was saved to the computer. Apparently, the sonotrode was not able to squeeze out all the ED and the displacement never reached the required 0.11 [mm].

Several conditions were changed to make the USW process work. a) First, smaller square 1 [cm²] EDs were used. However, again the displacement driver was never reached. b) Subsequently, the alignment plates were modified by removing material around the ED with a file, to prevent that the plates block the squeeze flow of molten ED. Moreover, a draft angle was given to the edges of the alignment plates, so that the upper sample would more easily find its place, and 0.5 [mm] space was given between the sample clip's edges and the alignment plates to minimize their interaction. Unfortunately, the problem was not solved. Next, c) the welding pressure was increased from 500 [N] to 1,000 [N] to speed up the squeeze flow and hopefully obtain higher displacement values. However, the displacement driver of 0.11 [mm] was still not reached. Therefore, d) the displacement driver was decreased to 0.08 [mm]. As a result, the USW process stopped by itself for the first time and the data was saved again to the computer. In the welding data (Figure 3-4), an abrupt stop of the sonotrode's displacement can be observed at values of approximately 0.08 [mm]. Although the USW process stopped in an early stage at 965 [J], sample clip USW140826-03 was already heavily damaged at the sides, as can be seen in Figure 3-5. In order to minimize the damage to the sample clips, e) the peak-to-peak amplitude was decreased to 51.8 [μm]. This provided satisfactory results as the damage to the clips was significantly reduced. However, sample clip USW140826-06 was still damaged, while the energy used to weld this sample was only 591 [J]. Finally, f) the welding force was increased to 1,500 [N]. As can be seen in Figure 3-5, the damage was again reduced, but sample USW140826-09 still presented visible damage at only 589 [J].

So several measures have been taken to make the USW process work when welding sample clips with flat square 1 [cm²] EDs. Despite the fact that slight improvements have been made and eventually, samples were welded with only minor damage to the sample clip, the results are not satisfactory. First of all, the samples are welded with a displacement of only 0.08 [mm] and are therefore probably imperfect. This can be derived from the fact that their power curves did not reach their second peak yet (Figure 3-4). This implies that they will not be optimal in terms of strength. Secondly, although the welds are unfinished, the sample clips are already damaged. Preferably, they should not be damaged at all. Finally, the displacement reaches an abrupt ceiling for a yet unknown reason. Unfortunately, due to the ceiling, the displacement cannot be used as the welding driver anymore, which also implies that the methodology of Villegas (2013a) cannot be applied. Given these three reasons, it is concluded that the flat square EDs, in the form presented, are not a good option when welding the CF/ PEKK sample clips. Therefore, another ED configuration has to be introduced.

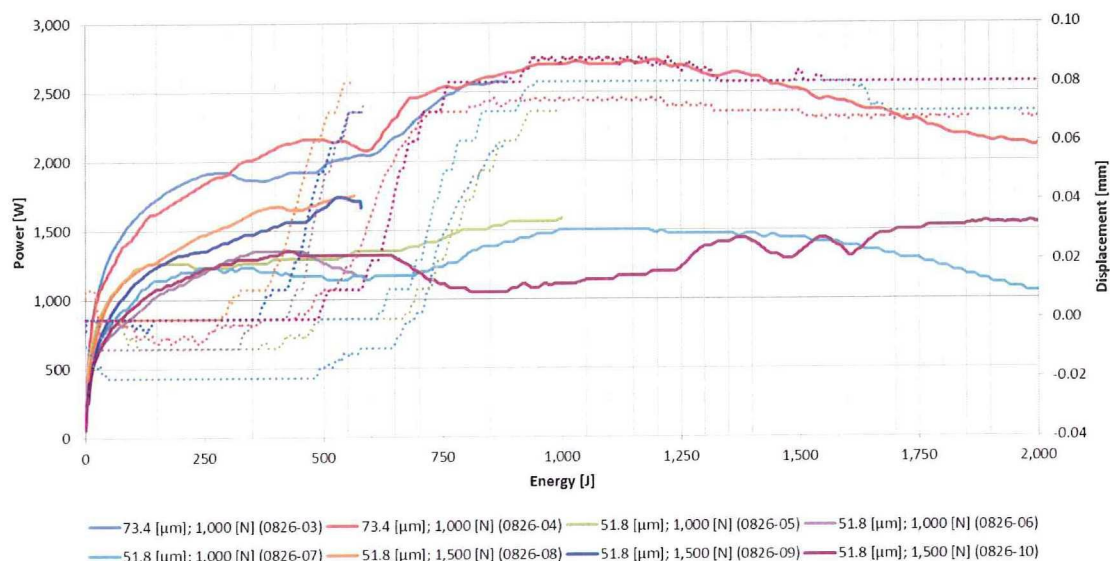


Figure 3-4: Power (solid) and displacement (dotted) plots of sample clips welded with flat square 1 [cm²] EDs with varying welding settings.

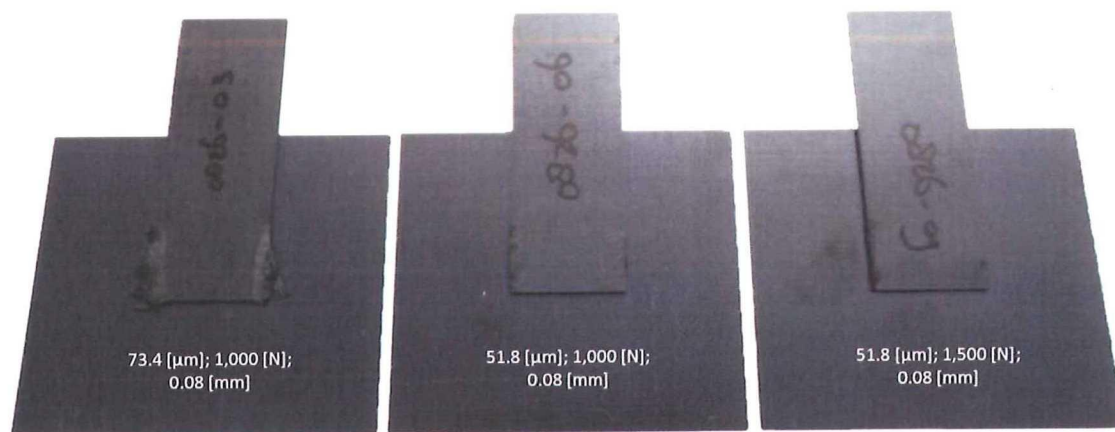


Figure 3-5: Three sample clips welded with flat square 1 [cm²] EDs and a displacement of 0.08 [mm] as the welding driver. All three clips are damaged at the edges, but the damage is visibly reduced for the later samples.

3.2. New energy director concept: flat strips

In the previous section, it was explained how the flat ED concept, as proposed by Villegas (2013a), provided unsatisfactory results when welding sample clips, because a) they were difficult to place, b) the sample clips were

being damaged in an early stage of the USW process, and c) the sonotrode's displacement experienced an abrupt ceiling, making the methodology of Villegas (2013a) inapplicable.

To solve the above mentioned issues, a new ED concept is proposed. This new ED concept implies using slender strips of flat ED (see Figure 3-6). The concept of ED strips is based on Villegas' flat ED and the traditional (triangular) ribs, already widely applied in the plastics industry.

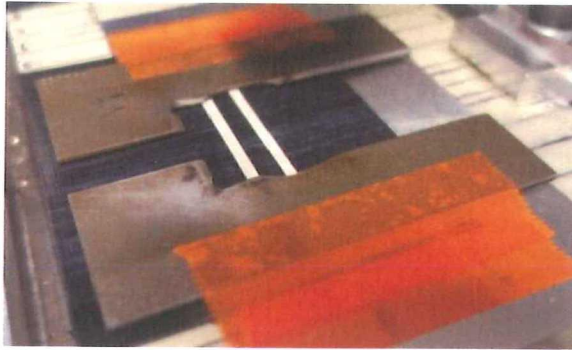


Figure 3-6: Slender ED strips are a new ED concept to weld sample clips. Both the ED strips and the alignment plates are fixed with tape.

The ED strips are expected to offer the following improvements: To begin with, the ED strips can be easily attached to one of the components to be welded by using tape (see Figure 3-6). Moreover, because slender strips offer a high perimeter-to-surface area ratio relative to flat EDs, it is expected that the molten ED will be squeezed out more easily, and hopefully this will result into the disappearance of the displacement ceiling (or at least its appearance at a higher value). Consequently, the displacement might be used as the welding driver again. In addition, the strips have a smaller initial surface area, which results in

the fact that a lower welding force is required to obtain a given welding pressure. Due to the small initial surface area and the high perimeter-to-surface area ratio, it should be easier to squeeze out the melted ED. Hopefully, this leads to a reduction in the damage to the sample clips. Although, the initial surface area covered by the ED strips is lower than when flat EDs are used, it might still be possible to obtain similar size welds. The downside of using ED strips, though, is that it is more complicated to design and manufacture them with respect to flat EDs.



Figure 3-7: Sample clip welded with two ED strips at 2,000 [J].

To determine whether or not ED strips are a good solution, five sample clips are welded with 2,000 [J]. Two strips with a width of 2 [mm] are chosen to approximately match the initial surface area of the square EDs (120 vs. 100 [mm²]). The thickness of the ED strips is still 0.25 [mm] as they are made from the same consolidated PEKK film as used for the flat ED. Moreover, a spacing of 3 [mm] is chosen to give the molten ED enough space to flow, but still allow the flow fronts of the squeeze flow to meet and merge into one weld. The same welding conditions (51.8 [μm]; 1,500 [N]), as those used for the last two sample clips welded with flat square 1 [cm²] EDs are applied, since these provided the best results in that setup. However, instead of using the displacement as the driver, an energy of 2,000 [J] is used. The configuration of the fixture is maintained.

As can be seen in Figure 3-7, the results are very satisfactory. First of all, although 2,000 [J] was used, the sample clips did not show any signs of damage, whereas the ones with square EDs already showed damage at energy levels below 600 [J]. Most likely, the damage is prevented because of the smaller perimeter-to-area ratio in combination with the fact that the strips support the edges of the sample clip that were previously damaged: In case of the square EDs, damage on the clips was found at the left and right edges which were not supported by ED and therefore probably could resonate. It is unknown why the lower edge did not show any damage. An explanation might be that the direction of the outer fibers has an effect on this. Furthermore, it can be seen that at the edges of the sample clip (Figure 3-7) ED has been squeezed out, even between the ED strips, which implies that they most likely merged into one weld. Unfortunately, as can be seen in the displacement curves in Figure 3-8, the displacement ceiling still exists. A positive observation, though, is that the average value of the ceiling

increased from 0.08 [mm] to 0.10 [mm]. This could be a result of the increased perimeter-to-area ratio, but more research is required to investigate this issue.

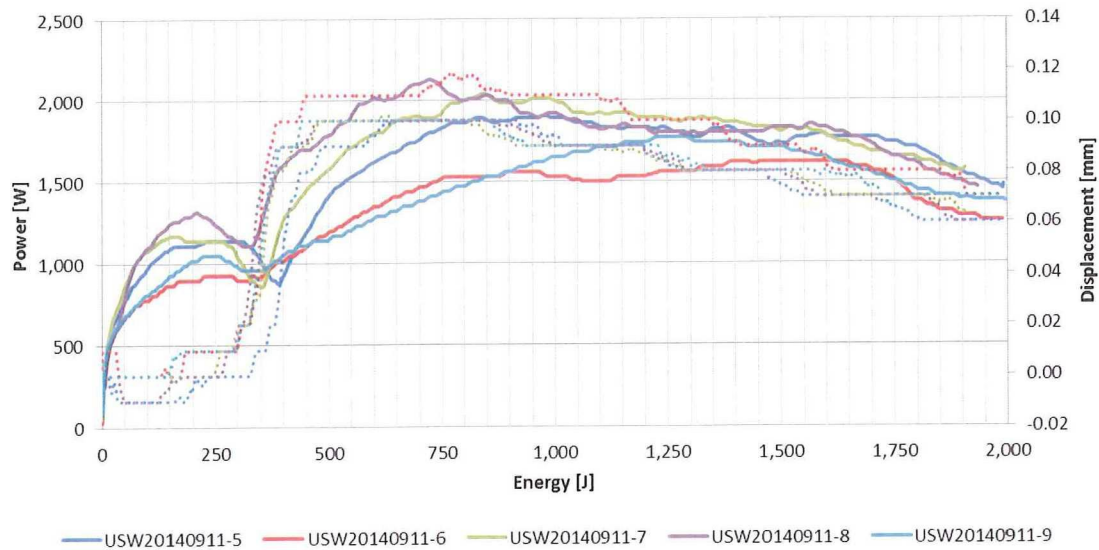


Figure 3-8: Power (solid) and displacement (dotted) plots of five sample clips welded with two ED strips under the same conditions.

3.3. Optimizing the ED strip configuration

In the previous section, it was determined that ED strips provide a better alternative to a flat ED when welding clips. Two ED strips with a width of 2 [mm], a spacing of 3 [mm] and a thickness of 0.25 [mm] were used as the ED configuration. The question remains if the configuration of ED strips can be optimized. In this section, the effects a) the width, b) the number, and c) the spacing between the strips have on the welding data, the weld quality, and damage to the clip are investigated.

Width of strip

First, the effect of the width of the strip on the USW process is investigated. Once again, the sample clip configuration is used. However, instead of two ED strips, only one strip is placed as the total area might otherwise become too large for the wider strips. The ED strip is placed at the center of sonotrode 3. ED strips with a width of 2 [mm], 4 [mm], 6 [mm] and 8 [mm] are used and they are welded with welding forces of 750 [N], 1,500 [N], 2,250 [N] and 2,500 [N], respectively. By applying these welding forces, the same welding pressure (12.5 [MPa]) is obtained as used in the experiments with the sample clips in section 3.2 (but for the last sample). For the last sample, with the 8 [mm] ED, a force of 2,500 [N] (equivalent to 10.4 [MPa]) had to be used instead of the preferred 3,000 [N], since the Rinco Dynamic 3000 'refused' to weld with such a force. Moreover, all samples were welded with a peak-to-peak amplitude of 51.8 [μ m]. Only one sample per configuration was welded, as this number proved to be sufficient to draw the required conclusions.

In Figure 3-9 it is observed that as expected, due to their larger volume, wider ED strips require more energy to melt (recognized by sudden increase in displacement and a valley in the power curve), and also require the use of more power because of probably their larger surface area. Furthermore, the location of the second peak in the power curve is also obtained at higher energy levels as the width increases; still, it should be noted that it is difficult to determine the exact location of the 'second peak' in some of the curves. These observations were anticipated and do not provide new insights. A surprising observation made in Figure 3-9 is the fact that the displacement ceiling is not influenced by the width of the ED strip, which actually means that it is not influenced by the perimeter-to-area ratio. There is variation in the ceiling, but this variation seems random as the strip of 2 [mm] and 8 [mm] have the same ceiling value. Another interesting observation is that the displacement of the

wider ED strips gradually increases in steps, whereas the displacement of the smaller ED strips increases at once. The step-wise squeeze out of the ED is probably caused by the fact that the nucleation and growth of hot spots is random in nature. Due to this randomness, the ED does not heat up uniformly and therefore, it might be squeezed out in steps. A hypothesis is that smaller EDs are less sensitive to this phenomenon as the hot spots are more closely located and therefore the ED heats up more uniformly.

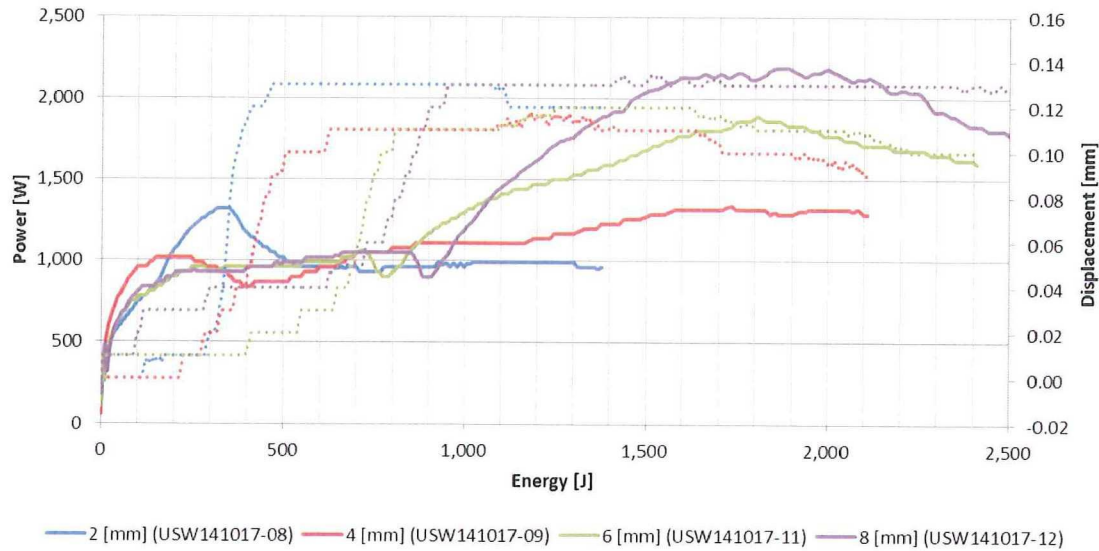


Figure 3-9: Power (solid) and displacement (dotted) plots of sample clips with single ED strips of varying widths.

In Figure 3-10, the resulting welds, ordered by the width of the ED strip, can be seen. It can be observed that none of the sample clips were damaged during the USW process, even though high levels of energy were used. Therefore, the perimeter-to-area ratio might not have as large an effect on the damage as was initially expected after all. Instead, resonations at the left and right edges of the sample clip – which were not supported by the ED when welding with the flat square EDs – were most likely the cause of the damage.

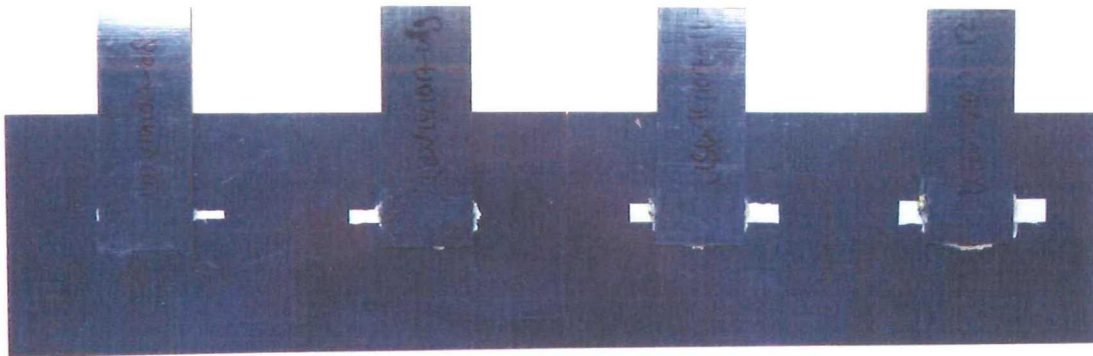


Figure 3-10: The welded sample clips ordered by the width of the ED strip from 2 [mm] to 8 [mm]. None of the sample clips is damaged.

Spacing between strips

Next, the effect of the spacing between the ED strips on the USW process and the welding data is investigated. In addition, the welding data is compared to determine whether or not the event of meeting flow fronts can be observed and if so, what exactly happens. This is important to know when determining the spacing of the EDs. The experiments in this subsection are conducted with the long lap shear samples and the double-side clamping configuration of the Z51414 fixture, as explained in more detail in section 2.3.3. No sample clips were used,

because they were not available at the time of the experiment, and the observations made with the long lap shear samples can also be projected to the sample clips. For the ED, two ED strips with a width of 2 [mm] and a thickness of 0.25 [mm] are used. Between the ED strips there is a gap of 3 [mm] and 12.7 [mm] for the first three and the last three samples, respectively. The lines of symmetry of the ED setup coincide with the center point of sonotrode 3. A welding force of 1,500 [N], which equals a welding pressure of 12.5 [MPa], is used in combination with a peak-to-peak amplitude of 51.8 [μm].

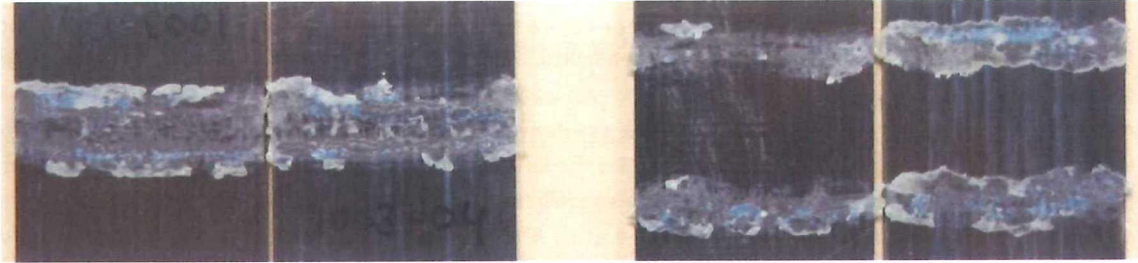


Figure 3-11: Fracture surfaces of sample USW141003-04 (left) with an ED spacing of 3 [mm] and welded with 750 [J] and sample USW141010-07 (right) with an ED spacing of 12.7 [mm] and welded with 1,000 [J]. In case of the left sample, the flow fronts have met.

Figure 3-11 displays the fracture surfaces of a sample where the two ED strips have a gap of 3 [mm] (left) and those of a sample where the two ED strips have a gap of 12.7 [mm] (right). It can be observed that the flow fronts met in the sample welded with 750 [J] and where the ED strips are 3 [mm] apart, whereas in case of the sample welded with 1,000 [J] and where the ED strips are 12.7 [mm] apart, the flow fronts did not meet.

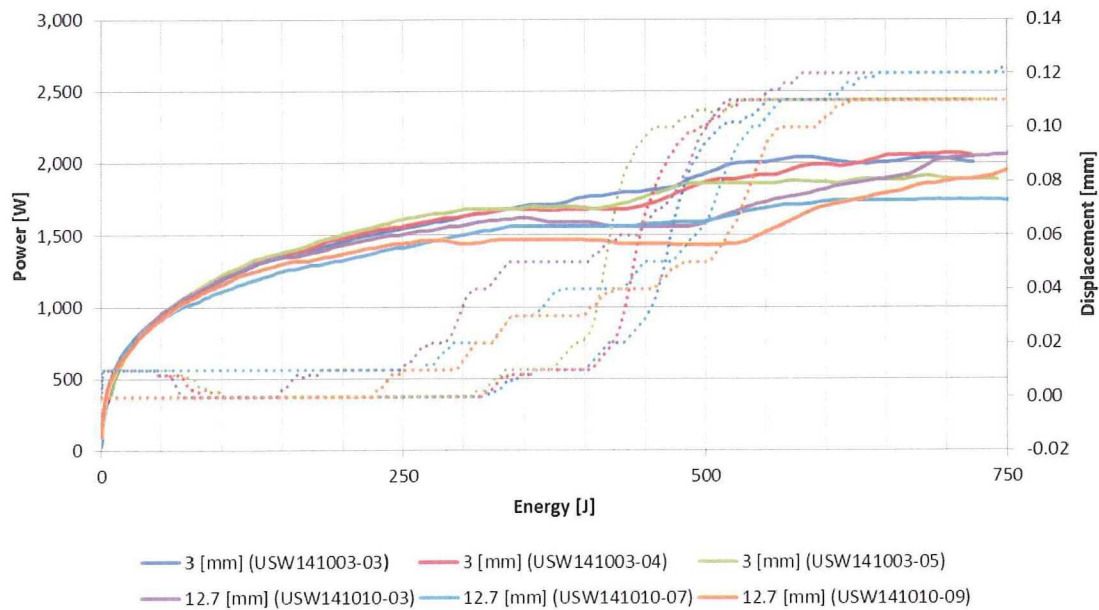


Figure 3-12: Power (solid) and displacement (dotted) plots of samples clamped at both sides with an ED spacing of either 3 [mm] or 12.7 [mm]. The displacement ceiling is similar for both ED configurations.

The power and displacement plots of the six samples are presented in Figure 3-12. The curves of the samples with an ED spacing of 3 [mm] are quite similar to the ones of the samples with an ED spacing of 12.7 [mm]: a) the power curves follow a similar trend; b) the displacement ceiling is reached at approximately the same energy level; and c) the ceiling has roughly the same value. However, the sudden increase in displacement, which occurs when the ED melted, shows a different pattern for the samples with 3 [mm] spacing than for the ones with 12.7 [mm] spacing: whereas the first occur at once, the latter ones have a step-wise evolution. This is actually similar to what could be observed in the previous section, where the wider ED strips also showed a step-wise increase

of displacement in contrast to the smaller ED strips. For that case, the hypothesis was established that the random nature of nucleation and growth of hot spots causes the ED to be squeezed out in steps as the ED does not melt uniformly. Moreover, it was expected that small ED strips would be less sensitive to this phenomenon as the hot spots are closely located. That explanation does not make sense in this situation, though, since two small strips are used. The only difference between the two configurations is the spacing between the ED strips. It is certain that the meeting flow fronts are not the cause, since the samples with the widely spaced EDs are the ones that experience a step-wise increase of displacement. In Figure A-1 an overview of the cross-sections of sample clips welded with various amounts of energy can be seen. These sample clips were also welded with two ED strips, and in the cross-sections of the samples welded with 300 [J] (Figure 3-13) and 400 [J], it can be observed that only one of the two EDs did melt. Measurements were performed on all cross-sections using the optical microscope's software and it was noticed that the gap between the two substrate composites was consistently larger on the right of the welding interface than on the left (258.1 [μm] vs. 225.8 [μm] in Figure 3-13). This is probably caused by a small misalignment of the sonotrode. Because of this misalignment, more pressure is exerted on one of the EDs than on the other and as a result, the first ED will heat up more effectively. Misalignment of the sonotrode would create a larger difference between widely spaced ED strips than between closely spaced ED strips, because the vertical offset is larger for the widely spaced. (Note that the samples with the 3 [mm] space EDs show a very small step increase). The hypothesis is established that: due to a misaligned sonotrode, one of the ED strips melts before the other one does. Subsequently, as the first ED strip has melted, it is squeezed out and the sonotrode drops until it is stopped by the second ED strip; this translates into the first step in the displacement curves.



Figure 3-13: Cross-section of the welding interface of a sample clip welded with 300 [J]. The left ED has melted, whereas the second one has not. The gap is 225.8 [μm] on the left side, whereas it is 258.1 [μm] on the right.

Experiments, in which the alignment of the sonotrode is changed, in combination with cross-sectional microscopy on the resulting samples, should be performed in order to confirm the hypothesis.

Benatar & Gutowski (1989), who welded CF/ PEEK composites with traditional EDs, concluded that the mechanical impedance quickly rises when the flow fronts meet. From Figure 3-12 it is unclear if the meeting flow fronts in the samples with the 3 [mm] ED spacing have any effect on the USW process as there are no apparent differences between the curves in addition to the step-wise increase in displacement. The power curves of the samples with the proximate EDs record slightly higher values than the others, but this might as well be a coincidence as this trend is already observed before the EDs have melted and the flow fronts could possibly meet. More research is required to investigate the effect of meeting flow fronts on the USW process when welding with ED strips. A starting point for additional experiments would be to reduce the spacing between the ED strips to, for instance, 1 [mm].

Preferred energy director configuration

The question remains which ED configuration is preferable: one wide ED strip or multiple small ED strips. The proposal surfacing from the performed experiments consists in using a setup with multiple small EDs, because equal sized welds can be obtained by using less ED. The utilization of less ED translates into less force being required to obtain a certain welding pressure, and also – as could be observed in Figure 3-9 – less power and energy being needed. A lower power requirement, possibly allows larger welds to be made. Regarding the spacing between EDs, it was observed that it is better to have proximately spaced ED strips, as this setup is probably less sensitive to misalignments in the setup. Moreover, by placing ED strips with a spacing of 3 [mm], the squeeze flows manage to merge into one weld. Therefore, an ED configuration of the two ED strips with a width of 2 [mm] and a spacing of 3 [mm] will be used again in the upcoming experiments.

3.4. Conclusions

In this chapter, an ED configuration for the welding of clips has been selected. Experiments pointed out that plunge-welded flat square EDs do not provide satisfactory results when welding clips, because: a) they were difficult to place, b) damage occurred in the clips, and c) an abrupt ceiling in the displacement was observed, which prevents the use of displacement as the welding driver, making the methodology of Villegas (2013a) inapplicable.

A new ED concept was introduced, which implies using (multiple) slender PEKK strips as EDs. These strips were manufactured by simply slicing flat EDs. Experiments indicated that a) the strips were easier to place, because they could be taped to the lower substrate composite, and b) no more damage occurred in the clips. However, the displacement ceiling was still present, with the improvement that the values at which it occurred were slightly higher than before.

Several experiments were conducted to investigate the effect of the ED strip configuration on the USW process and the related welding data: the width of the strips, and the spacing between the strips was varied. Based on the results, it was proposed to use multiple small strips instead of one wide strip, because a weld of similar size can be obtained while using less power, time, and thus, energy. Moreover, a lower welding force needs to be applied to obtain a certain welding pressure, due to the smaller initial surface area of the ED. Furthermore, it was observed that closely spaced ED strips are able to merge into one large weld, and are also – most likely – less sensitive to misalignments in the setup. As a result, it was proposed to use two ED strips with a width of 2 [mm] and a spacing of 3 [mm] to weld the CF/ PEKK clips.

The limitations of the research presented in this chapter consist in: a) the number of samples, and b) the range of performed analyses. Cross-sectional microscopy was applied only to a limited extent, and no fractography was performed at all. However, the experiments are sufficient to conclude that the new ED concept represents a better alternative to the flat ED when welding clips. Therefore, the new ED concept is used from this point onwards. Parameters whose effect on the USW process should be investigated in future research are: the thickness and the crystallinity of the PEKK ED.

4. Squeeze Flow & Weld Quality Development

In this chapter, 1) the squeeze flow of molten ED and 2) the development of the weld quality as a function of the welding energy are studied. Moreover, an effort is made to answer the question: why is there a ceiling observed in the displacement curves at approximately 0.11 [mm]? In section 4.1, the results of the experimental techniques applied and the various stages of the welding process are described. Next, in section 4.2, a validation set is tested and analyzed. Finally, in section 4.3, the conclusions are presented.

4.1. Analysis of various stages in the welding process

In this section, the relation between the energy used during welding and the squeeze flow of molten ED and the weld quality, respectively, is investigated. The goal is to understand what happens at the various stages of the USW process, so that the weld quality can be optimized. Of equal interest is the understanding of what the source of the abrupt displacement ceiling is, so that this phenomenon can be properly corrected.

All experiments in this section are conducted with sample clips and the Z51414 fixture in the corresponding configuration as described in section 2.3.1. As ED, two ED strips with a width of 2 [mm], a thickness of 0.25 [mm] and a spacing of 3 [mm] are used, as proposed in section 3.3. The lines of symmetry of the ED setup coincide with the center point of the $\varnothing 40$ [mm] sonotrode. Furthermore, all sample clips are welded with a force of 1,500 [N], equal to a welding pressure of 12.5 [MPa], and a peak-to-peak amplitude of 51.8 [μm]. In order to investigate what happens at the various stages of the USW process, the energy is varied between 300 [J] and 2,000 [J]. Figure 4-1 illustrates that this range covers all relevant stages of the USW process.

The welded samples are studied using the various experimental techniques, which are described in section 2.4. First, in section 4.1.1, the welding data is presented and theoretical optimal energy level is determined. Next, in section 4.1.2, the LSS results are analyzed. Subsequently, in section 4.1.3, the fracture surfaces are examined. Then, in section 4.1.4, the cross-sections are studied using microscopy. Next, the NDT results are examined in section 4.1.5. Finally, in section 4.1.6, the welding data is analyzed in more detail and related to observations in the preceding sections.

4.1.1. Welding data

In this section, five sample clips are welded under the same conditions with 2,000 [J]. The welding data of these clips can be observed in Figure 4-1.

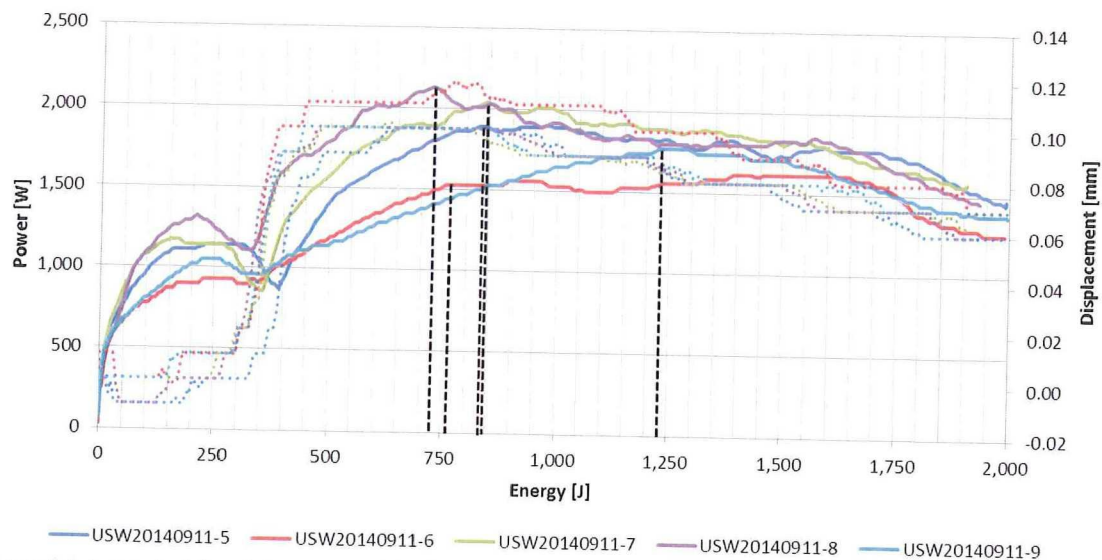


Figure 4-1: Power (solid) and displacement (dots) plots of five sample clips welded under the same conditions with 2,000 [J]. The black dashed lines indicate the location of the second peak. The location of the second peak of sample clip USW140911-09 is off from the locations of the others.

Villegas (2013a) explained that a weld is optimal at the moment the second peak in the power curve is reached, because after this point the substrate composites melt. The locations of the second peaks in the power curves are indicated by black dashed lines. It can be observed that the four leftmost peaks are reasonably close to each other and range between 720 [J] and 840 [J]. The second peak of the fifth weld, however, is located at a deviating value of 1,230 [J]. The analyses presented in the following sections, suggest that this value can be disregarded, since the displacement is already reducing for a while: a reduction in displacement after the ceiling has been reached, most likely, indicates the formation of voids as a result of material degradation.

4.1.2. LSS results

In this section, the LSS results are analyzed. The sample clips are tested by means of static single lap shear tests performed with a 100 [kN] Zwick/Roell universal testing machine, as described in more detail in section 2.4. The results can be seen in Figure 4-2, where both the tensile force values at which the welds broke and the resulting LSS values are presented. The LSS values are simply calculated by dividing the tensile force values by the surface areas of the fractures. The surface area values of the fractures were determined using the software ImageJ. It should be noted that only one sample was tested per data point. Although, a clear trend is observed, it is unknown how large the variation in this trend is and whether or not the optimum is always located at the same location.

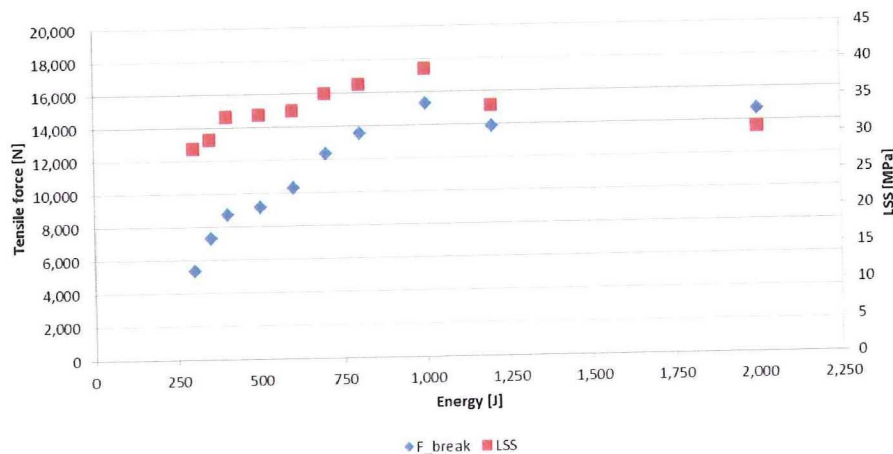


Figure 4-2: The tensile breaking force and associated LSS for sample clips welded with different amounts of energy.

In Figure 4-2, it can be observed that the tensile force increases almost linearly until 1,000 [J] where a maximum seems to have been reached. After this point, the tensile force is more or less stable. However, it can be expected that if more and more energy is added, the breaking force will eventually decrease as the material being welded deteriorates.

When the LSS is considered, it can be seen that it follows a similar linear trend up to 1,000 [J]. However, the slope of the LSS trend is less steep. This is due to the fact that the LSS is expressed as the strength per unit area. The fact that the LSS increases, but at a lower slope than the tensile force, implies that the joint becomes stronger as a result of both an increase in the welded area (squeeze out of ED) and a stronger bond per unit area (in the next section (4.1.3), it is observed that at some point first ply failure and/ or cohesive failure occur instead of the inferior adhesive failure). After 1,000 [J], the LSS drops, which implies that the material is probably degrading. It is interesting to note that at 1,000 [J], the power curves already go down for a while, so the optimum in terms of the point where the substrate composites start melting does not correspond with the optimum in terms of strength. It should be noted that the LSS values observed for the clips are considerably lower than the ones obtained for the reference samples in section 3.1, which had a value of 47.0 [MPa] on average. A possible explanation for this is that the ED near the flow fronts did not form a proper bond yet with the substrate material. This hypothesis is confirmed with cross-sectional microscopy in Figure 4-24.

4.1.3. Fractography

In this section, the fracture surfaces, which result from the tensile tests described in the previous section, are analyzed using optical microscopy. An overview of the fracture surfaces, ranked according to the amount of energy used, is presented in Figure 4-3. Fracture surfaces can be used to study: 1) the squeeze flow of molten ED, 2) the state of the material at the welding interface, and 3) the failure modes in the various stages of the USW process.



Figure 4-3: Fracture surfaces of sample clips in the order of the amount of energy used to weld. The two molten ED strips are merged between 700 [J] and 800 [J] and become one weld.

From the development of the fracture surfaces in Figure 4-3, it can be derived that the flow fronts of the two ED strips already meet at approximately 600 [J], but become one weld somewhere between 700 [J] and 800 [J]. When studying the associated welding curves (Figure 4-36), it can be observed that around the value where the flow fronts meet, the second peak in the power curve and a reduction in the displacement occur. However, this is most likely just a coincidence, as these phenomena were also seen in situations where there were no meeting flow fronts (Figure 3-9). After the two EDs have merged, the molten ED is further being squeezed out, as illustrated by the fracture surface area that keeps increasing. In the previous section, it was observed that the strength of the bond per unit area (LSS) decreases after 1,000 [J] and it was reasoned that the material at the welding interface was degrading. The fracture surfaces confirm this, since the fracture surface of the 800 [J] sample already shows the first voids (see Figure 4-4) and the fracture surface of the 2,000 [J] sample (see Figure 4-5) even displays brownish burn marks in addition to the voids. Next, optical microscopy, of which the equipment and procedure are explained in section 2.4, is applied in order to study particular areas of the fracture surfaces in more detail.

At approximately 400 [J], the EDs have melted and start to flow, as confirmed by the increase in displacement (see Figure 4-36). In Figure 4-6, it can be observed that at 400 [J] the flow fronts are almost meeting each other: they are now less than 1 [mm] apart, while the initial spacing between the EDs was 3 [mm]. In the middle of the flow fronts, the unaffected composite substrate can be observed. The substrate appears to be white as the surface is smooth and reflects light from the microscope. The black lines are carbon fibers. Interestingly, it looks like these fibers can still be observed underneath part of the squeeze flow as they continue, as illustrated in Figure 4-7. SEM microscopy should confirm this, though, by proving that these lines are not fiber imprints. If it is indeed light reflecting from the substrate material below the squeeze flow, then it can be concluded that the

squeeze flow is transparent and the PEKK ED thus became amorphous. Moreover, in case the squeeze flow is transparent and light is reflecting from the substrate below it, there is probably no, or at least a very poor bond, between the squeeze flow and the substrate composite. This hypothesis is supported by the fact that cross-section microscopy pictures show very thin gaps near the flow front between the squeeze flow and the substrate composites (e.g. Figure 4-23 and Figure 4-24). It would also not be surprising to observe a poor bond between the squeeze flow and the substrate composite near the flow front at 400 [J]. At this point, the substrate material is most likely still far below melting temperature, as the ED has just been squeezed out.

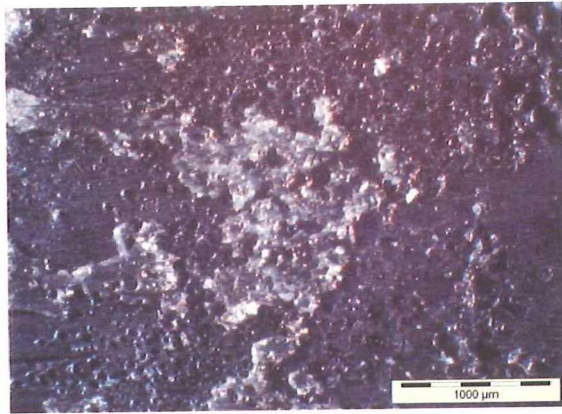


Figure 4-4: The presence of numerous voids at the welding interface indicates that PEKK started to degrade in a sample clip welded at 800 [J].

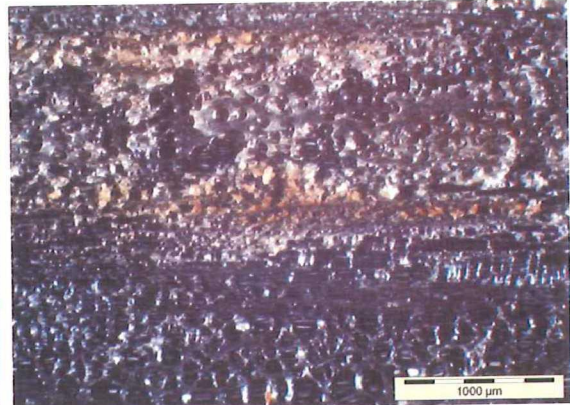


Figure 4-5: Clear signs of burned PEKK and countless voids at the welding interface of a sample clip welded at 2,000 [J].

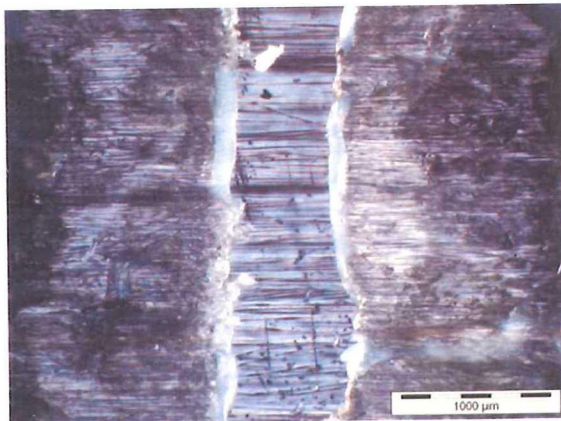


Figure 4-6: Flow fronts almost meeting each other in sample clip welded at 400 [J]. Reflecting light underneath the squeeze flow probably indicates that the ED became amorphous, and possibly that a poor or no bond has formed. The flow fronts light up due to the external cold light sources used.

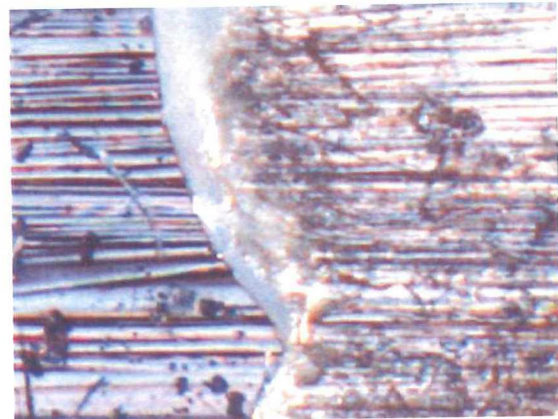


Figure 4-7: The fibers observed in the unaffected substrate seem to continue underneath the squeeze flow of ED. SEM microscopy should confirm that these lines are not fiber imprints in the squeeze flow, though.

In Figure 4-3, it could be observed that the flow fronts start meeting at around 600 [J] and become one weld somewhere between 700 [J] and 800 [J]. In Figure 4-8 and Figure 4-9, microscopy panoramas of the meeting flow fronts at 700 [J] and 800 [J] are presented, respectively. In the panorama of the 700 [J] weld, one flow front is still visible, which is a clear sign that the two flow fronts did not merge yet. It is expected that the other flow front is still attached to the sample's counterpart. Moreover, it can be observed that there is probably no or at least a poor bond at the centerline of the two ED strips, since the substrate composite is unaffected as indicated by the reflection of light from the substrate (white section). In contrast, at 800 [J] no flow fronts are visible anymore. In addition, most of the unaffected area at the centerline of the EDs disappeared. Therefore, it can be concluded that the two squeeze flows merged into one big squeeze flow and formed a proper bond with the substrate composite. Another interesting observation derived from both panoramas is that, near the edge of the sample clip (on the right), the whole area between the EDs is unaffected and it appears that no squeeze flow

whatsoever has been present. This phenomenon is most likely caused by the fact that the squeeze flow, after having found the path of least resistance, proceeds to flowing outside the welding interface. The flow directions are indicated with red arrows in the two figures.

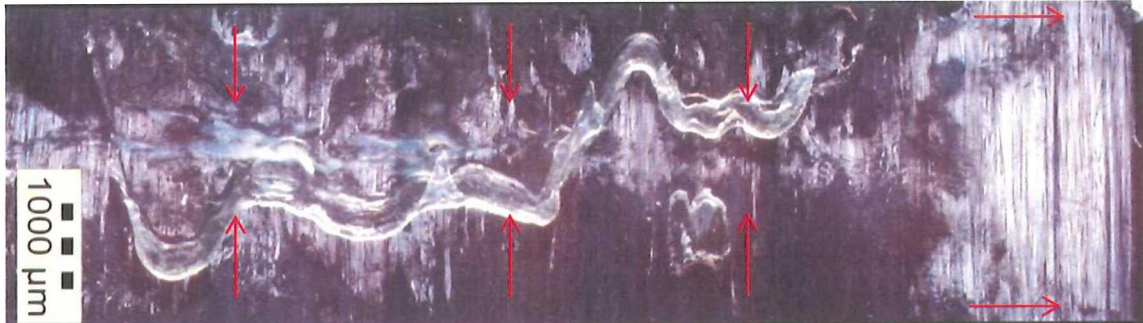


Figure 4-8: Merging flow fronts in a sample clip welded at 700 [J]. The reflection of light (white section) indicates that there was probably no or a weak bond at the centerline. Flow directions are indicated with the red arrows.



Figure 4-9: Merged flow fronts in a sample clip welded at 800 [J]. Flow directions are indicated with the red arrows.

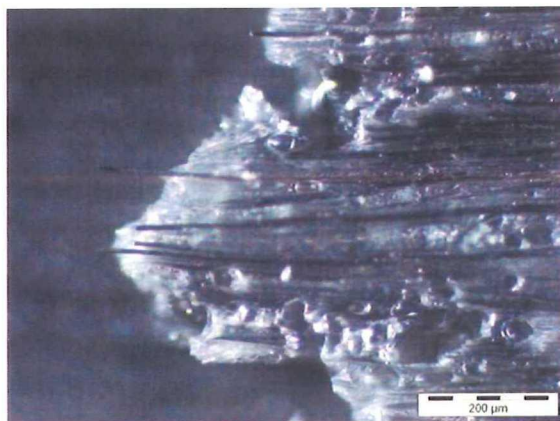


Figure 4-10: First ply failure at fracture surface of sample clip welded at 600 [J]. Fibers stick out of broken lamina.

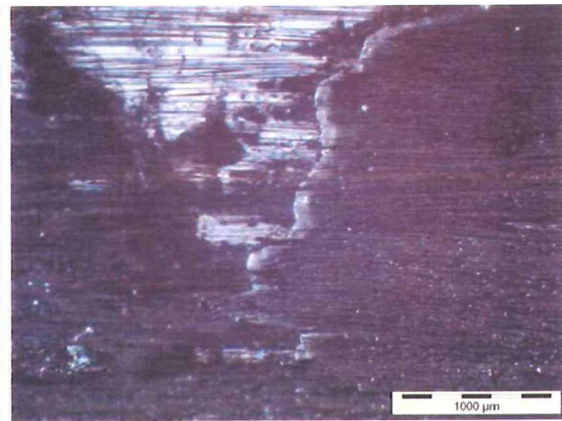


Figure 4-11: First ply failure at fracture surface of sample clip welded at 700 [J]. Fibers stick out of broken lamina.

In Figure 4-10 and Figure 4-11, it can be observed that some sections of the sample clips welded at 600 [J] and 700 [J] show signs of first ply failure, because a piece of lamina from the composite 'skin' is still attached to the sample clip. They are clearly pieces of lamina as fibers are sticking out. This observation is a good sign: first ply failure is preferred over adhesive failure due to former's higher strength. In case of adhesive failure, the squeeze flow of ED is simply ripped off the substrate material.

In the previous section, it was observed that a) the strength per unit area (LSS) decreases after 1,000 [J] and in Figure 4-3 it was observed that b) the fracture surfaces of the 1,200 [J] and 2,000 [J] sample clips contain many voids, with the latter displaying even burn marks. However, when using the microscope, large numbers of voids

can already be identified on the fracture surface of the 800 [J] sample, as can be seen in Figure 4-4. A hypothesis is that these voids are created by gasses that are released when the material deteriorates as a result of being overheated. When welding with higher energy levels, these gasses can be smelled during the USW process. The fact that the material already deteriorates at 800 [J] means that it is probably better to weld the sample clips at an energy level lower than 800 [J], which is in agreement with optimal energy level of 720 [J] defined in section 4.1.1. However, the LSS is still increasing, as observed in Figure 4-2.

4.1.4. Cross-section microscopy

In this section, the cross-sections of the sample clips are analyzed using optical microscopy.

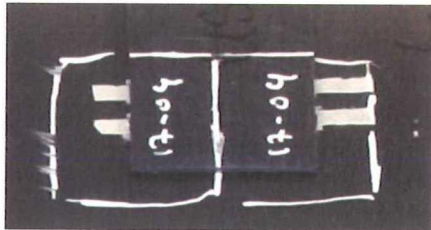


Figure 4-12: Two cross-sections are obtained from one sample clip.

Two cross-sections near the center of the weld are obtained per sample clip as the samples are sawn in half. The cross-sections offer a point-of-view perpendicular to the main squeeze flow direction. The white lines in Figure 4-12 indicate how the specimens are sawn. Because the samples have to be sawn, sanded and polished, there is a small offset – in the order of 1-2 [mm] – between the two cross-sections. Details about the potting, sanding, and polishing procedures are provided in section 2.4. The cross-sections are used to study 1) the

development of the squeeze flow, 2) the quality of the ED and the composites, and 3) the state of the material as reflected by the thickness of the composites. Moreover, the cross-sections are investigated to find a possible explanation for the cause of the abrupt displacement ceiling.

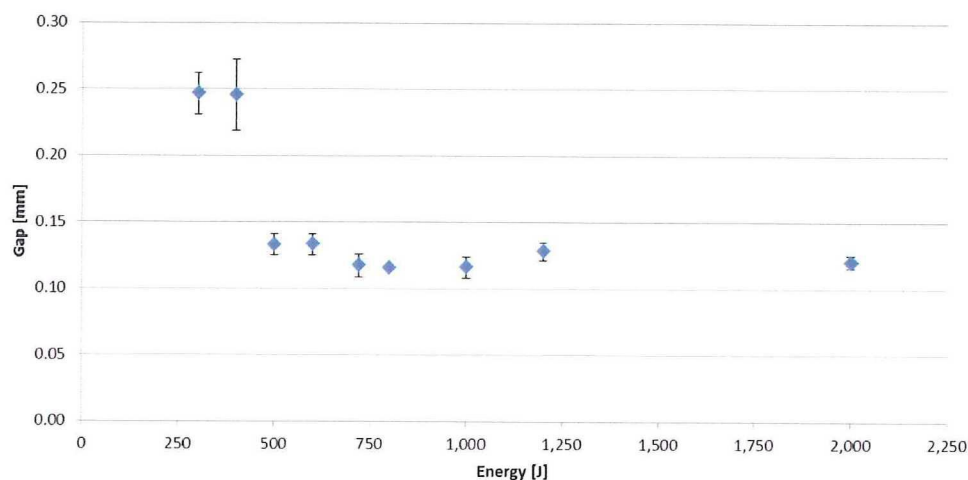


Figure 4-13: Development of the gap between the composite substrates measured in the cross-section micrographs at the locations of the flow fronts of the squeezed-out ED. The dots represent the average value and the error bars represent the standard deviation. Just one sample has been studied per data point. Four measurements per sample have been done.

The cross-sectional microscopy pictures are used to measure the distance between the two composite parts. The measurements are taken at the locations of the flow fronts and therefore, there are four measurements per sample clip. The average values and the standard deviations are illustrated in Figure 4-13. It can be observed that the gap starts at approximately 0.25 [mm], which is the original thickness of the ED strips. Then, somewhere between 400 [J] and 500 [J], the gap suddenly decreases by roughly 0.12 [mm] to 0.13 [mm], which corresponds exactly to the displacement ceiling observed in the welding data. The gap stays constant at 0.12 [mm]. Even at the high energy level of 2,000 [J], it does not seem to become smaller. The question remains why.

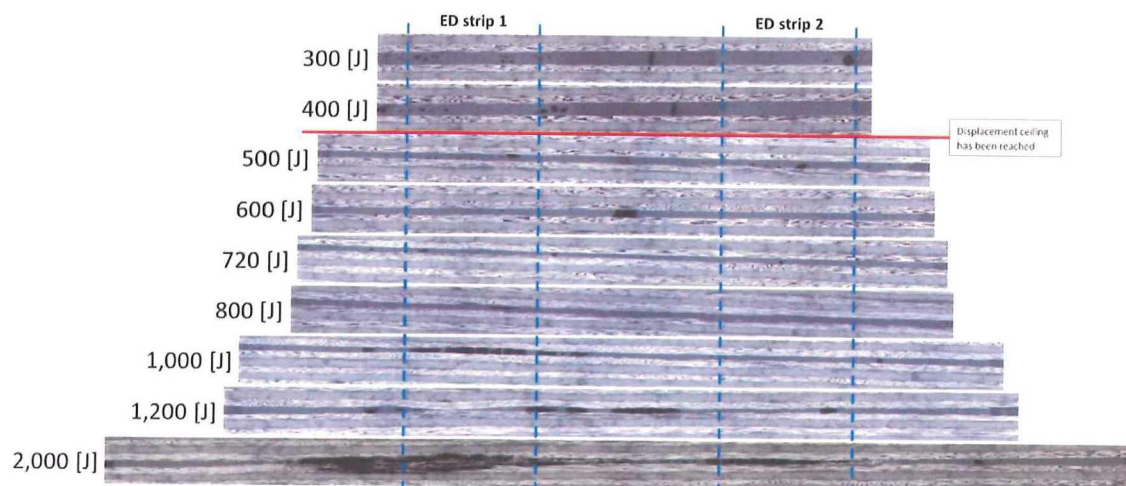


Figure 4-14: Overview of cross-section microscopy panoramas of sample clips' welding interfaces ordered by the amount of energy used during welding. The red solid line indicates the moment after the abrupt increase in displacement and the dashed blue lines indicate the initial size and position of the ED strips.

In Figure 4-14, an overview of the squeeze flows at the sample clips' welding interface can be seen. A large A3 version of this figure can be found in Figure A-1. In the overview, the initial positions of the two ED strips are indicated with the dashed blue lines. Furthermore, the moment at which the molten EDs are squeezed out and the displacement ceiling has been reached is indicated with a solid red line. The total width of the weld is indicated by the width of the cross-section micrograph.

In the overview, it can be observed that between 400 [J] and 500 [J], the thickness of the squeeze flow indeed decreases from 0.25 [mm] to the 0.13 [mm]. As a result, the total area covered by the ED increases by approximately, a factor 2. Between 500 [J] and 2,000 [J], the thickness of the squeeze flow at the flow fronts does not decrease any further as it was already observed in Figure 4-13. However, the area covered by the molten ED does increase. A likely explanation for this phenomenon is that the flow fronts are being pushed outwards by material in the center of the weld, and therefore are not really being squeezed anymore. This hypothesis is supported by the fact that the cross-sections of the 1,000 [J] to 2,000 [J] samples show that fibers from the outer plies are being squeezed into the molten ED at the welding interface (see Figure 4-14 or Figure A-1). Moreover, because the material at the center and/ or original location of the EDs starts to degrade as a result of overheating, gasses originate. This can be concluded from the high populations of voids. These gasses could also have a major role in pushing the squeeze flow out. Thermal expansion is another possible explanation for the fact that while the length of the squeeze flow increases, the thickness remains constant. Due to thermal expansion, the volume of the squeeze flow increases. As a result, since the ED thickness is constant, the area and in this case also the length of the squeeze flow have to increase. Most likely, a combination of these hypotheses explains the phenomenon. The question remains why the flow fronts are not being squeezed out any further and maintain their thickness of approximately 0.11 [mm]. In order to find an answer to this question, further enlarged microscopy images are studied next.

First, the flow fronts of the sample clip welded at 500 [J] are studied, because this sample is the first to experience the displacement ceiling. Three flow fronts of the sample clip welded at 500 [J] can be seen in Figure 4-15 and Figure 4-16. In the first figure, a flow front at the outer edge can be observed, whereas in the latter figure, two flow fronts that almost meet at the center are present. Interestingly, the flow fronts seem to consist of pieces of PEKK that have never melted, an insight derived from the fact that they retained a rectangular shape. This explains why the displacement ceiling is so abrupt: when the ED has almost fully melted and is rapidly being squeezed out, the movement of the sonotrode is suddenly blocked by solid particles of PEKK. Now, the following questions arise: 1) why does the ceiling always occur at approximately 0.12 [mm]? And 2) why does the PEKK not remelt, so that the squeeze flow can continue?

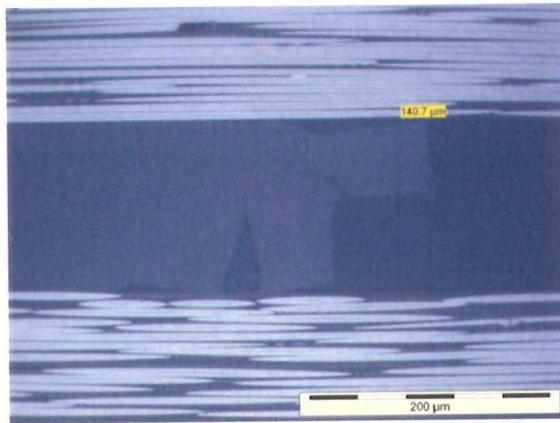


Figure 4-15: Flow front of ED at the welding interface of a sample clip welded with 500 [J]. There are small pieces of PEKK that have not been in a molten state as they retained a rectangular shape.

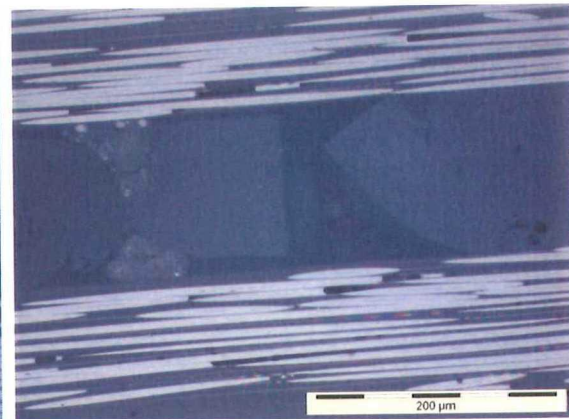


Figure 4-16: Meeting flow fronts of ED at the welding interface of a sample clip welded with 500 [J]. It can be observed that the molten squeeze flow on the left pushes a piece of unmelted ED forward.

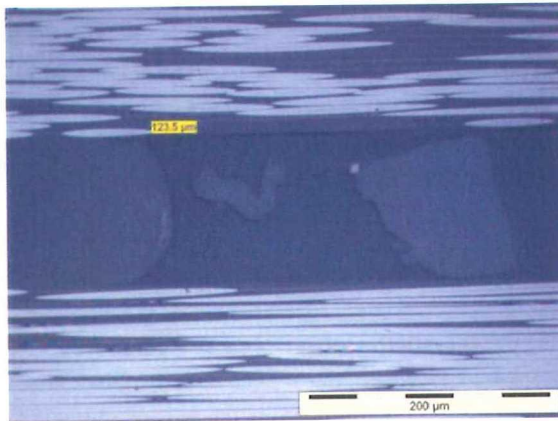


Figure 4-17: Squeeze flow of ED at the welding interface of a sample clip welded with 1,200 [J]. Even at the higher amounts of energy there are still pieces of PEKK ED which have not been in a molten state.

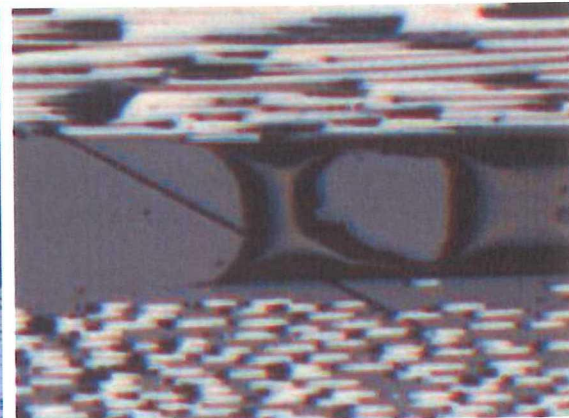


Figure 4-18: Squeeze flow of ED at the welding interface of a sample clip welded with 2,000 [J]. Still pieces of PEKK ED which have not been in a molten state are observed.

In Figure 4-17 and Figure 4-18, it can be observed that even at higher energy levels of 1,200 [J] and 2,000 [J], respectively, there are still pieces of unmelted ED present near the flow front.

A study of the partly molten flow fronts, at the stage where the ED has not been squeezed out yet, provides a valuable insight into why some pieces of ED are not melted at the moment of the squeeze out. In Figure 4-19 and Figure 4-20, the partly molten flow fronts of sample clips welded with 300 [J] and 400 [J], respectively, can be seen. In these figures, it can be observed that the ED does not melt uniformly. Instead, there seem to be layers in the ED that melt separately. These layers are actually the original 50 [μm] PEKK films from which the ED is manufactured as can be seen in Figure 4-21 and Figure 4-22. In Figure 4-21, an unmelted ED strip between the welding interfaces of a sample clip welded with 300 [J] can be observed. Using UV light, the boundaries between the original 50 [μm] PEKK films are revealed. The fact that the boundaries are still visible implies that the 5 PEKK films did not really consolidate into one layer of PEKK. This finding explains why the ED melts in layers, as could be observed in Figure 4-19 and Figure 4-20. In Figure 4-22, a SEM image of the fracture surface of a piece of unused ED can be seen. Again, a clear boundary between the 50 [μm] PEKK films is observed.

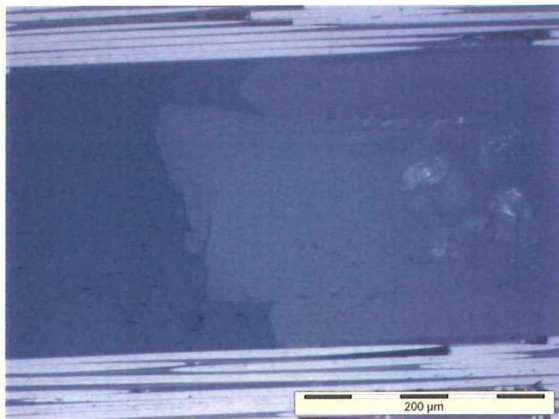


Figure 4-19: Squeeze flow of ED at the welding interface of a sample clip welded with 300 [J]. Only the two outer layers of PEKK film have been in a molten state. No bond between the squeezed out ED and the substrate composite has been formed near the flow front.

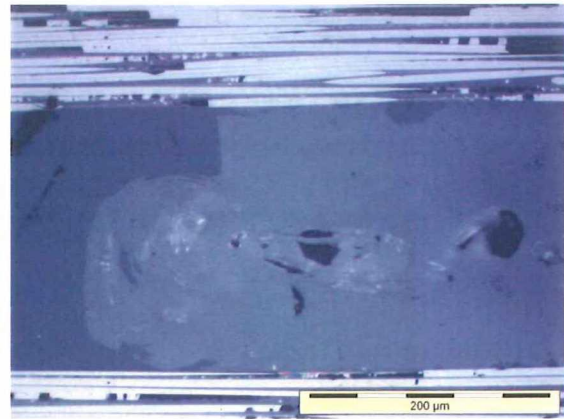


Figure 4-20: Squeeze flow of ED at the welding interface of a sample clip welded with 400 [J]. Only the lower layers of PEKK film have been in a molten state.

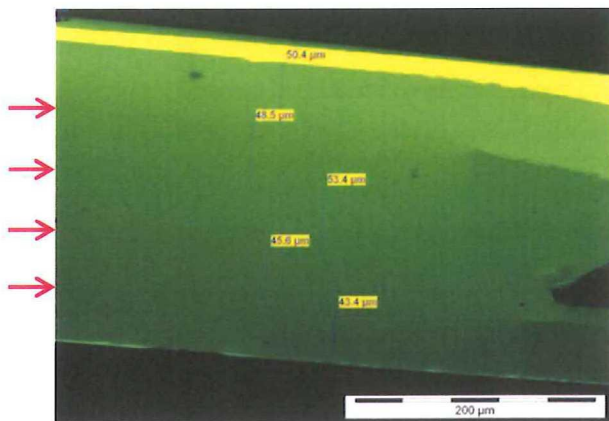


Figure 4-21: Cross-section micrograph with UV light of unmelted ED in a sample clip welded at 300 [J]. Separation between 50 [μm] PEKK films, as indicated by red arrows, can be observed.

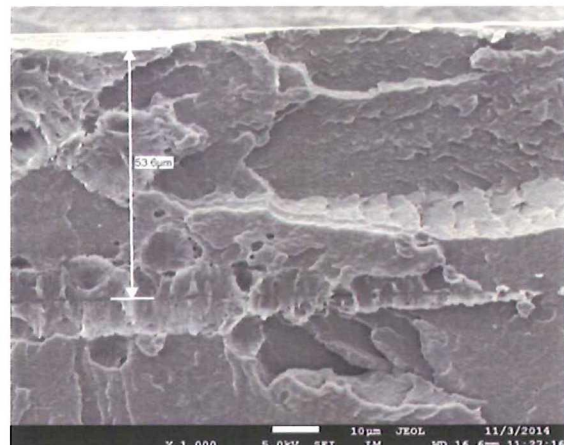


Figure 4-22: SEM scan of fracture surface of unused ED manufactured of 5 layers of 50 [μm] PEKK film. Separation between first and second film can be observed.

In Figure 4-23, a piece of ED that has not been in a molten state at the flow front of a sample welded at 720 [J] can be observed. Again, UV light is used to reveal the boundary between the original PEKK films. It can be seen that the piece of PEKK consists of two 50 [μm] PEKK films. A study of the other flow fronts with the use of UV light indicated that all pieces of unmelted ED consist of at most two films. This observation is in line with the fact that the gap is always around 0.13 [mm], because the gap allows a maximum of two films.

A hypothesis to explain these observations can be formulated as: because the PEKK ED does not melt uniformly, there are still unmelted pieces of ED left when the rest of the ED is being squeezed out. These pieces, most likely, remain unmelted due to nonuniform heating of the ED. These pieces block the displacement of the sonotrode and cause the abrupt displacement ceiling. At this point, sections of the squeeze flow, which are in contact with the colder substrate material, solidify again and prevent further squeeze out. This can be witnessed in Figure 4-24, where it is seen that the squeeze flow has no proper bond with the substrate composite, as there is a clear crack in between. However, at some point, it is expected that the solidified flow front will re-melt due to interfacial friction and bond properly with the substrate composite as well. At the same time, the material at the center of the squeeze flow of ED, which is already bonded to the substrate, continues to heat up due to viscoelastic heating. Phenomena such as thermal expansion of the material and the formation of gasses in both ED and the substrate material push the flow fronts outwards. The gap between the composites remains constant

as there are always pieces of unmelted ED present at the flow fronts that block the displacement of the sonotrode.

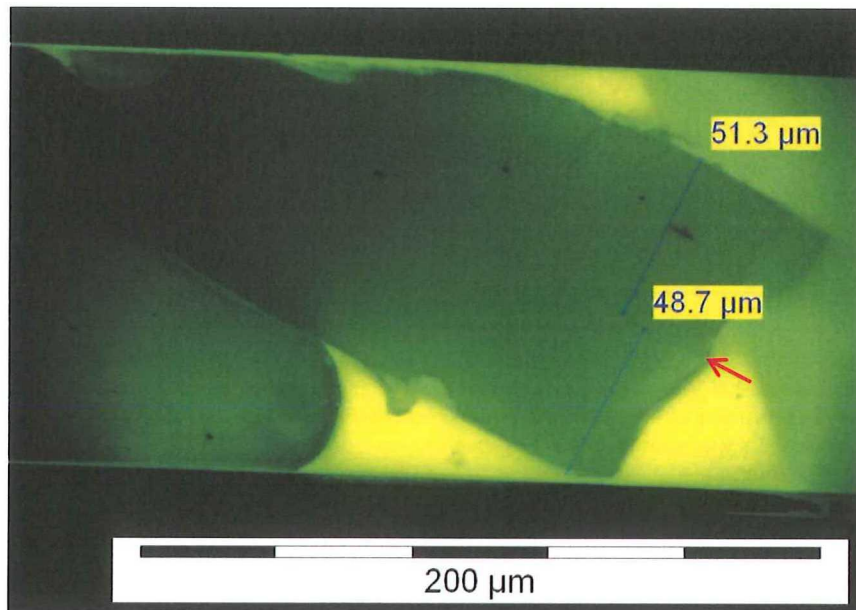


Figure 4-23: Cross-section micrograph with UV light of squeeze flow in a sample clip welded at 720 [J]. A piece of ED that has not been in a molten state can be observed. This piece consists of 2 layers of 50 [μm] PEKK film (red arrow indicates boundary). Moreover, there is no bond between the squeeze flow and the substrate composite near the flow front.

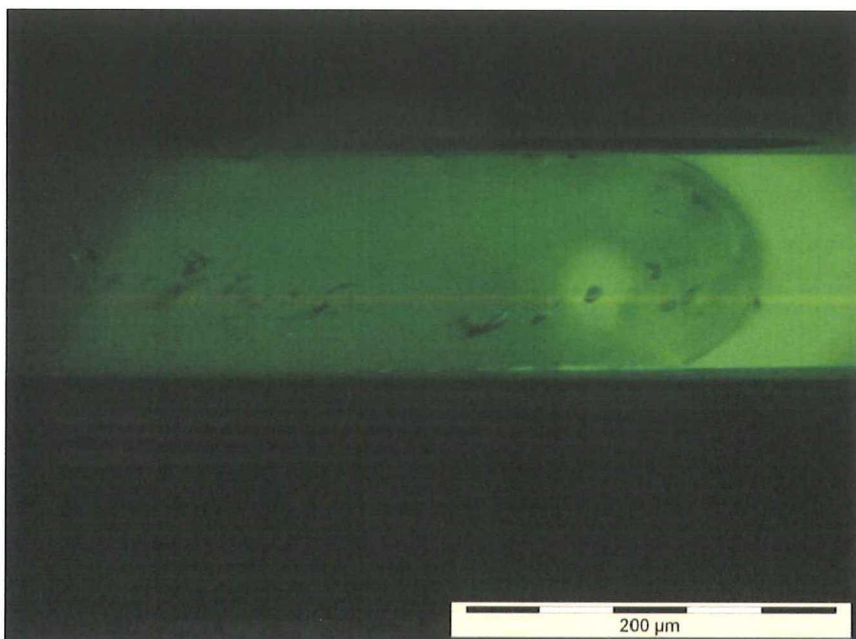


Figure 4-24: Cross-section micrograph with UV light of squeeze flow in a sample clip welded at 800 [J]. There is no bond between the flow front and bottom the substrate composite.

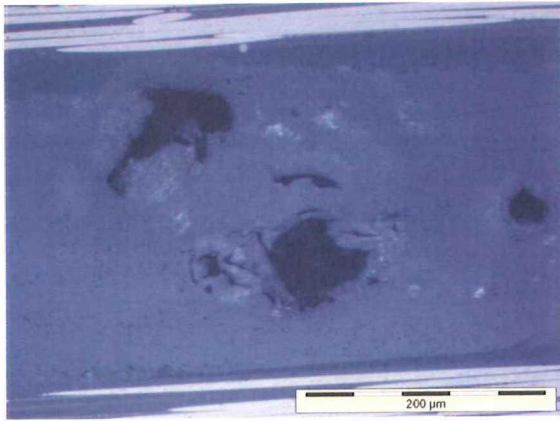


Figure 4-25: Unmelted ED at the welding interface of a sample clip welded with 300 [J]. There are already many voids present in the ED.

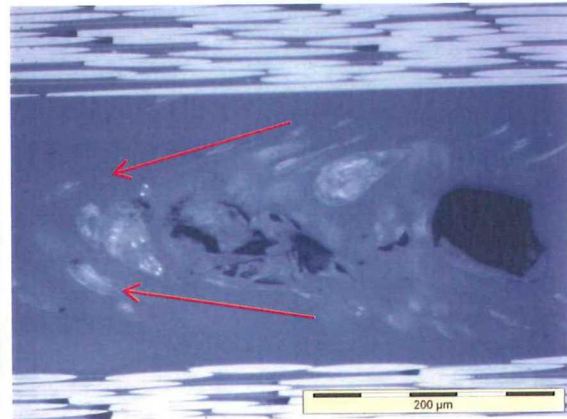


Figure 4-26: Squeeze flow of ED at the welding interface of a sample clip welded with 400 [J]. At least parts of the ED must have been in a molten state as there is a clear pattern in the squeeze out of the voids as indicated by the red arrows.

In addition to studying the squeeze flow, the quality of the ED is also analyzed using cross-sectional microscopy. In Figure 4-25, an unmelted ED in a sample welded at 300 [J] can be observed. The ED already contains some large voids, which most likely originate from combusted debris or air captured between the PEKK films. In Figure 4-26, the squeeze flow of ED in a sample welded at 400 [J] can be observed. The ED has been at least partly in a molten state as the voids flow towards the left side. The voids that are already present in the ED do not form a big issue as most of the air escapes in an early stage of the USW process. This can be concluded from the fact that the cross-sections of the samples welded with 600 [J] to 720 [J] have a limited number of voids as can be best seen in the panorama overview in Figure 4-14 (or in Figure A-1). At around 800 [J], the first voids are formed again, as can be seen in Figure 4-27. From this point onwards the number of voids increases rapidly, as can be seen in, for instance, Figure 4-28. The voids are a product of the gasses formed by the degrading PEKK. Subsequently, at approximately 1,200 [J] the first voids are discovered between the first and second plies of the substrate composites. In Figure 4-29, it can be observed that these interlaminar voids push the first ply towards the molten ED. If any voids were present in that section of the molten ED, they are most likely pushed aside, as can be seen in the panoramas of Figure 4-14. Finally, at 2,000 [J] numerous voids are present throughout the molten ED and the first layers of the substrate composites (see Figure 4-30). Furthermore, the fibers have redistributed and therefore, it became hardly possible to spot the location of the welding interface.

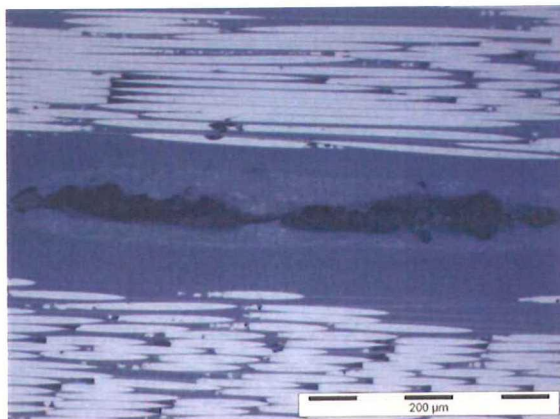


Figure 4-27: Welding interface of a sample clip welded with 800 [J]. A few large voids are present in the squeeze flow of ED.

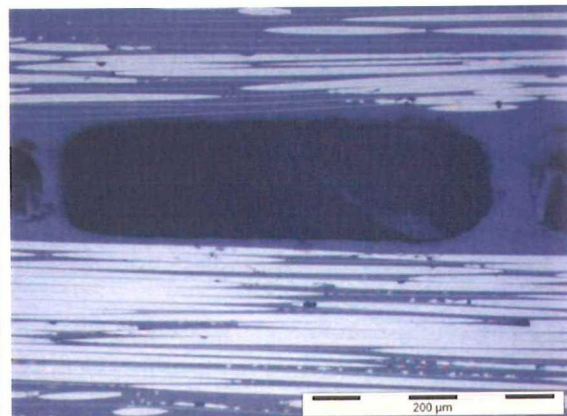


Figure 4-28: Welding interface of a sample clip welded with 1,000 [J]. Numerous large voids are present in the squeeze flow of ED.

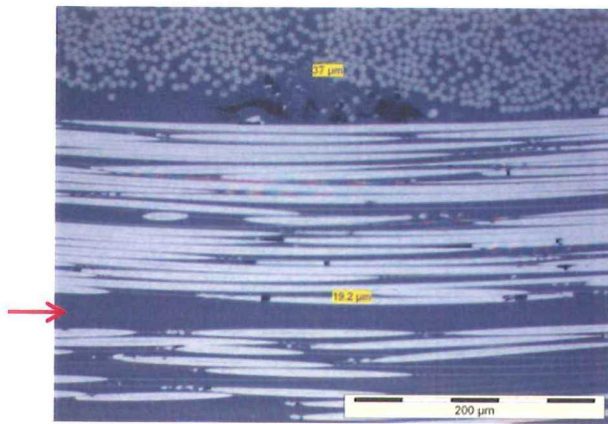


Figure 4-29: Welding interface (indicated with red arrow) of a sample clip welded with 1,200 [J]. Voids between the first and second ply start to develop, which push the first ply towards the molten ED at the welding interface.

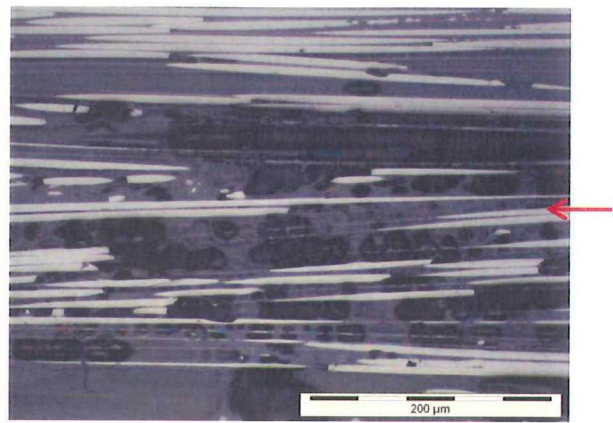


Figure 4-30: Welding interface of a sample clip welded with 2,000 [J]. Fibers from the first ply have redistributed through the squeeze flow and as a result the exact location of the welding interface can hardly be identified anymore. The red arrow indicates the approximate location, though.

4.1.5. NDT analysis

In this section, NDT scans are analyzed and compared to the observations made in the previous sections. The NDT scans are made with an Olympus OmniScan MX using the phased array technique, as described in more detail in section 2.4. A detailed explanation of how to read the scans is also provided in this section. The goal of this section is to understand the PA scans of the welds so that in the future (almost) no destructive tests are required anymore to understand what happened at the welding interface. In order to understand the PA scans, the observations made in the previous sections have to be linked to patterns in the scans. First the complete PA scans (A, S, and C scan) of the four most interesting sample clips are discussed and compared to the observations made in the previous sections. Subsequently, the development of the weld quality is analyzed using an overview of the C-scans.

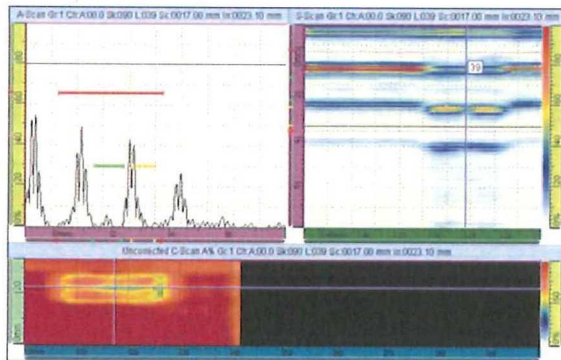


Figure 4-31: PA scan of USW141017-04 which is welded with 600 [J]. The A, S, and C-scan show that the two ED strips have melted and formed two proper welds. However, the flow fronts did not merge yet.

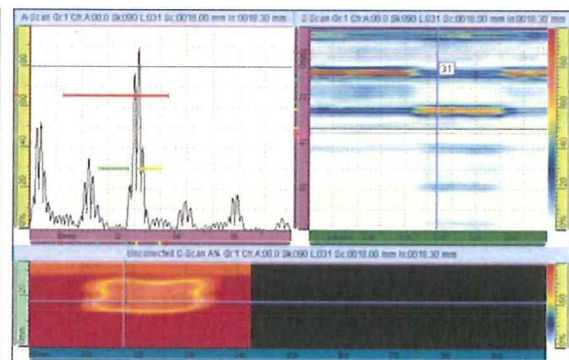


Figure 4-32: PA scan of USW140912-10 which is welded with 700 [J]. The A, S, and C-scan show that the two ED strips merged into a proper uniform weld.

In Figure 4-31, the PA scan of a sample clip welded with 600 [J] can be seen. It can be concluded from both the C and S-scan that the two ED strips have melted and formed a proper bond, as a strong signal returns from the bottom of the lower composite. However, the squeeze flows did not merge and therefore no proper bond has formed yet in between the ED strips. This can be derived from the fact that, at the center of the weld, a signal returns from the welding interface in the A, S, and C scans. In Figure 4-32, the PA scan of a sample clip welded with 700 [J] can be seen. From the A, S, and C scans it can be concluded that the flow fronts have merged and a high quality weld has been obtained, as the signal returns from the back of the lower composite throughout the

whole weld. It is interesting to note that, when the fracture surface of this sample (USW140912-10) is studied, it can be observed that the flow fronts met, but did not fully merge yet - as can be seen in Figure 4-3 and Figure 4-9. In the PA scan this aspect is probably not visible because its resolution is too low.

In Figure 4-33, the PA scan of a sample clip welded with 800 [J] can be seen. It can be observed in the C-scan that the left part of the weld has a good quality, but that the right part of the weld has a very poor quality. The A and S-scan confirm that the right section of the weld is of poor quality since the signal is almost completely lost. The fracture surface of the right section, illustrated in Figure 4-4, shows that the welding interface is indeed of poor quality as it is full of voids. It is assumed that the signal is lost, because the geometry of the voids makes it scatter in all directions. In Figure 4-34, the PA scan of a sample clip welded with 2,000 [J] can be seen. The A, S, and C-scans show that the weld quality is poor throughout the whole weld. It is interesting to note that the C-scan illustrates that in the left section of the weld quite a strong signal returns. However, the A and S-scan show that the signal returns from the welding interface and not from the back of the lower sample. The C-scan is compared to the related fracture surface, as can be seen in Figure 4-3. From this comparison, it can be derived that wherever the fracture surface shows brownish burn marks, a strong signal returns from the welding interface. The fact that a strong signal returns again probably has to do with the structure and roughness of the material at the interface. Whereas it is expected that the signal scatters and is lost when many small voids are present and the welding interface is coarse, it is likely that the burn marks have a finer structure which allows the signal to return. Figure 4-5 illustrates that the burn marks indeed have a finer structure than sections with many voids. In addition, it can be derived that wherever voids are found at the fracture surface, the signal is weak.

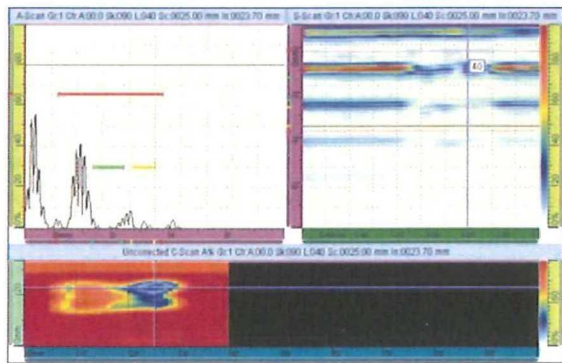


Figure 4-33: PA Scan of USW140912-02 which is welded with 800 [J]. The A, S, and C- scan show signs of material degradation on the right side of the weld as the signal is lost.

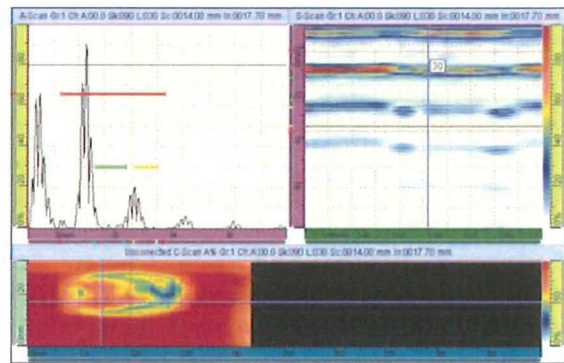


Figure 4-34: PA scan of USW140911-08 which is welded with 2,000 [J]. The A, S, and C-scan show that the two ED strips have merged but the weld quality has deteriorated.

In Figure 4-35, an overview of the C-scans of all sample clips can be seen. The C-scans are ordered according to the amount of energy used to the weld the sample clip. In the first column, the sample clips welded to perform LSS tests and fractography are shown, whereas in the second column, the sample clips welded to perform cross-sectional microscopy are shown. Two observations stand out.

The first observation is that there is a clear pattern in the development of the weld quality. It can be seen that in the range 300 [J] to 500 [J], the ED strips melt, are squeezed out (as indicated by blue lines), and eventually form two proper bonds. At 600 [J] the flow fronts start meeting, and at around 700 [J] the two EDs are (almost) completely merged and form a strong bond. Subsequently, from approximately 800 [J] onwards the material at the welding interface, and at some point also the material in the substrate composite, starts degrading. Based on the C-scans, it can be concluded that an energy of 700 [J] provides the best weld quality.

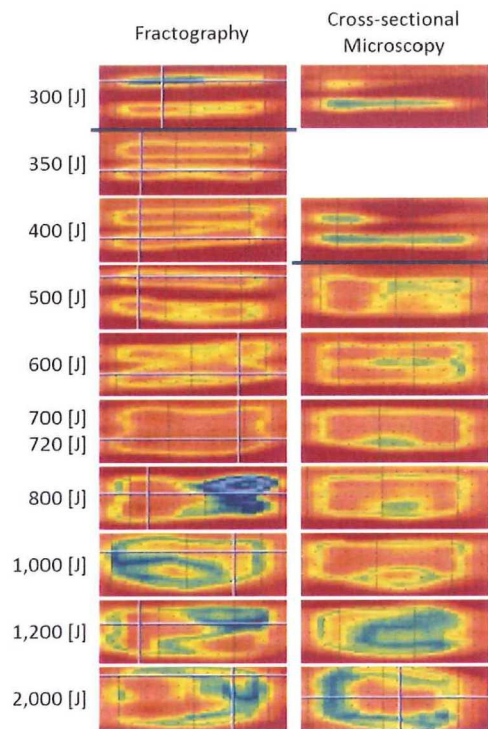


Figure 4-35: C-scan overview of welded sample clips. An energy of 700 [J] provides the best weld quality. The solid blue lines indicate from which point onwards the samples experienced the squeeze out.

The second observation that stands out is the scatter in the results. For instance, whereas, the first 800 [J] weld is of poor quality, the second one can be considered of reasonable quality. This inconsistency is explained by the fact that, as the detailed analysis of the welding data in the next section also points out, something unusual occurred to the 800 [J] weld used for fractography. Another large deviation in weld quality can be observed between the 400 [J] welds. While the EDs in the first weld are already squeezed out and formed a proper bond, the EDs in the second weld have not yet fully melted as they were not squeezed out. Most likely, deviations can be expected in an early stage of the USW process due to the random nature of nucleation and growth of hot spots (Villegas, 2013a).

When analyzing just the C-scans, caution should be used as the C-scans only provide a map of the strength of the signal. The A and S scans have to be analyzed as well in order to identify the location at which the signal returns. Therefore, Figure 4-31 to Figure 4-34 were analyzed as reference to what the colors indicate at the various energy levels. For example, at lower energy levels, an orange/ red surface implies that there is a strong bond as the signal returns from the back of the lower sample. However, at higher energy

levels, an orange/ red surface implies that material at the welding interface is heavily degraded and shows burn marks, as the signal is returning from the welding interface.

In this section, the PA scans were analyzed and compared to the observations made in the previous sections so that in the future, the A, S, and C-scans can be linked to the weld quality; it was observed that the PA scans can give an accurate impression in case the A, S, and C-scan are all analyzed.

4.1.6. Analysis of welding data

In this section, the welding data generated during the USW process is analyzed and compared to the observations made in the previous sections. Only the welding data of the sample clips used for fractography is considered here; the welding data of the sample clips used for cross-sectional microscopy can be found in Figure A-3. The power and displacement curves of the sample clips are compared to the observations made in the previous sections, so that patterns in the data can be related to events in the USW process. The welding data can eventually be used for in situ quality monitoring of USW as suggested by Benatar & Gutowski (1989) and Villegas (2013a).

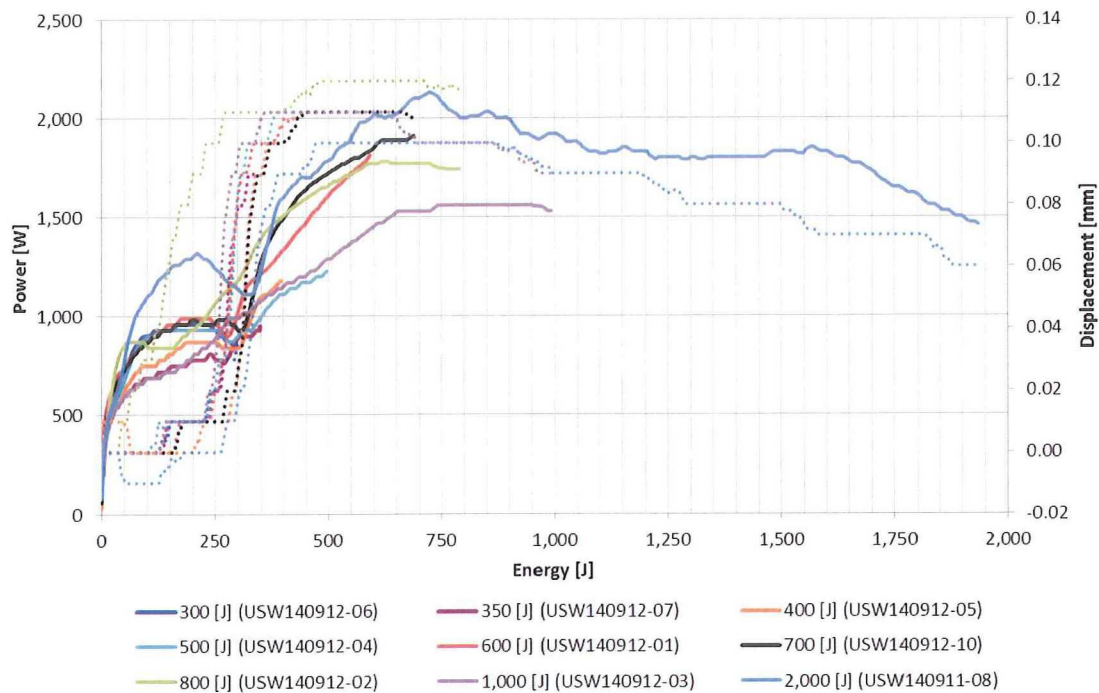


Figure 4-36: Power (solid) and travel (dotted) plots of sample clips used for fractography.

The welding data of sample clips used for fractography can be seen in Figure 4-36. Note that the data for the sample clip welded at 1,200 [J] (USW100912-09) is missing because, for unknown reasons, the Rinco Dynamic 3000 did not save the data for that weld. It can be observed that the plots are similar for almost all welds. Only the plots of USW140912-02, which is welded with 800 [J], are significantly different than the plots of the other samples, as the displacement already increases at a very low energy level. This does not come as a surprise as the NDT scan of this weld, illustrated in Figure 4-35, already stood out from the others. Since the sudden increase in displacement already started in a very early stage of the USW process and the PA scan showed that the weld has one poorly welded side, the sample was most likely welded with a small angle. Even after having established that one of the samples has an unusual weld (because of yet unknown reasons), this sample provides a great illustration of how informative the welding data is: before testing or scanning the weld with NDT techniques, the welding data can already tell whether the weld is good or bad. If the USW machine would be able to recognize deviating patterns during the USW process, it could stop or correct the process 'in situ'.

Villegas (2013a) indicated that at the moment the power curve reaches a valley, the ED has already melted and will be squeezed out. This conclusion is in line with the observation that all samples presented in Figure 4-36 show a sudden increase in displacement at the moment of the valley. Moreover, Villegas indicated that at the moment the power curve reaches the second peak, the weld is optimal and the vibrations should be stopped, since the decline in the power curve is caused by melting of the substrate composite. Again, this is confirmed by the fact that the first observations of deformations in the substrate material are made in the cross-sections of sample clips welded with 800 [J], which can be seen in Figure 4-14 and Figure A-2. The sample clips welded with 800 [J] are also the first samples to show a decrease in power after a second peak has been reached.

Additional observations that can be made is the fact that: a) all the samples that did not reach the second peak of the power curve yet, do not show any signs of material degradation, whereas b) the samples that passed the second peak do show clear signs of degradation. However, no explanation has been found for how the degradation of PEKK would contribute to a decline in power. A rise in force and/ or a decrease in displacement could be expected though, because the gasses released by the degradation of the PEKK will result in an increase in volume (in addition to the increase in volume due to thermal expansion) and therefore, exert pressure on the

sonotrode. It is assumed that the increase in volume results into the reduction of displacement, whereas the pressure exerted by the overheated material onto the sonotrode translates into the increase in force, as can be seen in Figure 4-37. However, it cannot be explained why the force already increases before the 'optimal' energy. Are these the first signs of degradation or merely thermal expansion?

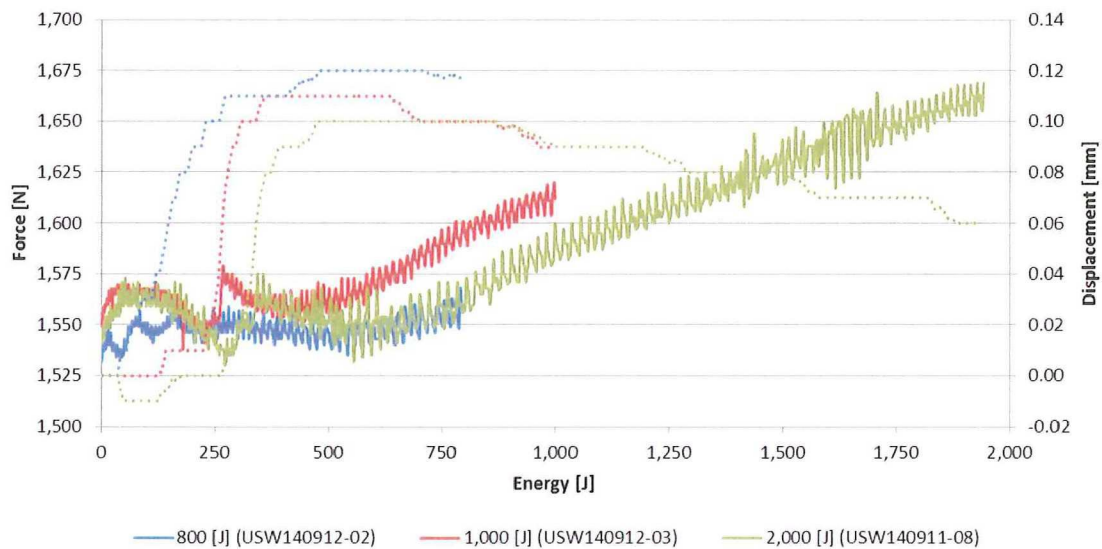


Figure 4-37: Three examples of force (solid) and travel (dotted) plots of clips used for fractography.

A last observation that can be made in Figure 4-36 is the fact that the displacement ceiling consistently occurred between 350 [J] and 450 [J] with a value ranging between 0.10 [mm] and 0.12 [mm]. In all cases where more energy was added than required to obtain an optimal weld, the displacement reduced again.

4.2. Optimal energy level & validation experiments

In the previous section, various techniques were applied to study the development of the squeeze flow and the weld quality as a function of the energy. Using the methodology of Villegas (2013a) and the welding data presented in Figure 4-1, it was determined that the theoretical optimal energy lies between 720 [J] and 840 [J]. Cross-sectional microscopy and fractography, however, indicated that the first signs of material degradation at the welding interface were already found at energy levels of 800 [J]. The NDT scans confirmed this and showed that the conservative energy value of 720 [J] would probably provide the best weld quality, as the chances of material degradation are minimized.

In this section, five sample clips are welded under the same conditions as in the previous section with 720 [J]. The goal is to verify that an energy of 720 [J], which is assumed to be (close to) the optimal energy level, consistently provides a good weld quality. The quality and consistency of the validation welds is assessed with the help of NDT scans, tensile tests, and fractography. Moreover, the welding data is analyzed.

The resulting C-scans of the PA scans can be seen in Figure 4-38. The C-scans show that all five samples have an outstanding weld quality, given that a strong signal (orange/ red) returns. The A and S-scans, as can be seen in Figure A-4 to Figure A-8, confirm the conclusion that the weld quality is good, given that the signal returns from the back of the lower composite and not from the welding interface.

In order to quantify the quality of the bond, LSS tests have been performed as well. The results of the LSS tests can also be seen in Figure 4-38. The average breaking force is 11,374 [N] with a CoV of 4.87 [%], which implies that the weld quality is very consistent. By dividing the breaking force by the area of the fracture surface, a LSS of 36.9 [MPa] with a CoV of 2.63 [%] is obtained. These numbers correspond to the ones in Figure 4-2, where the sample clip welded with 700 [J] had a higher than average breaking force of 12,334 [N] and a slightly lower than

average LSS of 36.0 [MPa]. It should be noted that the CoV is lower for the LSS than for the breaking force, because the breaking force is directly proportional to the area of the fracture surface. This relationship is confirmed by the fact that the welds with a relatively low breaking force also had a lower area welded.






USW141001-01	USW141001-02	USW141001-03	USW141001-04	USW141001-05
				
11,095.51 [N] 37.59 [MPa]	11,874.55 [N] 36.64 [MPa]	11,398.72 [N] 38.24 [MPa]	12,018.05 [N] 36.61 [MPa]	10,485.59 [N] 35.39 [MPa]

Figure 4-38: C-scans of five sample clips welded in the same conditions with 720 [J]. The C-scans validate the consistency of the welding quality using these settings as five good welds are obtained. The average breaking force is 11,374 [N] with a CoV of 4.87 [%] and the average LSS is 36.9 [MPa] with a CoV of 2.63 [%].



Figure 4-39: Fracture surfaces of five validation samples welded in the same conditions with 720 [J]. The fracture surfaces are similar in terms of area and failure mode as expected.

In Figure 4-39, the fracture surfaces of the five validation samples are shown. It can be observed that the fractures surfaces are very similar: a) the fractures surface areas are comparable; b) in all cases, the squeeze flows of ED met and merged into one weld (with the exception of the first weld, in which the EDs have only partly merged); c) the failure modes are comparable and show first-ply failure (see Figure 4-40); and d) there are no signs of degradation as the number of voids is limited.

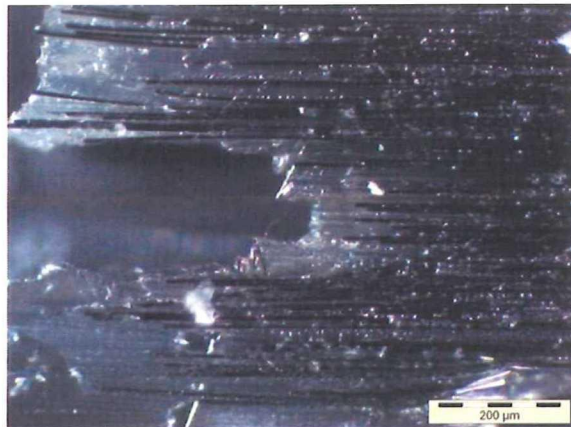


Figure 4-40: First-ply failure observed at the fracture surface of USW141001-01 which is welded with 720 [J].

Last, but not least, the welding data of the validation set, illustrated in Figure 4-41, is analyzed. All power and displacement curves show expected behavior. There is, however, a bit of deviation when it comes to the moment when the steep increase in displacement occurs. As mentioned before, such deviation is completely normal due to the random nature of nucleation and growth of hot spots in the ED. Moreover, it appears that not all power curves reached their second peak. Unfortunately, there is no way to find out how close they were.

Based on all the observations made in this section, it can be concluded that all five samples in the

validation set are of excellent quality and the results are consistent. Therefore, it has been confirmed that the line of reasoning – established in previous section to determine the optimal amount of energy – is indeed valid.

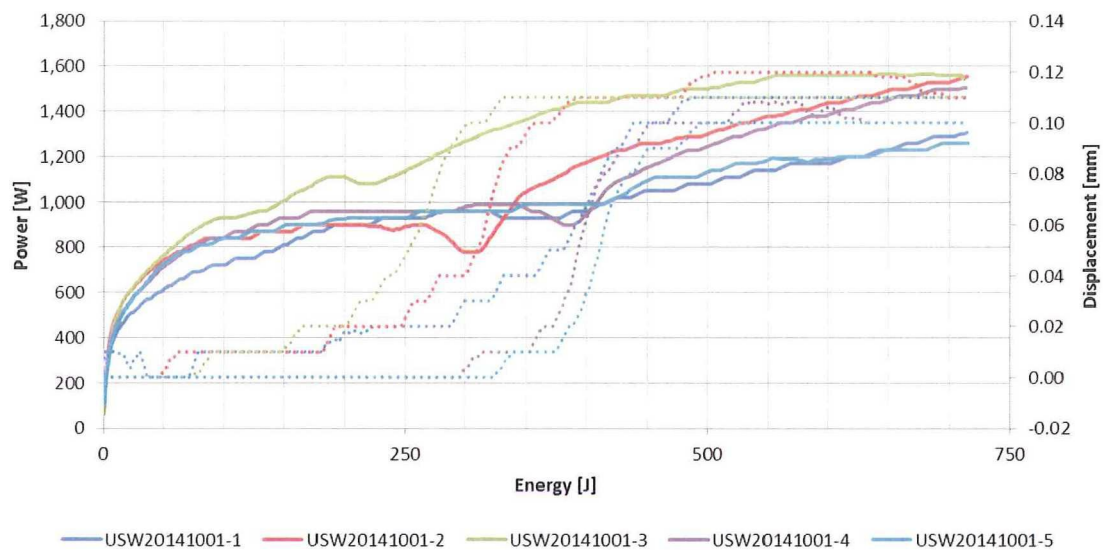


Figure 4-41: Power (solid) and displacement (dotted) plots of five validation samples welded in the same conditions with 720 [J]. The plots show that the theoretical optimum is approximately reached as the slopes of the power curves approach zero.

4.3. Conclusions

In this chapter, a) the squeeze flow of molten ED and b) the development of the weld quality as a function of the welding energy have been studied. Various techniques, such as NDT scanning, LSS testing, fractography, and cross-sectional microscopy were applied to determine the state of the welding interface, as well as of the substrate composite at the various energy levels. Subsequently, the observations were linked to patterns in the welding data, following the example of Benatar & Gutowski (1989) and Villegas (2013a), so that the various stages in the welding process could be identified and the optimal welding energy could be determined. The conclusion is that the weld quality is optimal at the moment the second peak occurs in the power curve. However, the position of this second peak deviates. Since the PEKK is expected to already show the first signs of degradation, as can be derived from the rise in force and the decrease in displacement, at energy levels close to the second peak in the power curve, it is best to take a conservative value. Cross-sectional microscopy and fractography confirmed that the material at the interface was degrading at the moment the force curve increases and the displacement decreases.

Five validation samples were welded using 720 [J], which was believed to be (close to) the optimum. These samples were analyzed in terms of the quality and consistency of the welds. The results confirmed that the chosen energy level was adequate as the weld quality was good and consistent for all welds.

Furthermore, the source of the displacement ceiling was most likely identified in this section. Cross-sectional microscopy exposed that small pieces of the PEKK ED, which had not melted, cause the abrupt displacement ceiling. These small pieces of ED are, most likely, a result of the fact that the ED is not melting uniformly. They do not melt uniformly because the five layers of 50 [μm] PEKK film have not been consolidated well when the ED was manufactured and therefore the films can still interact with each other during the USW process. The incomplete bond between the films could be observed with both optical and SEM microscopy. Further research is required to investigate if a well consolidated ED can prevent the appearance of the displacement ceiling.

The present research was conducted using one fixed set of welding parameters. A similar investigation should be performed using other sets of parameters to see whether the conclusions still hold. A lower welding force or amplitude, for instance, might slow down the rate of heating and delay the moment at which the material starts degrading. Moreover, the scope of future similar research should be expanded to include different applications and materials.

5. System Clips

In this chapter, real composite system clips are welded together with the ultimate objective to weld the first demonstrator: system clips welded to a rib of the horizontal stabilizer of the Gulfstream G650. First, in section 5.1, the design of the system clip is described. Secondly, in section 5.2, the choice of the ED configuration is explained. Next, in section 5.3, an effort is made to determine the optimal welding energy for the system clip using the welding data and NDT scans. Finally, in section 5.4, the welded demonstrator is presented and the results are discussed.

5.1. System clip design

In this section, the design of the composite system clip is discussed. The design of the composite clip is based on that of an existing aluminum clip, which is used to attach brackets holding various systems, such as wire harnesses and pipes. The original aluminum clip is attached to a rib of the horizontal stabilizer of the Gulfstream G650, as can be seen in Figure 5-1, Figure F-1 and Figure F-2.



Figure 5-1: Original position of the aluminum clip on a rib of the horizontal stabilizer of the G650, as indicated by the red ellipse. The clip is fastened by three rivets.

The original aluminum system clip is illustrated in Figure 5-2. The clip is fastened to the rib with three rivets, while two floating nuts are riveted to the clip with two rivets per unit. Special brackets holding the wire harness are bolted to the floating nuts. It can be seen in Figure 5-2 that extra material has to be built-in around the rivet holes, as it is standardly required for a hole to always be away from an edge by a distance equal to 2.5 times its diameter. In case of the composites this would be 3 times, as indicated by Fokker.

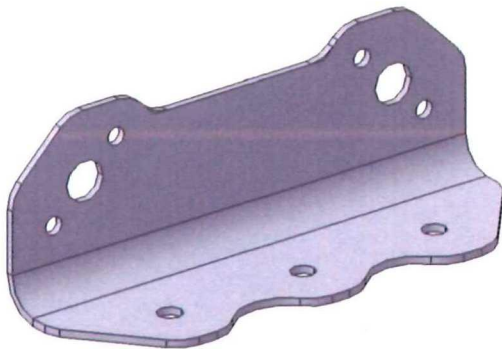


Figure 5-2: Original aluminum clip. The three holes at the bottom flange are used to rivet the clip to the rib. Two floating nuts are riveted to the other flange.



Figure 5-3: Composite clip based on the dimensions of the original aluminum clip. The clip is welded to the rib. The floating nuts could be integrated in the design or welded as well as there are already thermoplastic floating nuts.

The composite version of the clip, which can be observed in Figure 5-3, is expected to be smaller and lighter than its aluminum counterpart. This is due to the fact that: a) it is made of composites with a high specific stiffness/strength and b) since the clip will be welded to the rib, rivet holes are no longer necessary. Because of the latter reason, no additional material has to be added. Therefore, the composite clip's dimensions are similar to those of the aluminum clip minus the added material. The detailed design including the dimensions of the aluminum and composite clip can be found in Figure B-1 and Figure B-2, respectively.

5.2. Energy director configuration

Before any clips are welded to a demonstrator, experiments are conducted to determine: a) the best configuration for the EDs, and b) the right amount of energy needed to obtain a good weld quality. In this section, the EDs configuration is described. The welding setup used to conduct the experiments is described in section 2.3.2.

The clips are made of 8 layers of Cytec PEKK FC, have an exact thickness of 1.14 [mm], and the following layup: $[45/90/-45/0]_s$, as explained in detail in section 2.1.3. The samples are welded using the Z51414 fixture in the system clip configuration (section 2.3.2). Furthermore, sonotrode 1 is used as it completely overlaps the bottom flange of the clip. The clips are welded with a welding force of 1,500 [N], a peak-to-peak amplitude of 63.4 [μm], and a holding time of 4,000 [ms].

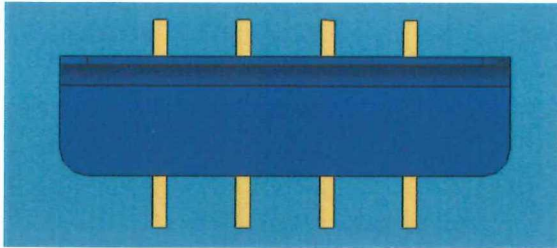


Figure 5-4: ED configuration 1 – Four EDs with a spacing of 10 [mm] are placed in the transverse direction.

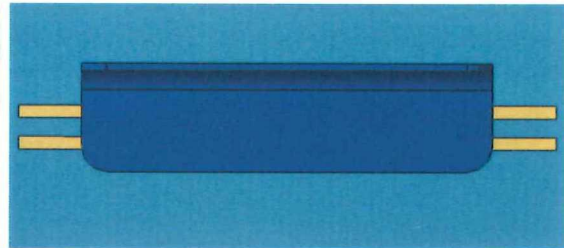


Figure 5-5: ED configuration 2 – Two EDs with a spacing of 3 [mm] are placed in the longitudinal direction.

First the orientation of the ED strips is investigated. Two ED configurations are proposed: 1) Four strips in the transverse direction of the clip, and 2) two strips in the longitudinal direction of the clip. Configuration 1 and 2 are illustrated in Figure 5-4 and Figure 5-5, respectively. The ED strips are temporarily fixed using tape.

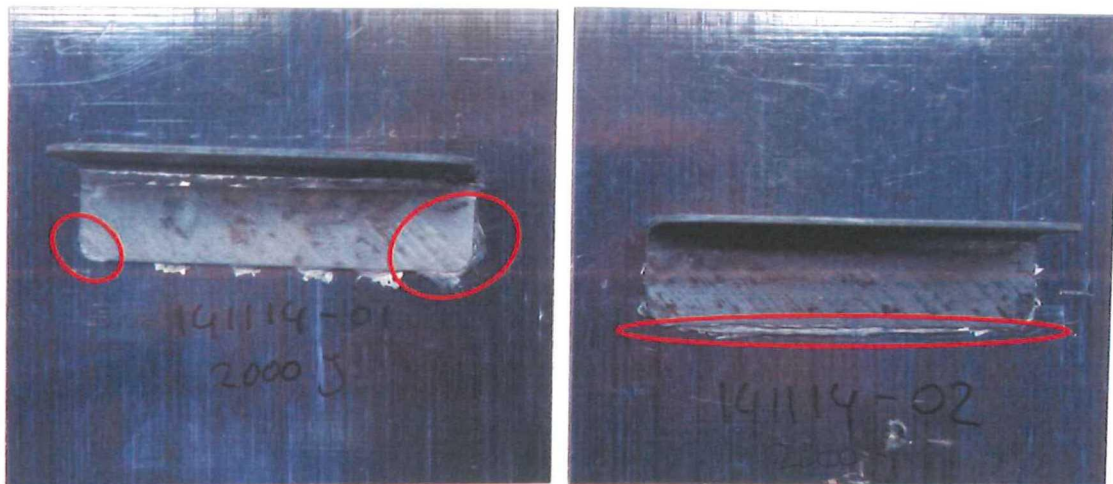


Figure 5-6: A clip welded with ED configuration 1 (left) and a clip welded with ED configuration 2 (right). It can be observed that clip welded with ED configuration 1 is damaged at the sides, and the one welded in configuration 2 is slightly damaged at the lower edge. The damages are indicated with the red ellipses.

The resulting clips welded in both configurations with 2,000 [J] can be seen in Figure 5-6. It can be observed that both clips are damaged. However, the clip welded with ED configuration 1, shows more severe damage at the edges as fibers are squeezed out over a relatively long distance. The damage is similar to the damage observed in section 3.1, where sample clips were welded with a plunge welded square ED. Just as with the square EDs, the clip was not supported by ED at the edges and therefore, the edges were, most likely, able to resonate, causing damage. This damage might be prevented, though, by adding more EDs near the edge. The damage of the sample welded with ED configuration 2 seems to be less severe, as only some fibers from the first plies, with respect to the welding interface, seem to have joined the squeeze flow of molten ED: This type of damage can probably be

prevented by welding at a lower energy level. Therefore, from the 'damage' point of view, configuration 2 is preferred. However, there are more factors to consider than just damage. For instance, it is much easier to install the second ED configuration, as only two strips have to be placed. Furthermore, it is a concern that in the first configuration, the sonotrode cannot fully overlap the area of ED that supports the clip due to the radius near the flange (see Figure 5-7). In case the molten ED is able to flow towards areas which are not overlapped by the sonotrode, it will probably solidify and will not be able to remelt.

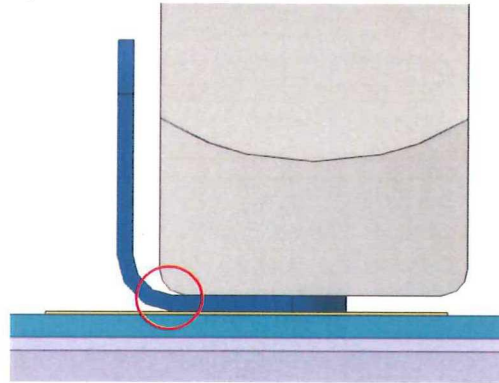


Figure 5-7: Side-view of configuration 1. The sonotrode cannot fully overlap the area of the ED that is supporting the clip in the area marked by the red circle.

Only one clip was welded per configuration, as multiple arguments converge to support a preference for ED configuration 2: the configuration is easier to install, the clip is less prone to damage in this configuration, and the ED can be fully covered by the sonotrode. Since the ED width and ED spacing of 2 [mm] and 3 [mm], respectively, provided satisfactory results in the experiments described in Chapter 0, the same ED width and ED spacing are also used for the clips.

5.3. Energy determination

In this section, an effort is made to determine the optimal amount of energy to weld the clips. First the welding data is studied. The power and displacement curves are illustrated in Figure 5-8. It can be observed that the curves show familiar behavior and are consistent with exception of the ceiling, which varies between 0.09 [mm] and 0.13 [mm]. It is unknown why the ceiling varies considerably. However, due to fluctuations in the power curve from the moment the displacement ceiling is reached, it is difficult to identify a second peak. It should be noted that the displacement curves of the system clips also shows more fluctuations than the displacement curves of the sample clips (e.g. Figure 4-1 and Figure 4-36) after the moment the ceiling is reached.

The force curves, which can be seen in Figure F-5 to Figure F-9, also show irregular behavior. It is assumed that the fluctuations are caused by the more complex geometry of the clip. However, more research is required to confirm this. Given the fluctuations, no conclusions about the optimal energy level can be drawn yet. The only useful observation is that the optimum is to be found at a value of or above 1,000 [J]. This insight is based on the fact that the ED has just been squeezed out and the displacement ceiling has been reached at this point.

Another technique has to be applied in order to find the optimal energy level. NDT technology is the most convenient way to do this, as this approach proved to be quite effective in section 4.1.5. Therefore, five more clips are welded with an energy between 1,000 [J] and 2,000 [J] and an interval of 250 [J]. Subsequently, PA scans are made of the welds and compared to identify the optimum. The orientation of the clip in the C-scans is the same as the orientation of the clip in Figure 5-5.

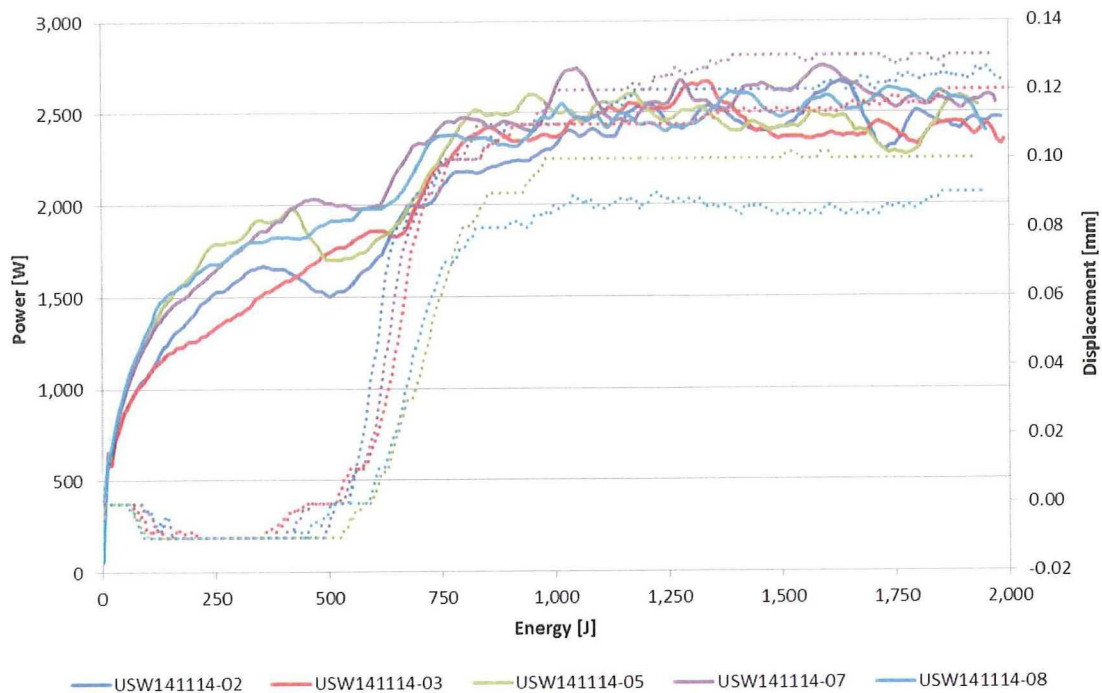


Figure 5-8: Power (solid) and displacement (dotted) plots of five clips welded with 2,000 [J]. The plots are similar, however, no clear second peak can be identified.

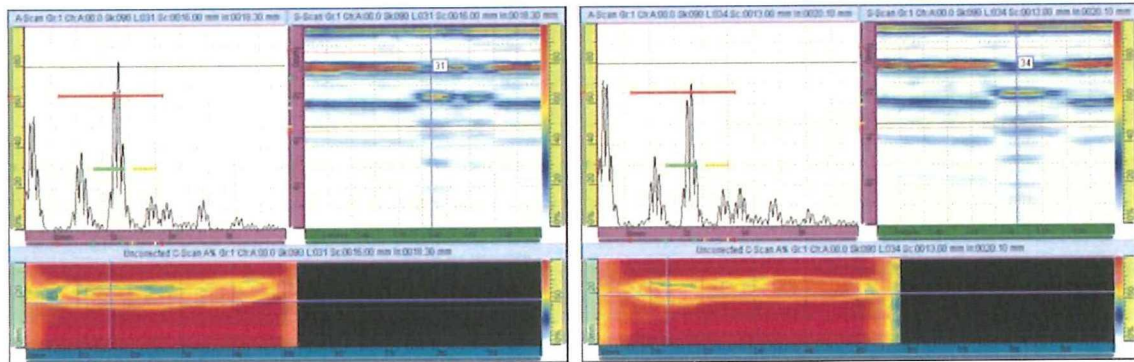


Figure 5-9: PA scan of clip (USW141114-11) welded with 1,000 [J]. The S-scan indicates that the two EDs have not merged yet. The lower ED formed a strong bond, but the upper ED did not as can be seen in the C-scan.

Figure 5-10: PA scan of clip (USW141114-12) welded with 1,250 [J]. The weld has improved w.r.t. the previous weld. However, the upper left section of the weld is not optimal as can be seen in the C-scan.

A PA scan of the first weld, with an energy of 1,000 [J], can be seen in Figure 5-9. It can be observed that the two ED strips have not merged yet, as the S-scan shows that the signal returns from the welding interface in between the two strips. Moreover, the C and S-scan illustrate that whereas the lower ED strip formed a proper bond, the upper ED strip formed only a mediocre bond.

In a PA scan of the clip welded with 1,250 [J], as can be seen in Figure 5-10, it can be observed that weld quality improved with respect to the previous weld. The squeeze flows of the molten ED merged, as illustrated by the S-scan, and a good weld has been formed throughout the whole right section. However, the S and C-scan show that the quality of the upper-left section of the weld is not yet optimal. In Figure 5-15, which presents the welded clip, it can be seen that no squeeze out can be observed in the bottom-left section (upper-left in C-scan) yet, whereas squeeze out is already present in bottom-right section.

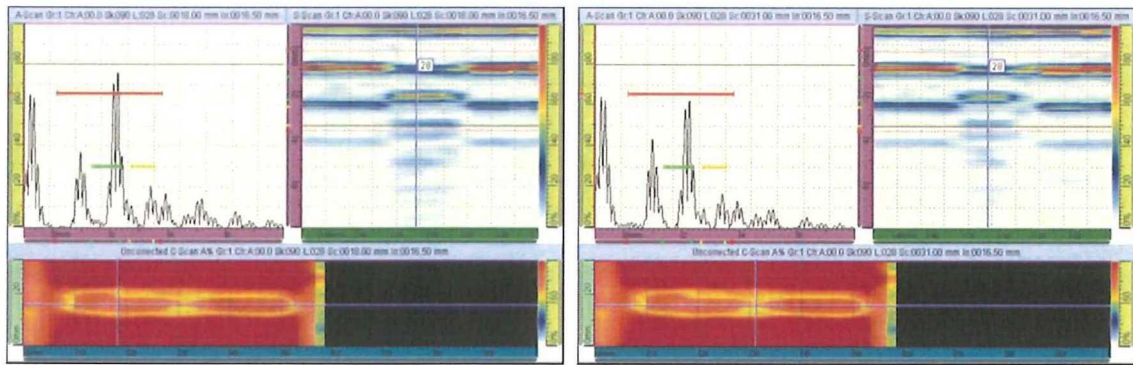


Figure 5-11: PA scan of clip (USW141114-09) welded with 1,500 [J]. The A, S, and C-scan confirm that an excellent weld has been obtained, with the exception of a small area at the center of the weld, as can be seen in the C-scan.

Figure 5-12: A second PA scan of clip (USW141114-09) welded with 1,500 [J]. The A and S-scan show that the quality of the section at the center is still acceptable as the signal returns from the back of the lower composite.

In Figure 5-11 and Figure 5-12, PA scans of the clip welded with 1,500 [J] can be seen. The S-scan of the first figure shows that the two squeeze flows of molten ED have merged into one large weld, as the signal is not interrupted at the center line. Moreover, the C-scan indicates that the weld has an excellent quality over the whole area of the weld, with the exception of a small section at the center. However, the latter figure illustrates that the weld quality at the center section is still reasonable, as the S-scan shows that a relatively strong signal returns from the back of the lower composite.

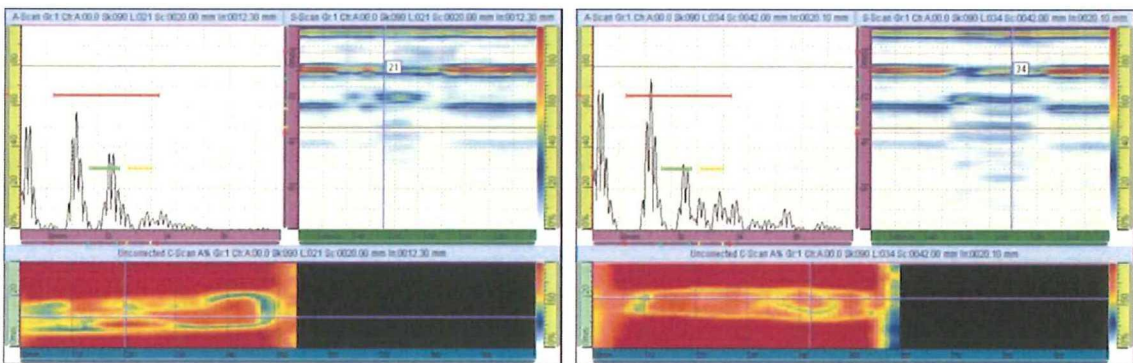


Figure 5-13: PA scan of clip (USW141114-13) welded with 1,750 [J]. The A, S, and C-scan show that the weld is deteriorating at the left side.

Figure 5-14: PA scan of clip (USW141114-08) welded with 2,000 [J]. The A and S scan indicate that a strong signal returns from the welding interface, which implies that the material at the welding interface has degraded.

A PA scan of a clip welded with 1,750 [J] can be seen in Figure 5-13. It can be observed that the weld quality has strongly deteriorated with respect to the clip welded with 1,500 [J] as the signal is lost or returning from the welding interface. In section 4.1.5, it was observed that a poor signal at higher energy levels, most likely, indicates that voids are present, whereas, a strong signal returning from the welding interface at a high energy level, presumably, implies that the material has started to degrade heavily and is showing burn marks. The right section of the weld still has a good quality, as can be seen in the C-scan. The PA scan of the clip welded with 2,000 [J], illustrated in Figure 5-14, shows that material at the welding interface, in the section where the A-scan is made, is most likely degraded: The A and S-scan show that a strong signal returns from the welding interface. The other sections of the weld, highlighted in orange/red in the C-scan, do exhibit good quality levels, though, since the signal returns from the back of the lower sample.

From the NDT scans it can be concluded that the optimal welding energy is close to 1,500 [J]. No tensile tests and/ or cross-sectional microscopy are performed, as section 4.1.5 indicated that the scans provide a sufficiently good impression of the weld quality. It should be noted, though, that since only one sample has been studied per energy level, no conclusion can be made about the consistency and reliability of the results.

The clips welded with 1,250 [J] and 1,500 [J] can be seen in Figure 5-15. It can be observed that while the clip welded with 1,250 [J] has no damage and only shows squeeze out of resin, the clip welded with 1,500 [J] also shows squeeze out of fibers in addition to that of resin. Because the demonstrator is used for commercial purposes, it is decided to weld the clips with the conservative energy level of 1,250 [J]. This choice supports the objective of minimizing the chances of having damaged clips on the demonstrator. The energy level of 1,250 [J] is still expected to provide a reasonable welding quality, as it could be observed in Figure 5-10.

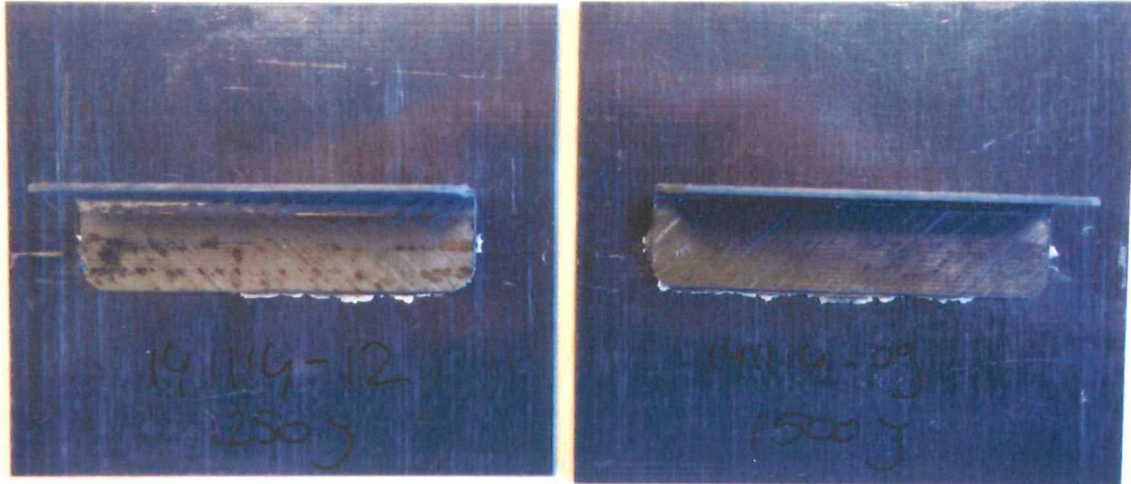


Figure 5-15: A clip welded with 1,250 [J] (left) and a clip welded with 1,500 [J] (right). In case of the right clip, fibers are squeezed out.

5.4. Demonstrator

In this section, it is explained how the clips are welded to the rib. Moreover, the welding data and the resulting welds are briefly discussed. The rib is press-formed by Dutch Thermoplastic Components (DTC) and is made of Cytec CF/ PEKK FC. The exact layup can be provided by DTC if required. The clips are welded with the same ED configuration, the same sonotrode, and the same settings as those used in the previous section. A welding energy of 1,250 [J] is used as driver, based on the insights and decisions explained in the previous section. Two CF/ PEKK clips and one carbon fiber/ polyphenylenesulfide (CF/ PPS) clip were welded to the rib. Moreover, one aluminum clip was riveted to the rib. The CF/ PPS clip was only welded to the CF/ PEKK rib to demonstrate another possibility of USW of CFRTPCs, and will not be discussed in this section. The aluminum clip was riveted to the demonstrator as a reference to the current situation.



Figure 5-16: Clamping of the rib onto the anvil of the Rinco 3000. The rib is simply clamped with two glue clamps. Wooden sticks are placed in between to prevent damage.

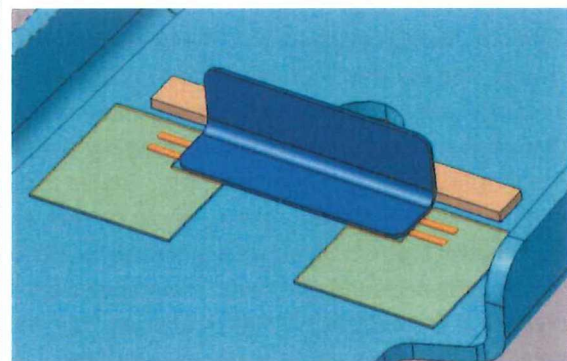


Figure 5-17: Positioning plates (transparent orange) and a wooden bar (brown) prevent the clip from moving sideways during the USW process. The plates and the bar are taped to the rib.

The rib is clamped onto the anvil of the USW machine with glue clamps, as can be seen in Figure 5-16. The clip is not clamped but freely placed between the positioning plates and a wooden bar that should prevent the clip from moving sideways due to the vibrations of the USW process. The position plates are made of 0.7 [mm] thick aluminum. Since the plates also cover the ED, the combined thickness of a) the plate and of b) the ED must be smaller than the thickness of the clip (1.14 [mm]) to prevent the sonotrode from being blocked by the plates. The positioning plates and the bar are simply taped onto the rib. A spacing of approximately 0.5 [mm] is kept between the clip and the positioning plates to prevent friction between them.



Figure 5-18: CFRTPC clips ultrasonically welded to a CFRTPC rib. The left-most clip is the original aluminum clip and it is riveted to the rib. The second clip is a CF/ PPS clip and the two right-most clips are CF/ PEKK clips. The CF/ PPS clip is welded with PEKK EDs.

The welded demonstrator can be seen in Figure 5-18. The clips seem to be properly welded to the rib without having incurred any damage. Even the PPS clip seems to have bonded well, although, a destructive test should be performed to determine the strength of the joint. The welding sequence is: 1) third leftmost clip, 2) fourth leftmost clip, and 3) second leftmost – the PPS clip. The first clip unfortunately moved during the USW process as a result of poor clamping and is therefore poorly aligned. For the other clips more tape was used and as a result, they did not move anymore. Obviously, a proper fixture has to be designed if this application is going to be industrialized. However, the fact that the clip can be kept in position during the USW process by merely some aluminum plates held in place by tape, implies that designing a fixture should not extremely be complicated.

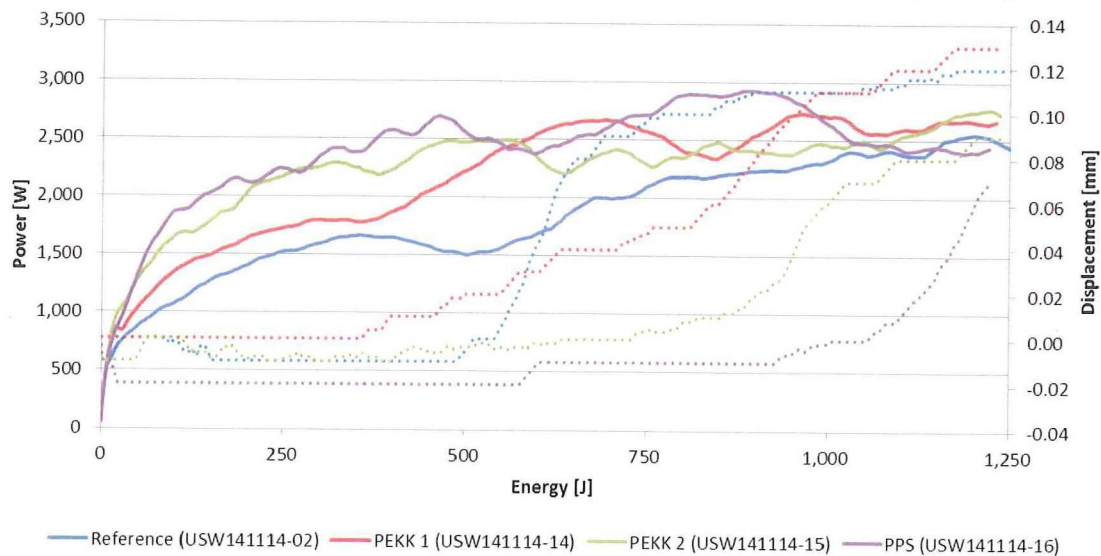


Figure 5-19: Power (solid) and displacement (dotted) plots of the clips welded to the rib. The data of one clip from the previous section is provided as a reference.

The welding data of the clips is illustrated in Figure 5-19. It can be seen that there is a lot of variation between the two CF/ PEKK clips. This is, most likely, caused by the inconsistency of clamping and the fact that the clips are welded at different locations of the rib. When comparing the welding data of the two clips to the welding data of a clip from the previous section of this report, it can be seen that a) more power is used, and b) also more energy needs to be applied before the EDs are melted. This is probably due to the fact that the rib and its simplistic fixture absorb more energy than the compact fixture and the well clamped composite plate used for

welding the reference clip. Since more energy is lost, it is expected that the welds are still in an early stage and the optimal condition has not yet been reached. It is recommended that, when welding with energy as the driver, welds should be optimized again in the real setup. Such re-adjustment is required given the large deviation between the currently considered experimental setup and the real situation. Another option is that, if applicable, the more consistent displacement is used as the driver, like Villegas (2013a) suggested. Unfortunately, the displacement ceiling prevented the use of this method.

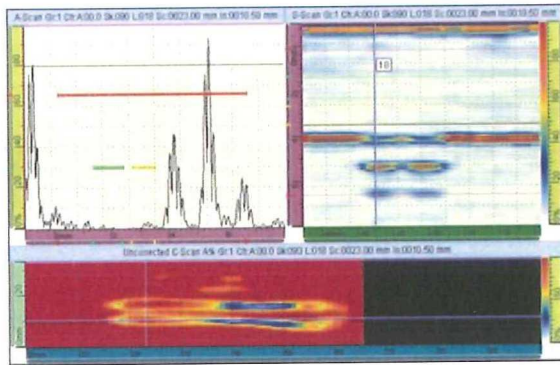


Figure 5-20: PA scan of the first clip welded. The weld is still in an early stage as some sections of the ED strips have not formed a proper bond yet.

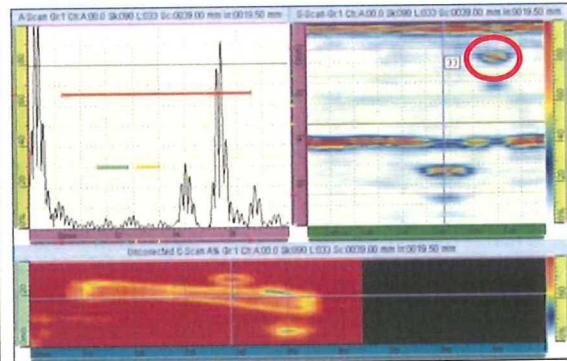


Figure 5-21: PA scan of the second weld. The squeeze flows of the EDs seem to have merged and formed a proper bond. A delamination has been observed close to the weld as indicated with the red circle in the S-scan.

The PA scans of the first and second PEKK clips from the previously described welding sequence can be seen in Figure 5-20 and Figure 5-21, respectively. The first figure illustrates that not all sections of the two ED strips have formed a proper bond yet. The fact that the first clip moved sideways during the USW process, parallel to the longitudinal direction of the EDs, might provide an explanation for this observation. In the other sections, as indicated by the red/orange sections of the C-scan, a good bond has indeed formed. The second figure illustrates that a very good bond has formed in which the EDs have even merged. However, the welded area is rather thin. Therefore, it is expected that the EDs strips moved towards each other during the USW process. Moreover, two delaminations in the rib can be spotted close to the weld. The location of a delamination is indicated in the S-scan with a red circle. It is unknown if these delaminations were already present or have been caused by the USW process. It is equally unknown if the delaminations had any (significant) effect on the USW process.

III – New Concepts & Fuselage Frame

6. Integrated Triangular Energy Directors

The research conducted on ED strips in section 3.2 resulted in the finding that ED strips provide a good weld quality when welding clips. However, from an industrial point-of-view, ED strips are not at all favorable: 1) they have to be manufactured separately (as explained in section 2.1.2.), 2) they have to be placed on one of the substrate composites, and 3) they have to be kept in position during the USW process by tape or a plunge weld, because otherwise the vibrations characteristic to the USW process will displace them. The three aforementioned issues can be solved by integrating EDs into one of the composites to be welded. Integrated triangular ribs are widely used in the plastics industry: because, just like the ED, thermoplastics are generally non-reinforced, EDs can be integrated in the design of the component to be welded without adding process steps. Unfortunately, this method does not apply to composites as they are fiber reinforced. In this chapter, a method to integrate triangular ED ribs into CFRTPC components is proposed: the elements are consolidated by a) vacuum-bagging the product and b) subsequently consolidating it in an autoclave. In section 6.1, the manufacturing method is explained. Next, in section 6.2, sample clips with integrated EDs are welded and the results are discussed. Finally, in section 6.3, recommendations are provided.

6.1. Materials & manufacturing

A laminate with a $[(0/90)_3]_s$ lay-up is manufactured, as explained in section 2.1.1. However, on top of the laminate two additional 50 [μ m] films of PEKK are placed. Moreover, the stainless steel cover plate, illustrated in Figure 2-1, is replaced by an aluminum plate with small triangular channels, as can be seen in Figure 6-1. These channels are spaced 10 [mm] apart, have a depth of 1 [mm] and angles of 60 [$^\circ$], as illustrated in Figure 6-2. Angles of 60 [$^\circ$] were chosen, because Devine (2001) experimented with the shape of the triangular EDs and concluded that 60 [$^\circ$] EDs provide the best bond for semi-crystalline TPCs. The mold is positioned in such a way that the channels are perpendicular to the direction of the fibers in the outer ply. This positioning is meant to prevent the fibers from being pressed into the channels.



Figure 6-1: Aluminum cover plate with triangular channels.

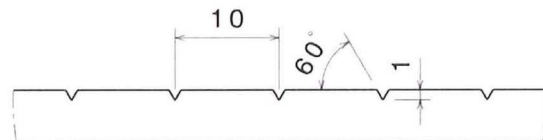


Figure 6-2: The triangular channels are spaced 10 [mm] apart, have a depth of 1 [mm], and have angles of 60 [$^\circ$].

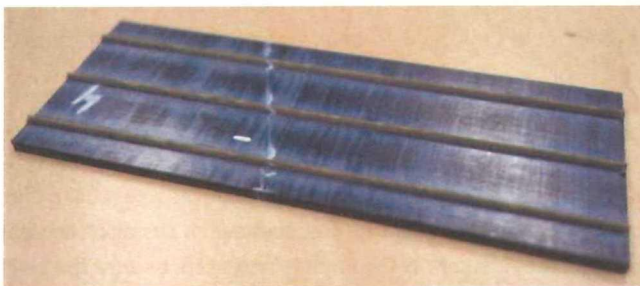


Figure 6-3: Sample clip with integrated triangular ED ribs.

Furthermore, the Upilex release film – normally placed between the cover plate and the product – is left out, because the film might prevent the molten PEKK from filling the channels. Instead, the mold is first treated with Frekote B-15 Mold Release Sealer and then with Frekote 700-NC Mold Release Agent. The laminate is vacuum bagged and spends one hour in the autoclave under high pressure at 375 [$^\circ$ C] like the other composites manufactured for this thesis, as explained in section 2.1.1. Finally, sample clips of 80

[mm] by 30 [mm] are sawn out of the laminate using a water-cooled circular saw with a diamond-coated blade.

The result can be seen in Figure 6-3. The attempt to integrate triangular ribs in a composite product was successful as the molten PEKK flowed into the channels and consistent ribs were obtained. Moreover, only a little bit of excess PEKK resin

remains at the surface of the substrate material (whitish area around the ribs). The presence of excess resin can, most likely, be prevented by matching the volume of the PEKK films and the volume of the channels. Currently, the volume of PEKK was slightly higher to ensure that all channels would be filled.

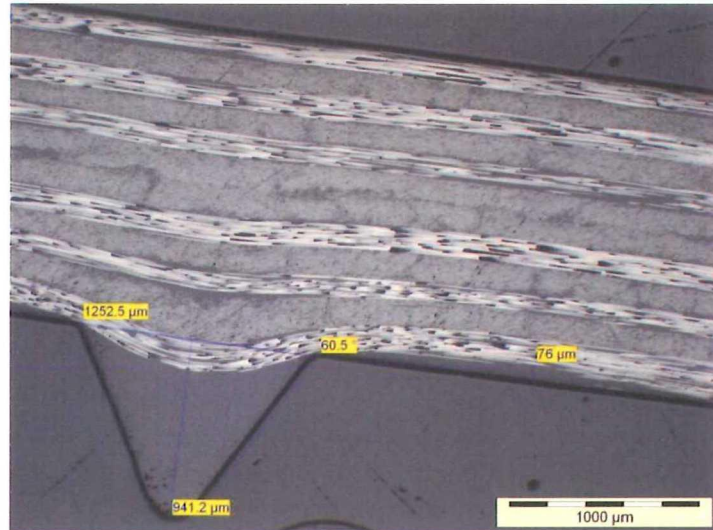


Figure 6-4: Integrated triangular ED onto sample clip. Fibers in the laminate are slightly disturbed. Near the ribs, there is excess resin on top of the first ply.

A cross-sectional microscopy picture of an integrated triangular ED is presented in Figure 6-4. It can be seen that, even though the fibers of the first ply were placed perpendicular to the channels, the fibers in the laminate are slightly disturbed. Especially the first two plies of the laminate are significantly affected. Villegas and Bersee (2010) experimentally observed that using multiple smaller EDs instead of a larger one reduces the disturbance of fibers in the outermost layers of the substrate. Furthermore, excess resin is observed near the rib. This excess has a thickness of approximately 76 [μm] at its thickest point. The triangular rib itself has a good quality as it does not contain significant voids. Moreover, its dimensions match those of the mold, which implies that whole cavity was filled with the molten PEKK.

6.2. Welding of sample clips with integrated energy directors

In order to test if the integrated EDs can be successfully used to weld CFRTPCs, sample clips with integrated EDs are welded. A setup similar to that applied for the sample clips, described in section 2.3.1, was used. However, the overlap of the two samples is reduced to 22.5 [mm], so that sonotrode 3, which has a diameter of 40 [mm], can fully cover it. This is required, as the ED ribs continue over the full length of the sample clip (see Figure 6-1) and would block the downwards displacement of the sonotrode if sections of the ED, overlapping the lower composite, did not melt. The samples are welded using the same settings as those used for the sample clips: peak-to-peak amplitude of 51.8 [μm] and welding force of 1,500 [N].

Four samples were welded at 2,000 [J] and one sample was welded at 1,000 [J]. The welding data is illustrated in Figure 6-5 and Figure 6-6. In the latter one, it can be seen that the power curves show similar behavior as those of the sample clips with ED strips: 1) the power increases until it reaches a first peak; 2) the power reduces to a local minimum; 3) the power increases again until it reaches a second peak; and 4) finally, the power reduces again. The displacement curves are completely different, though: a) The displacement increases steadily as the force is increased; b) once the vibrations start, the displacement increases abruptly; c) the slope reduces significantly, but the displacement keeps increasing gradually; d) the displacement decreases again; e) once the vibrations stop, the displacement abruptly increases again; and f) finally, the displacement gradually increases until the welding interface has solidified. It is interesting to note that the total displacement is approximately equal to the height of the triangular EDs, which implies that everything has been squeezed out. The displacement curves are very similar to the ones observed by Troughton (2008), as can be seen in Figure D-1, who welded plastic components also using integrated triangular EDs.

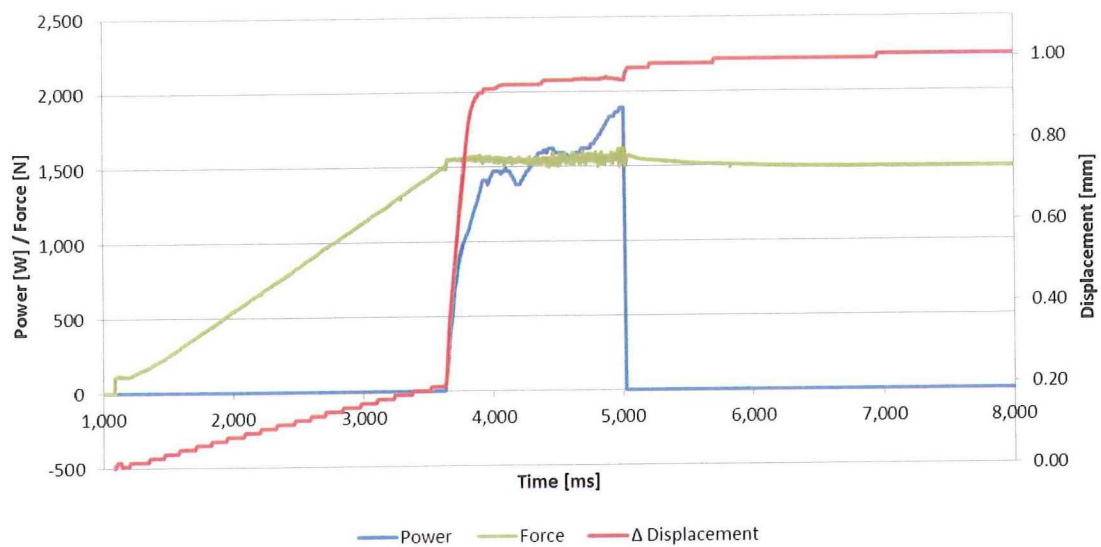


Figure 6-5: Power, force and displacement curves of sample USW141117-03 welded at 2,000 [J].

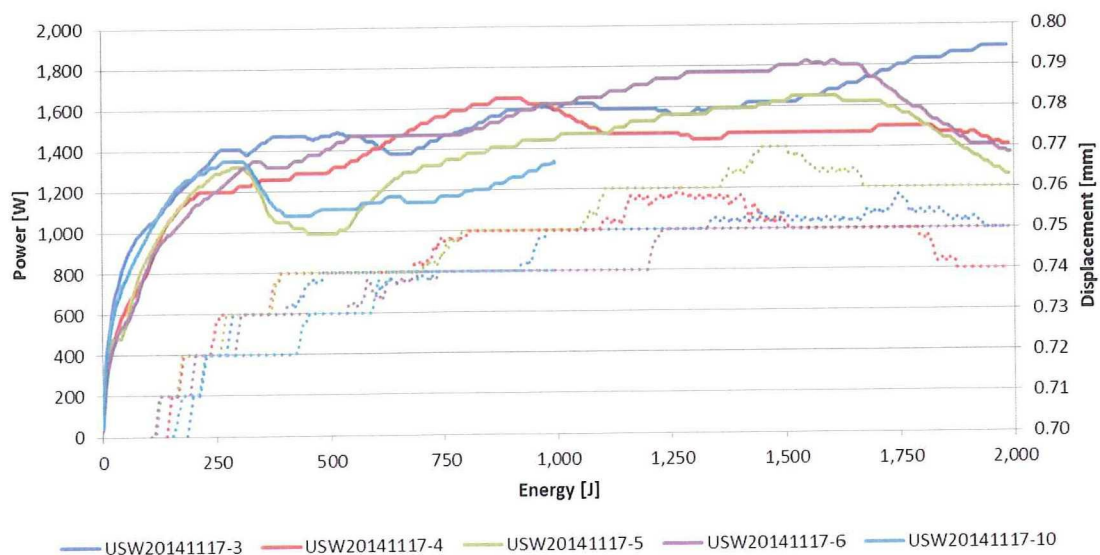


Figure 6-6: Power (solid) and displacement (dotted) curves of five samples with integrated triangular ED ribs. The scale of the displacement has been adjusted to study the 'ceiling' (see Figure D-2 for normal scale).

The displacement curve does not experience an abrupt ceiling, as was the case with flat EDs and ED strips, but it keeps increasing until a local maximum is obtained at a relatively high energy value. Because of the absence of an abrupt displacement ceiling, the methodology proposed by Villegas (2013a) might be applicable again. Further research should focus on this.

A welded sample clip with integrated EDs can be seen in Figure 6-7. Squeeze out of PEKK and fibers is observed near the edge of the sample.



Figure 6-7: Sample clip USW141117-03 welded with 2,000 [J]. The triangular EDs are integrated in the upper sample. Squeeze out of ED and fibers is observed.

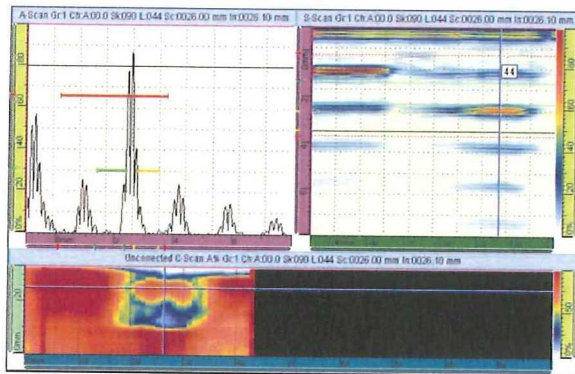


Figure 6-8: PA scan of sample clip USW141117-03 welded with 2,000 [J]. The weld quality is excellent near the upper edge, but poor near the lower edge.

In Figure 6-8, a PA scan of sample clip USW141117-03 indicates that the weld has a) an excellent quality near the upper edge, as a strong signal returns from the back of the lower composite (A, S and C-scan), but b) a poor quality near the lower edge, as the signal is almost lost (S and C-scan). The orientation of the PA scan is similar to the orientation of the sample in Figure 6-7. There are no traces of the original ED ribs in the S or C-scan, and therefore it seems that the three squeeze flows (three ribs) have merged. Further research is required to find the optimal welding energy and to see if a good quality level can be obtained throughout the whole weld.

6.3. Recommendations

This chapter discussed a production method meant to integrate triangular EDs into composites: the elements are consolidated by a) vacuum-bagging the product and b) subsequently consolidating it in an autoclave. The conclusion is that this method is effective in integrating triangular ED ribs into composites. The only downside of the method is that the fibers in the outer plies are lightly disturbed, but by optimizing the production process and the ED design, it is most likely possible to minimize the disturbance. Moreover, the abrupt displacement ceiling was not observed in the welding data, so the methodology of Villegas (2013a) might be applicable again. Therefore, it is strongly recommended that the integration of triangular EDs into CFRTPCs is further investigated. A study should be performed into the optimization of the ED configuration in order to: 1) minimize the disturbance of the fibers, and 2) optimize the joint strength. Moreover, it should be investigated if the methodology of Villegas (2013a) is applicable again and displacement can be used as a more consistent driver. Furthermore, a study similar to the one performed in chapter 0 should be conducted to determine the development of the squeeze flow and weld quality as a function of the applied energy level. It is expected that many similarities exist between the using integrated triangular EDs in a) the USW of plastics versus b) the USW of CFRTPCs. Therefore, the associated literature should be carefully reviewed.

7. Clamping & Sequential Welding

In order to weld the orthogrid panel, a sequential spot welding approach is required. A challenge of the sequential welding process is that welding conditions change for every subsequent weld, as noticed by Lu et al. (1991). For instance, whereas the upper composite is free to vibrate when making the first weld, it is fixed on one-side by the first weld when making the second weld. This issue is illustrated in Figure 7-1, where it can be seen that the welded section on the right 'clamps' the upper composite to the lower one, while the section on the left still has to be welded. It is expected that the spacing between subsequent welds has a significant influence on the USW process, and it is highly likely that there is a minimum spacing value below which no proper welds can be obtained. Therefore, it is important that effects of the distance between a weld and a 'clamped' spot on the USW process are thoroughly investigated.



Figure 7-1: A schematic drawing of the welding interface of a sequential weld. The section on the left side has not been welded yet, whereas the right section has been. The grey rectangles represent EDs.

Moreover, the two composites have to be tightly clamped together to prevent them from moving during the USW process, as can be seen in, for instance, Figure 2-9 – the fuselage frame fixture (Z51430). It is expected that clamping the two components also has a substantial influence on the USW process. Two factors that are expected to have a major influence on the process are: a) the clamping force, and again, b) the clamping distance. In this chapter, the relation between these two factors and the USW process is examined. In section 7.1, experiments are conducted on single-side clamped samples. Next, in section 7.2, experiments are performed on double-side clamped samples. Finally, in section 7.3, recommendations are presented.

7.1. Welding of single-side clamped samples

In this section, ASTM D1002 samples are welded using the Z51414 fixture in the single-side clamping configuration, as presented in section 2.3.3 and illustrated in Figure 7-2. The experiments have been performed at Aeson B.V. using a 2,000 [W] version of the Dynamic 3000 and sonotrode 1. Furthermore, the samples are welded using a flat ED with a thickness of 0.25 [mm], a peak-to-peak amplitude of 70.4 [μm], a welding force of 500 [N], and a displacement of 0.11 [mm] as the welding driver. These settings are similar to the ones used when welding single lap shear samples with flat EDs in the 9109 jig, as described in section 3.1. However, the amplitude is slightly lower (70.4 [μm] instead of 72.6 [μm]), because a different sonotrode is used and the amplitude can only be adjusted in increments of 5 [%]. However, the difference is assumed to be (almost) negligible. Moreover, it should be noted that flat EDs are used again, as they prove to work well when welding ASTM D1002 samples.

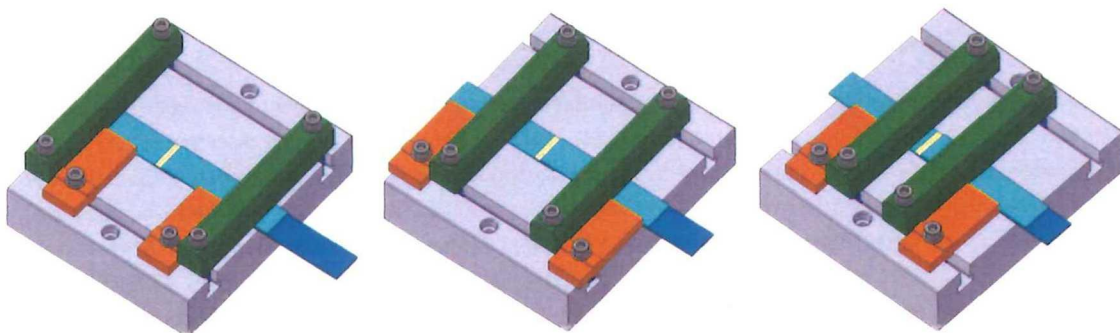


Figure 7-2: The position of the clamps is varied when welding the single-side clamped ASTM D1002 samples to investigate the effects of the clamping distance on the USW process and weld quality. From left to right: the clamps are placed at a distance of 6 [cm], 3.5 [cm], and 1.5 [cm] w.r.t. the centerline.

The distance between the clamps and the centerline, varies between: 6 [cm], 3.5 [cm], and 1.5 [cm], as illustrated in Figure 7-2. Moreover, the clamping force is varied by tightening the bolts with either 2.5 [Nm] or 7.5 [Nm]. Per combination of the clamping force and the distance, five samples are welded and subsequently, single lap shear tests are performed on the Zwick/Roell 100 [kN] universal testing machine. The welding data of all thirty samples can be seen in Figure E-1 to Figure E-6. The statistics of a) the energy, b) maximum power, c) welding time, and d) LSS value, are illustrated for a torque of 2.5 [Nm] and 7.5 [Nm] in Figure 7-3 and Figure 7-4, respectively.

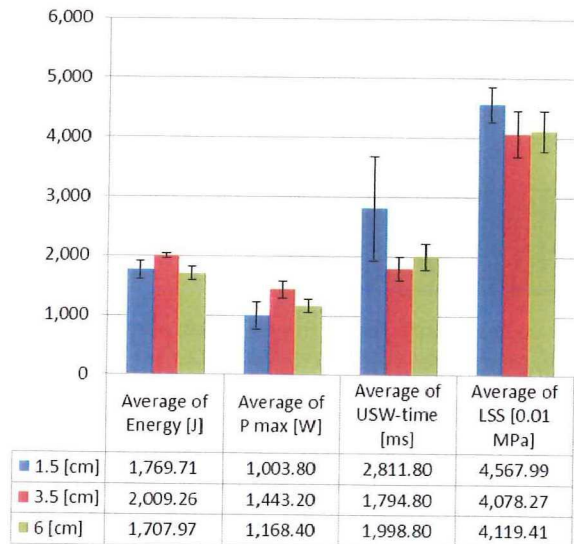


Figure 7-3: Averages and standard deviations (error bars) of welding data of single-side clamped ASTM D1002 samples clamped at 1.5, 3.5, or 6 [cm] distance from the centerline with rubber pads and a torque of 2.5 [Nm] per bolt. Welding settings: 70.4 [μm]; 500 [N]; 0.11 [mm].

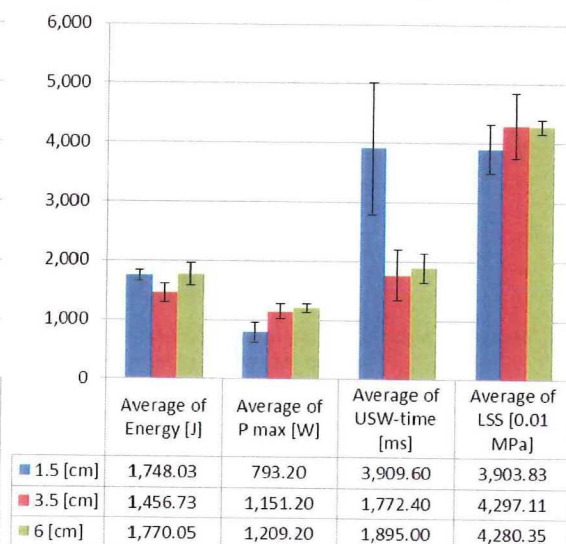


Figure 7-4: Averages and standard deviations (error bars) of welding data of single-side clamped ASTM D1002 samples clamped at 1.5, 3.5, or 6 [cm] distance from the centerline with rubber pads and a torque of 7.5 [Nm] per bolt. Welding settings: 70.4 [μm]; 500 [N]; 0.11 [mm].

In both Figure 7-3 and Figure 7-4, it can be observed that when the samples are clamped very closely to the sonotrode at 1.5 [cm] from the centerline, the average maximum power is substantially lower and the average welding time is noticeably higher. Furthermore, by comparing the two figures, it can be seen that this effect becomes even greater as the clamping force is increased. The hypothesis is that the closer and harder the composites are clamped, the stiffer the area to be welded becomes. Consequently, the USW machine has more difficulties passing on the vibrational energy to the samples. This might explain why the power curves of the samples clamped at 1.5 [cm], in Figure E-3 and Figure E-6, are relatively low and flat compared to those of the other samples. Further research should be conducted to confirm this hypothesis and investigate if there is a bottom threshold for distance and an upper threshold for the clamping force outside of which proper welds can no longer be obtained. It is probably better to use a low clamping force rather than high one, as long as the force is sufficient to keep the components in place during the USW process.

The clamping force mainly has an effect on the samples that are clamped closely to the weld zone. Samples clamped further away from the weld zone, most likely, have enough flexibility in the direction of the vibrations of the sonotrode to minimize the effect of the clamping force. It is unknown why superior LSS values were obtained when clamping at 1.5 [cm] with a low force, whereas inferior results were obtained when clamping at 1.5 [cm] with a high force. Moreover, it is unknown why, when compared to samples clamped at other distances, samples clamped at 3.5 [cm] require on average more energy when clamping with a low force, while they require less energy when clamping with a high force. This can be 1) a coincidence or 2) the result of complex vibrational dynamics. The experiments should be repeated and/ or compared to a finite element method (FEM) analysis to see if these results can be reproduced.



Figure 7-5: The related fracture surfaces of USW140827-05 clamped at 6 [cm] and with a torque of 2.5 [Nm]. There are 1) two resin rich areas in the middle; 2) fiber squeeze-out near the side edges; and 3) voids on one side of the weld.

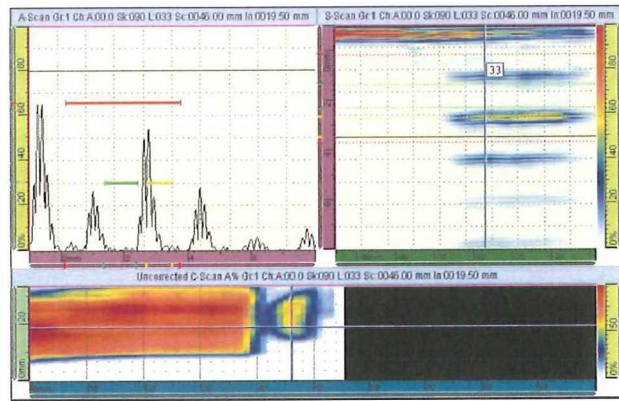


Figure 7-6: The PA scan of USW140827-05 clamped at 6 [cm] and with a torque of 2.5 [Nm]. The left section of the C-scan represents the sample, whereas the right section represents the weld. The middle of the weld has a good joint quality. However, the quality is poor near the edges of the weld.

In Figure 7-5, the fracture surface of a sample, clamped at 6 [cm] from the centerline and tightened with a torque of 2.5 [Nm], is presented. It is observed that the center shows a nice and 'clean' fracture with two small resin rich areas. However, the side edges show fiber squeeze-out and one side of the weld contains many small voids. In the overview of the fracture surfaces in Figure E-7 and Figure E-8, it is observed that all samples clamped at 6 [cm] have a similar fracture surface, where the voids and the resin rich areas are located at more or less the same locations. The samples clamped at 3.5 [cm] also show similar fractures surfaces, but the area that contains voids is smaller (Figure 7-7). Almost no voids and no resin rich areas are visible at the fracture surface of the samples clamped at 1.5 [cm]. However, the samples clamped at 1.5 [cm] seem to show a more intense first ply failure (Figure 7-8). The hypothesis formulated to explain these differences is: the fracture surfaces vary as a function of the clamping distance, because it is expected that a) the flexibility of the upper sample, and b) the slope of the clamping distance, because it determines how easily vibrational energy is transferred to the composites, whereas the slope is expected to contribute to these results because it basically determines the distribution of the welding pressure, which is directly related to the dissipation of energy. The latter reason might explain why one side consistently displays voids, while the other side exhibits proper weld quality.



Figure 7-7: The related fracture surfaces of USW140805-06 clamped at 3.5 [cm] and with a torque of 2.5 [Nm]. There are 1) resin rich areas; 2) fiber squeeze-out near the side edges; and 3) voids on one side of the weld.

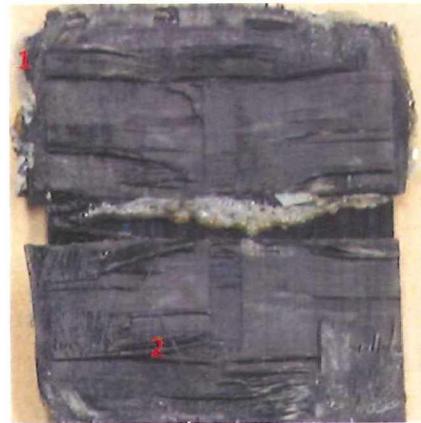


Figure 7-8: The related fracture surfaces of USW140804-20 clamped at 1.5 [cm] and with a torque of 2.5 [Nm]. The sample shows 1) fiber squeeze out, and 2) intense first ply failure.

When comparing fractures surfaces of the samples clamped with 2.5 [Nm] and 7.5 [Nm] tightened bolts, respectively (see Figure E-7 and Figure E-8), no obvious differences are observed. Therefore, it is expected that whereas the clamping distance bears substantial influence on the weld quality, the clamping force only has a limited effect.

Moreover, NDT scans of the samples (see Figure 7-9 to Figure 7-12), are analyzed. Note that the samples clamped at 3.5 [cm] are not shown, as only the extremes are analyzed. The C-scans of the samples clamped at 3.5 [cm] can be seen in Figure E-9 and Figure E-10.

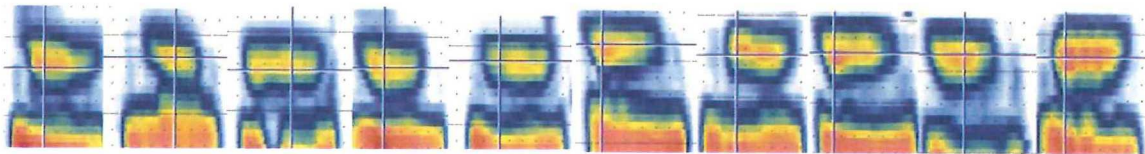


Figure 7-9: The C-scans of samples clamped at 6 [cm] and with a torque of 2.5 [Nm].

Figure 7-10: The C-scans of samples clamped at 6 [cm] and with a torque of 7.5 [Nm].

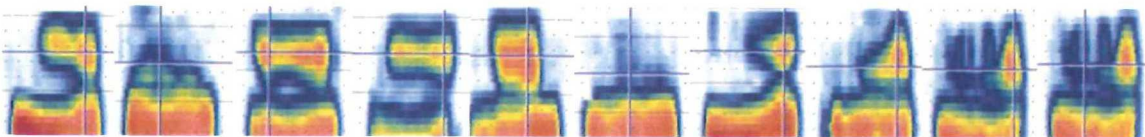


Figure 7-11: The C-scans of samples clamped at 1.5 [cm] and with a torque of 2.5 [Nm].

Figure 7-12: The C-scans of samples clamped at 1.5 [cm] and with a torque of 7.5 [Nm].

It is observed that the welds of the samples clamped at 6 [cm] are relatively consistent. The quality of these welds seems to be slightly better for the ones where the bolts are tightened with 7.5 [Nm], as the returning signals are generally stronger in Figure 7-10 than in Figure 7-9. This observation was also made in the LSS data presented in Figure 7-3 and Figure 7-4. The welds of the samples clamped at 1.5 [cm], on the other hand, are far from consistent, as can be seen in Figure 7-11 and Figure 7-12. By comparing these figures, it is seen that, for samples clamped at 1.5 [cm], the weld quality is superior when a low clamping force is applied. Again, this observation is supported by the LSS data. It is noteworthy that the samples clamped at 1.5 [cm] with 7.5 [Nm] generally have a small area where a strong signal returns on the right, while the remaining area, most likely, has a poor bond quality as the signal is lost. A possible explanation for this pattern could be the fact that the clamps applied more pressure on one side than on the other. This is actually likely as each clamp has to be individually tightened at both sides. Although a torque wrench was used, it was observed during the experiments that the clamps were not always perfectly aligned with respect to the composite. It is considered that the use of rubber pads allowed for this misalignment.

Next, the welding data of samples clamped at 6 [cm] with a torque of 2.5 [Nm] is studied (see Figure 7-13), and subsequently compared to the data of the ASTM D1002 samples welded with the 'ideal' 9109 jig, as presented in section 3.1. This comparison is interesting as it directly shows the influence of clamping: the samples welded in 9109 jig can move freely in the vertical direction, whereas the clamped ones obviously cannot. It can be seen that both the power and displacement curves of the clamped samples actually show a similar pattern to the ones observed by (Villegas 2013a): 1) the power curves ramp up to a first peak; 2) the displacement suddenly increases when a local minimum in the power curve is reached; and 3) the power curves approach a second peak. A very interesting observation is that the optimal displacement value, determined when welding using the 9109 jig, seems to consistently also provide the optimum for the clamped samples: the USW process stops vibrating at approximately the same moment as the second peak in the power curve is reached. This implies that the methodology of Villegas (2013a) can also be applied to clamped ASTM D1002 samples using flat EDs, and that the optimal displacement value is indeed independent of the fixture.

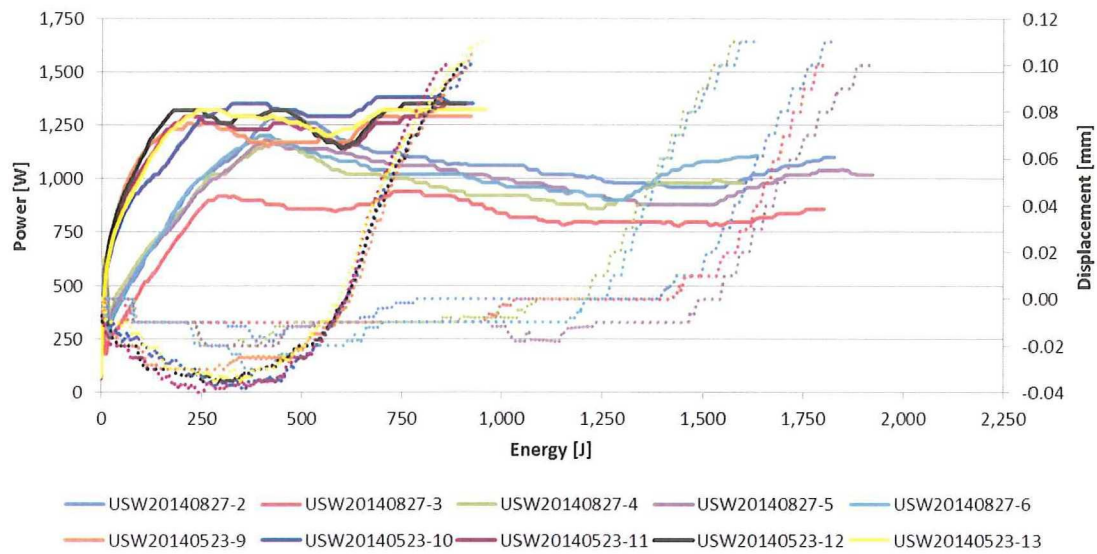


Figure 7-13: Power (solid) and displacement (dotted) curves of ASTM D1002 samples with 0.25 [mm] flat EDs, welded using the Z51414 fixture (1-5) and the 'ideal' 9109 jig (6-10) under the same conditions: 70.4 - 72.6 [μm]; 500 [N]; 0.11 [mm].

Furthermore, in Figure 7-13, it is observed that the clamped samples require more energy before they melt and become a good weld. This was expected because the upper composite, most likely, absorbs a substantial amount of energy as it is clamped and needs to vibrate. Moreover, more deviation is present in the energy curves recorded for the clamped samples. Again, such deviation is to be expected as most probably some misalignment between the samples and the clamps is already present when the Z51414 fixture is used, whereas the 'ideal' 9109 jig offers a consistent alignment.

7.2. Welding of double-side clamped samples

In this section, longer lap shear samples (25.4 [mm] x 203.2 [mm]) are welded using the Z51414 fixture in the double-side clamping configuration, as presented in section 2.3.3 and illustrated in Figure 7-14. The experiments have been performed at TU Delft with sonotrode 3. Furthermore, the samples are welded using two ED strips with a width of 2 [mm], a spacing of 3 [mm], and a thickness of 0.25 [mm]. Flat EDs are not used as these EDs have too few free edges, as illustrated in Figure 1-11. Similar settings to those of the clips with ED strips are used: a) a peak-to-peak amplitude of 51.8 [μm]; b) a welding force of 1,500 [N]; and c) an energy level of 750 [J] as the welding driver.

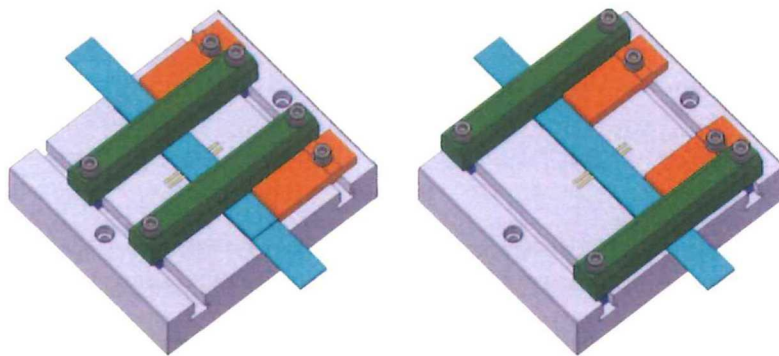


Figure 7-14: The position of the clamps is varied when welding the double-side clamped long lap shear samples to investigate the effects of the clamping distance on the USW process. The clamps are placed at a distance of 6 [cm] (left) and 2.1 [cm] (right) w.r.t. the centerline.

Five samples are welded with a clamping distance of 6 [cm] and five are welded with a distance of 2.1 [cm], as illustrated in Figure 7-14. A value of specifically 2.1 [cm] is chosen, since this is as close as possible to the sonotrode, which has a diameter of 4 [cm]. The bolts of the clamps are tightened by 2.5 [Nm]. Moreover, single lap shear tests are performed on the Zwick/Roell 100 [kN] universal testing machine. The welding data can be seen Figure 7-16. The statistics of a) maximum power, b) welding time, and c) LSS, are illustrated in Figure 7-15.

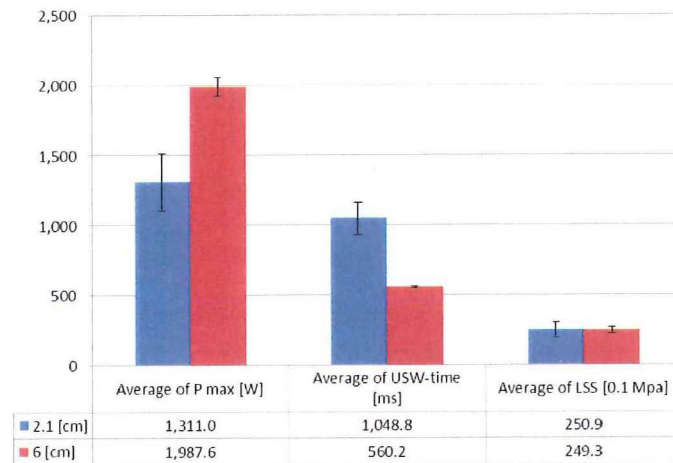


Figure 7-15: Averages and standard deviations (error bars) of welding data of double-side clamped long lap shear samples with two ED strips clamped at 2.1 [cm] or 6 [cm] distance from the centerline with rubber pads and a torque of 2.5 [Nm] per bolt. Welding settings: 51.8 [μ m]; 1,500 [N]; 750 [J].

Figure 7-15 illustrates that when the samples are clamped closely to the sonotrode at 2.1 [cm], the maximum power is substantially lower and the welding time is considerably longer than when the samples are clamped far away from the sonotrode at 6 [cm]. Moreover, the deviations of the samples clamped at 2.1 [cm] are also larger. The exact same observations were made when analyzing the results of the single-side clamped samples.

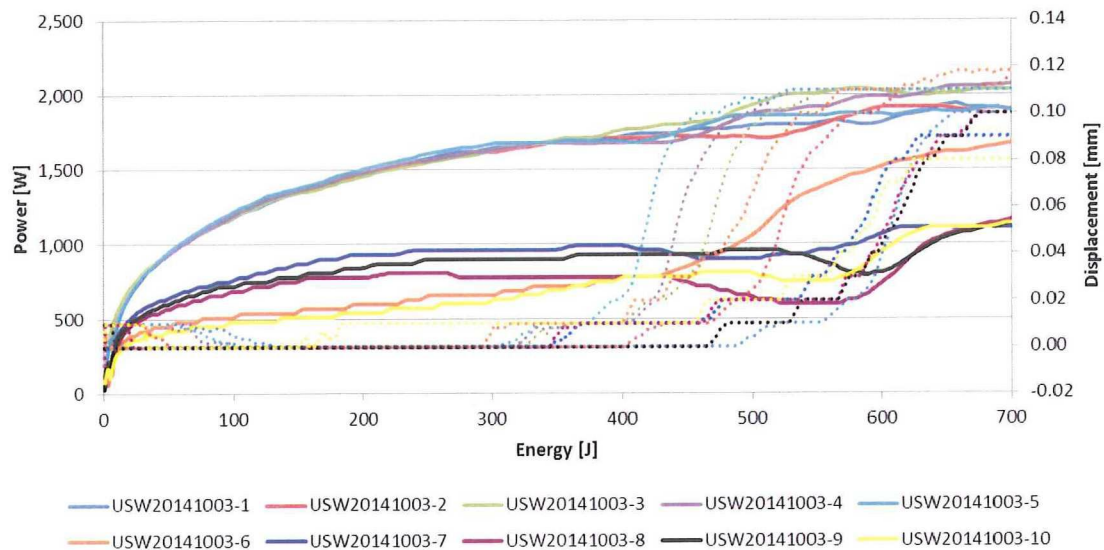


Figure 7-16: Power (solid) and displacement (dotted) curves of double-side clamped long lap shear samples with two ED strips clamped at 6 [cm] (1-5) or 2.1 [cm] (6-10) distance from the centerline with rubber pads and a torque of 2.5 [Nm] per bolt. Welding settings: 51.8 [μ m]; 1,500 [N]; 750 [J].

In Figure 7-16, it can be observed that the power curves of the samples clamped at 2.1 [cm] from the centerline are much lower than the power curves of the others. Most likely, the USW machine has problems passing on the vibrational energy because the composites are clamped very tightly. This explains why the process takes longer

than when the samples are clamped further away. Furthermore, it can be seen that the EDs of the samples clamped closely to the sonotrode generally need more energy before they melt. Most likely, this is the case because more vibrational energy goes into the fixture of tightly clamped composites.

7.3. Recommendations

In this chapter, the effects of clamping on the USW process were investigated. The experiments were conducted in two setups: 1) a single-side clamped, and 2) a double-side clamped configuration. In the first setup both the clamping force and distance were varied, whereas in the latter setup only the clamping distance was. In both setups, it was observed that when the samples are clamped closely to the sonotrode or weld area, the USW machine transfers the vibrational energy to the composites less effectively. As a result, the USW process takes more time. Moreover, it was observed that the deviations in the process and the weld quality increase considerably. It is expected that these results are due to the fact that, when samples are clamped closely to the sonotrode, the system is more sensitive to small misalignments because it has less flexibility to correct for them. In the experiments conducted on single-side clamped samples, it was observed that the clamping force mainly influences the process when the clamps are positioned near the sonotrode. If this is the case, a higher clamping force makes it even more difficult for the USW machine to transfer vibrational energy to the composites. It is strongly recommended that a FEM model is made to simulate the vibrations in the composites and the fixture. This might provide more insights into how clamping affects the vibrations and thus the USW process.

These results do not only provide more information about clamping, but possibly also about sequential welding: when making a sequential weld, the previous welds basically 'clamp' the composites. The experiments presented in this chapter indicate that sequential welding is probably possible: successful welds could be obtained with tightly clamped together composites. Future research should point out how closely to each other sequential welds can be placed. Moreover, it should be investigated if the stiffness of the composites has an effect on this minimum distance. Finally, it is recommended that these experiments are conducted in a real sequential setup.

8. Fuselage Frame

In this chapter, it is described how the fuselage frame was welded to a section of the orthogrid panel. The welding of the fuselage frame is highly experimental and the goal of this activity is to demonstrate the potential of the USW technique to sequentially weld larger CFRTPC components. The analysis of the resulting welds lies outside the scope of the research project, and is therefore not performed. Moreover, only one frame is welded. Since demonstration purposes require it to be intact, its structural performance was not tested.

In section 1.2.3, a number of challenges were identified when it comes to welding a fuselage frame to an orthogrid panel in an industrial setting. Since these challenges lie outside the scope of this project, simplifications are made. A section with a width of 1 [dm] is sawn out of the orthogrid panel (see Figure 8-1), so that it fits under the Dynamic 3000 and the skin panel does not interfere with the sonotrode. On a full scale orthogrid panel, the fuselage panel has to be welded under an angle with a chamfered sonotrode to prevent the sonotrode from interfering with the orthogrid panel, as illustrated in Figure 1-10.

The fuselage frame and the orthogrid panel are clamped onto the Z51430 fixture, as explained in section 2.3.4 and illustrated in Figure 8-1. The two components are kept in place by two Destaco toggle clamps, which can be simply opened and closed by pulling and pushing the red handles, respectively. A side-view of the setup is illustrated in Figure G-2 and a front-view in Figure G-3. A photo of the real setup can be seen in Figure G-4.

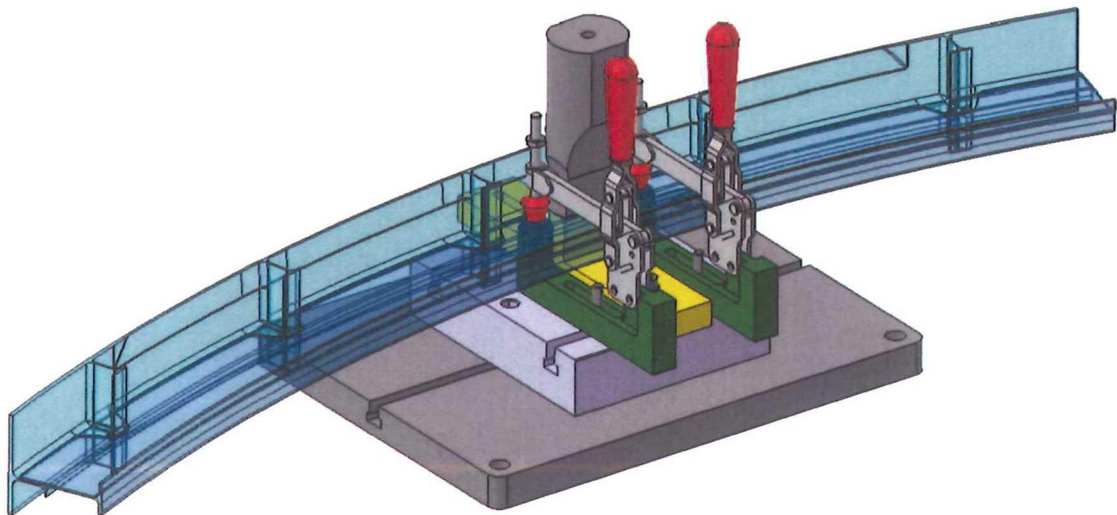


Figure 8-1: Isometric view of the Z51430 fixture to weld the fuselage frame to the orthogrid panel.

The fuselage frame is welded with sonotrode 2, a peak-to-peak amplitude of 52.8 [μm], a force of 1,500 [N], and energy as the welding driver. The first three spots are welded with 1,000 [J]. However, since in these initial welds the fuselage frame was being damaged at the edges, the remaining spots are welded with 800 [J]. Two ED strips with a thickness of 0.25 [mm], a width of 2 [mm], and a spacing of 3 [mm] are used per spot. The ED strips are taped to the stiffener of the orthogrid panel as illustrated in Figure 8-2.

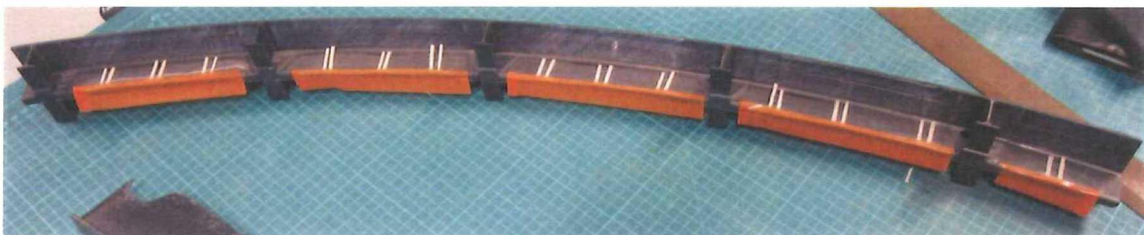


Figure 8-2: Two ED strips with a thickness of 0.25 [mm] and a width of 2 [mm] per weld are taped to the orthogrid panel.

The top and bottom view of the resulting fuselage frame welded to the orthogrid panel can be seen in Figure 8-3. The red numbers indicate the locations and sequence of the spot welds. An inside-out approach is used, as this is believed to minimize misalignment of the frame with respect to the skin panel. The associated welding data is illustrated in Figure G-5.



Figure 8-3: The fuselage frame welded to a section of the orthogrid panel. Upper: top-view of the fuselage frame; lower: bottom-view of the fuselage frame. The red numbers indicate the locations and sequence of the spot welds. See Figure G-1 for a larger version of this picture.

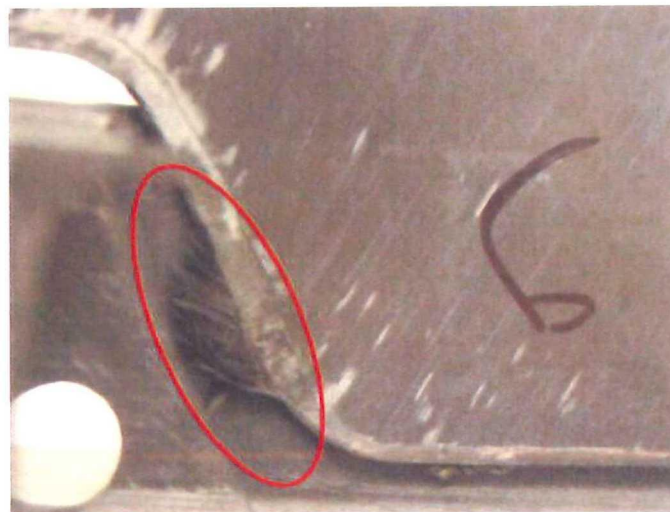


Figure 8-4: Damage to the fuselage frame as indicated with the red ellipse.

The fuselage frame seems to be fixed quite well to the orthogrid panel. However, a structural test would have to be performed in order to quantify this aspect. As observed in Figure 8-4, there are some small damages at the edges of the fuselage frame. As suggested in chapter 0 and 5, this can probably be prevented with a different ED configuration: it was noticed that the upper components have a large chance to be damaged at the edges that are not supported by an ED.

The first known demonstrator product ultrasonically welded using a sequential approach is manufactured. It is strongly recommended that the research on sequential USW is continued as the process is thought to have a huge potential for the mass assembly of larger structural components.

IV – Conclusions & Recommendations

9. Conclusions

In this research, an effort has been made to identify the potential and feasibility of USW of CFRTPCs (CF/ PEKK) in an industrial setup and specifically within the aerospace industry. Both the potential and feasibility were tested by welding two demonstrator products: 1) spot welded system clips to a rib, and 2) a sequentially welded fuselage frame to a section of the orthogrid panel.

First, clips were welded. The following results were derived from welding samples in an experimental setup: a) a new tooling concept – in which the clips were not clamped but merely kept in position by alignment plates – was successfully used to weld sample clips; b) a good ED configuration – the use of multiple slender ED strips – was discovered; and c) an ‘optimal’ energy level – to consistently reproduce high quality welds – was found. Subsequently, these results were used to design the setup for welding the first demonstrator product: CF/ PEKK clips were welded to a rib. The first demonstrator was a success that confirmed the feasibility of welding CFRTPC clips to larger CFRTPC structures. Moreover, a study performed by the cost engineering department of Fokker Aerostructures pointed out that it is 35 [%] cheaper to ultrasonically weld a composite clip (in case the ED is integrated) than to rivet an aluminum equivalent (Hoogenboom, 2014). Not to mention the weight savings that welded composite clips, most likely, offer in comparison to riveted aluminum clips. Because on a large passenger plane there are thousands of small clips (and brackets) to be found, spot welding of small CFRTPC components has a huge potential. It is recommended that efforts to certify USW of small CFRTPC components are made soon, as this thesis indicated that the USW process is already mature enough: high quality welds can be obtained consistently.

Next, the fuselage frame was welded. This demonstrator is really pushing the frontiers of current possibilities, because no known CFRTPC components of this size have ever been ultrasonically welded using a sequential approach. Before the second demonstrator was welded, fundamental research was performed on clamping of the upper sample as: a) the fuselage frame had to be clamped to the orthogrid panel, and b) it was believed that a first spot weld basically creates a clamped situation for the consecutive weld. It was observed that successful welds can still be made when the composites are tightly clamped, although the process does indeed become more challenging. Subsequently, a dedicated fixture for the fuselage frame was designed and produced. Using this fixture, the frame was successfully welded to a section of Fokker’s orthogrid panel. Although the joints are far from perfect, the second demonstrator indicates that it is possible to ultrasonically weld CFRTPC structures using a sequential approach. If the sequential USW process is perfected, it stands to have a huge potential for industry wide application. Therefore, it is stressed that the research on sequential USW should be continued.

In addition to or as part of welding the demonstrators a number of interesting observations were made and/ or hypotheses were formulated:

- Plunge welded square flat EDs did not provide satisfactory results when welding clips, because a) they were difficult to place, b) damage occurred at the clips’ edges, and c) an abrupt ceiling in the displacement was observed. Such a ceiling prevents the use of displacement as the welding driver, which renders the methodology proposed in Villegas (2013a) as inapplicable to this research. It is expected that the clips are damaged at the edges because they were not fully supported by the ED and therefore could resonate, which resulted in the dissipation of heat in the clips’ edges.
- Instead, multiple slender ED strips were used to weld clips. Experiments pointed out that: a) they were easier to place and b) no damage occurred at the clips’ edges anymore. However, the displacement ceiling was still present, with the improvement that the values at which it occurred were slightly higher than before.
- When multiple ED strips are used with a small enough spacing between them, their squeeze flows are able to merge and form one strong bond. However, this moment could not be recognized in the welding data as Benatar & Gutowski (1989) indicated.

- It is probably better to weld with multiple EDs instead of one large flat ED, because welds of similar size can be obtained while using less power, time, and thus energy. Moreover, a lower welding force needs to be applied to obtain a certain welding pressure, due to the smaller initial surface area of the ED strips.
- Cross-sectional microscopy of sample clips welded at various energy levels showed that small pieces of unmelted ED are found near the flow fronts of the squeeze flow of molten ED. Since the size of these pieces is exactly equal to the size of the gap that remains between the two composites to be welded after the displacement ceiling has been reached, it is expected that these unmelted pieces cause the abrupt displacement ceiling because they block the downward displacement of the sonotrode. The hypothesis formulated to explain the presence of the unmelted pieces is: these small pieces of ED remain because the ED is not melting uniformly. Most likely, the ED is not melting uniformly as microscopy pointed out that the five layers of 50 [µm] PEKK film had not been well consolidated during the manufacturing process. When welding ASTM D1002 samples, the ceiling does not occur because all edges of the ED are free and the unmelted pieces are squeezed out as soon as the ED is being squeezed out.
- It was confirmed that the substrate material starts melting after the second peak in the power curve is reached as indicated by Villegas (2013a). Therefore, this peak indicates the optimal state of the weld. Unfortunately, the location of the second peak varies in terms of energy.
- Using the 'optimal' energy level, high quality welds were consistently obtained. It should be noted that a conservative approach was preferred when establishing the 'optimal' energy level value: close to the second peak, the first signs of degradation were already observed in the materials.
- The hypothesis is formulated that: because gasses are formed when PEKK degrades, it is inferred that the material at the welding interface starts degrading when the displacement reduces and the force increases after the displacement ceiling has already been reached. These gasses released in the PEKK degradation result into an increase in volume and therefore exert pressure on the sonotrode, which as a result is slightly pushed back.
- When consolidating vacuum bagged composites in an autoclave, triangular EDs can be successfully integrated by adding additional films of pure thermoplastic resin on top of the laminate and replacing the cover plate with a mold that contains triangular grooves.
- Promising results, in terms of weld quality and welding data, were obtained when welding samples with integrated triangular EDs. The fact that no abrupt ceiling was observed implies that the methodology suggested by Villegas (2013a) might be applicable again.
- The effects the distance between clamps and the weld area has on the USW process were investigated. The experiments were conducted in two setups: 1) a single-side clamped, and 2) a double-side clamped configuration. In both setups, it was observed that, when the samples are clamped closely to the weld area, the USW machine transfers the vibrational energy less effectively to the composites. As a result, the USW process takes more time. Moreover, it was observed that the deviations in the process and the weld quality increase considerably. It is expected that these results are due to the fact that, when samples are clamped closely to the sonotrode, the system is more sensitive to small misalignments because it has less flexibility to correct for them.
- In the single-side clamped experiments, it was observed that the clamping force mainly influences the process when the clamps are positioned near the weld area. If the clamps are located closely to the weld area, a higher clamping force makes it even more difficult for the USW machine to transfer vibrational energy to the composites.

10. Outlook

This chapter provides an outlook of the large-scale application of USW of CFRTPCs in the aerospace industry. This research project indicated that the USW technique offers the possibility to spot-weld small CFRTPC components – such as clips and brackets that are used in the thousands on a passenger plane – to a CFRTPC structure in only 5-6 seconds. Moreover, this thesis pointed out that, in the near future, USW can probably be used to spot weld larger CFRTPC components using a sequential approach. Although a number of continuous welding techniques are currently available for joining larger CFRTPC components – such as induction welding and to some extent resistance welding, sequential USW is expected to be a superior alternative because of the short duration it requires to make a weld. The following methods to apply USW in an industrial setting are proposed:

- 1) Small CFRTPC components can be spot welded to flat small or mid-sized sub-assemblies, such as a rib, using a fixed machine like the Dynamic 3000. In this case, the components have to be manually manipulated and clamped onto an anvil by an operator. This method is basically similar to the one presented in Figure 5-16. However, specialized tooling should support the operator in positioning and clamping the components faster and more consistently. For every subsequent weld, the components have to be repositioned.
- 2) A low-cost automated method to (sequentially) weld CFRTPC components to flat mid or large-sized sub-assemblies is to place an actuator and a welding stack onto a simple Cartesian robot, as illustrated in Figure H-1. This robot can move over the in-plane axes and position the welding stack. Subsequently, the actuator can press the sonotrode onto the composites with a certain welding pressure. If the Cartesian robot is also able to rotate over its in-plane axes, it can also be used to weld slightly curved components. The composites are clamped onto an anvil.
- 3) To (sequentially) weld CFRTPC components to more complex mid or large-sized structures, a six-axis robot arm that holds a welding stack and an actuator can be used, as illustrated in Figure H-2 and Figure H-3. If the robot arm needs more range, it can be placed on rails, as can be seen in the same figures. Dependent on the shape of the larger structure, a pre-installed jig or a C-frame, which is attached to the robot (see Figure 1-10), can be used to provide a counterforce to the sonotrode.

The positioning of EDs before welding is no longer a concern as they can already be integrated into one of the composites to be welded. Moreover, the EDs are used as a shim between the two composites to correct for deviations.

In the aerospace industry, adhesive bonds are scanned using NDT technology to ensure that proper joints are obtained. This is very time-consuming and therefore expensive. Fusion bonds also have to be scanned using NDT techniques. Fortunately, USW offers the possibility for 'in-situ' monitoring by analyzing the evolutions recorded in the welding data. In the ultrasonic welding line of the future, computers will 'in-situ' study the welding data and interrupt, or if possible correct, the welding process if deviant evolutions in the welding data are observed. In this way, NDT post-scanning no longer has to be performed for the non-critical components – such as system clips. Structural bonds will always have to be scanned though.

11. Future Research Recommendations

This thesis indicated that USW has a huge potential to become a preferred method for joining CFRTPCs in the aerospace industry. Therefore, it is strongly recommended that research into using USW of CFRTPCs is continued and efforts are made to certify the first industrial applications. A number of areas for future research are identified:

- The welded fuselage frame demonstrator pointed out that it is possible to ultrasonically weld larger CFRTPC components using a sequential approach. The process is, however, not yet fully understood. Given its large potential, it is strongly recommended that the research on sequential ultrasonic welding is continued. First of all, it should be investigated which ED configuration is best suited for sequential USW. Subsequently, it should be established if a) a minimum distance has to exist between every consecutive weld, or b) the welds can overlap. Next, it should be researched if the stiffness of the composites has an effect on this distance. Finally, it should be investigated if there is a method to use the same settings for every consecutive weld. Lu et al. (1991) suggested using clamps with rubber pads to minimize the zone affected by the vibrations, so that the circumstances and therefore, the settings would become more similar.
- The results derived from this research do not only provide more information about clamping, but possibly also about sequential welding: when making a sequential weld, the previous welds basically 'clamp' the composites. The experiments presented in this thesis indicate that sequential welding is probably possible: successful welds could be made with tightly clamped together composites. Future research should point out how closely sequential welds can be placed next to each other. Moreover, it should be investigated if the stiffness of the composites has an effect on this minimum distance. Finally, it is recommended that these experiments are conducted in a real sequential setup.
- It is recommended that research on the integration of the EDs is continued, since it is too time-consuming to place the EDs after the composites are consolidated. Moreover, due to their small size, separate EDs are likely to also be a source of inconsistency in the weld size and quality. In this research project, it was already demonstrated how triangular EDs can successfully be integrated into a composite laminate, which is consolidated in the autoclave while being vacuum bagged. A suggestion is that the configuration of the triangular EDs is improved so that fiber distortion in the outer plies is minimized and the weld quality is optimized.
- In order to allow a larger number of aircraft components to be ultrasonically welded, welding under a small angle needs to be possible. Therefore, it is recommended that a first effort is made to weld composites under an angle by using a chamfered sonotrode. When designing a conceptual welding tool, it was observed that, at the very least, an angle of 10 [°] would probably be required to access difficult-to-reach spots.
- Significantly high welding forces were used, as they delivered good results in early experiments. Building on these good results, welding parameters were kept constant throughout the rest of the research in order to be able to compare the outcomes of the various experiments. It is recommended that parameters used to weld clips are reassessed in the final welding configuration and an optimal setting and/ or processing window is determined.
- The USW process focuses energy dissipation at the welding interface, which makes USW an extremely fast welding technique. A possible downside of the implicit rapid cooling is that the resin at the welding interface becomes amorphous, as could be observed in the fracture surfaces. It should be investigated what the consequences of having an amorphous welding interface are. If the amorphous interface proves to be problematic, an effort should be made to make to crystallize the interface.
- While welding the clips, a displacement ceiling was observed. This prevents the ED from being further squeezed out, causes a gap between the two composites, and prevents the use of the methodology

proposed by Villegas (2013a), in which the displacement is used as the driver. An effort should be made to solve this issue. The abrupt displacement ceiling is probably caused by the presence of unmelted pieces of PEKK, which are, most likely, the result of non-uniform ED melting. It is recommended that the experiments are repeated with well consolidated EDs, to see if the poorly consolidated EDs are the cause of the non-uniform heating. It should be noted that, when welding with integrated triangular EDs, no abrupt ceiling was observed. This might be explained by the fact the shape of the triangles probably makes them melt more uniformly.

- Research on 'in-situ' weld quality monitoring needs to be continued. It is recommended that an algorithm distinguishing a bad weld from a good one is written. Preferably, this algorithm is able to do this in an early stage of the USW process while the process is still taking place, so that the process can be stopped or altered.
- It would be useful to know what the relationship between the maximum power used and the weld area is, so that the maximum weld area that can be covered within one spot weld can be determined for every setup.
- Experiments should be conducted with composite sonotrodes and multiple converter setups to find out if larger structural welds can be obtained using a spot welding approach.
- It is recommended that a FEM model is built to simulate the vibrations in the composites and the fixture. This might provide more insights into how clamping affects the vibrations, and thus the USW process.
- USW of CFRTPCs with 35 [kHz] tooling should be investigated. The smaller dimensions of this tooling make it more suitable for hand tooling or for welding difficult to reach areas.
- Only single lap shear tests have been performed. It is recommended that also peel tests (G1c) are performed on the clips, as peeling is likely the load case on which they most easily fail.
- If welded components have a poor weld quality or have to be replaced at some point, they have to be removed. It should be investigated what the best approach to do so is. Moreover, it should be researched whether and how poor welds can be repaired.
- It is unknown what the effects of contamination – such as grease or dust – on the USW process and on the weld quality are. This topic should also be investigated.
- It is expected that deviations in the geometry of the composites can lead to issues in the USW process. Therefore, it is important to investigate how these issues can be mitigated. One suggestion would be to use the ED as a shim.

References

- Ageorges, C., Ye, L. & Hou, M., 2001. Advances in fusion bonding techniques for joining thermoplastic matrix composites: a review. *Composites Part A: applied science and ...*, 32(2001), pp.839–857. Available at: <http://www.sciencedirect.com/science/article/pii/S1359835X00001664> [Accessed April 2, 2014].
- Agricola, F.M., 2014. *Up-scaling of the Ultrasonic Welding Process for Joining Carbon Fibre PEEK Composites - A Clean Sky Eco-Design Specific Case*. Delft University of Technology.
- Beevers, A., 1991. Welding: the way ahead for thermoplastics. *Engineering(London)(UK)*, 231, pp.11–12. Available at: <http://scholar.google.nl/scholar?hl=nl&q=beevers+the+way+ahead+for+thermoplastics&btnG=&lr=#0> [Accessed April 18, 2014].
- Benatar, A., 1987. *Ultrasonic welding of advanced thermoplastic composites*. Massachusetts Institute of Technology. Available at: <http://dspace.mit.edu/handle/1721.1/14668> [Accessed April 2, 2014].
- Benatar, A. & Gutowski, T.G., 1989. Ultrasonic welding of PEEK graphite APC-2 composites. *Polymer Engineering and Science*, 29(23), pp.1705–1721. Available at: <http://doi.wiley.com/10.1002/pen.760292313>.
- Chuah, Y.K. et al., 2000. Effects of the shape of the energy director on far-field ultrasonic welding of thermoplastics. *Polymer Engineering & Science*, 40(1), pp.157–167. Available at: <http://doi.wiley.com/10.1002/pen.11149>.
- Cytec, 2009. *APC (PEKK-FC) Thermoplastic Polymer Prepreg - Revision 1.2*,
- Destaco, 2014. *Series 207 Product Overview - Vertical Hold Down Clamps*,
- Devine, J., 2001. Ultrasonic Plastic Welding Bascis. *Welding Journal*, pp.29–33.
- Fokker, 2013. *Thermoplastic Affordable Primary Aircraft Structure 2 (TAPAS2) Project*,
- Grewell, D.A., Benatar, A. & Park, J.B., 2003. Ultrasonic Welding. In *Plastics and Composites Welding Handbook*. Munich: Hanser Publishers, pp. 141–188.
- Harras, B., Cole, K. & Vu-Khanh, T., 1996. Optimization of the ultrasonic welding of PEEK-carbon composites. *Journal of Reinforced Plastics and Composites*, 15, pp.174–182. Available at: <http://jrp.sagepub.com/content/15/2/174.short> [Accessed April 2, 2014].
- Hoogenboom, J., 2014. *Trade Riveting versus Ultrasonic Welding of Clips*,
- Van Ingen, J.W., 2014. *TW-14-131 Frame to grid panel weld concept*,
- Levy, A., Le Corre, S. & Fernandez Villegas, I., 2014. Modeling of the heating phenomena in ultrasonic welding of thermoplastic composites with flat energy directors. *Journal of Materials Processing Technology*, 214(7), pp.1361–1371. Available at: <http://linkinghub.elsevier.com/retrieve/pii/S0924013614000508> [Accessed April 2, 2014].
- Ling, S.-F. et al., 2006. Input electrical impedance as signature for nondestructive evaluation of weld quality during ultrasonic welding of plastics. *NDT & E International*, 39(1), pp.13–18. Available at: <http://linkinghub.elsevier.com/retrieve/pii/S0963869505000745> [Accessed April 2, 2014].

- Liu, S. & Chang, I., 2002. Optimizing the weld strength of ultrasonically welded nylon composites. *Journal of composite materials*, 36(5), pp.611–624. Available at: <http://jcm.sagepub.com/content/36/5/611.short> [Accessed April 2, 2014].
- Liu, S.-J., Chang, I.-T. & Hung, S.-W., 2001. Factors affecting the joint strength of ultrasonically welded polypropylene composites. *Polymer Composites*, 22(1), pp.132–141. Available at: <http://doi.wiley.com/10.1002/pc.10525>.
- Lu, H., Benatar, A. & He, F., 1991. Sequential ultrasonic welding of PEEK/Graphite composites plates. In *Proceedings of the annual technical conference ANTEC*, pp. 89–92. Available at: <http://scholar.google.com/scholar?hl=en&btnG=Search&q=intitle:Sequential+Ultrasonic+Welding+of+PEEK+/+Graphite+Composites+Plates#0> [Accessed July 7, 2014].
- Nonhof, C. & Luiten, G., 1996. Estimates for process conditions during the ultrasonic welding of thermoplastics. *Polymer Engineering & Science*, 36(9), pp.1177–1183. Available at: <http://onlinelibrary.wiley.com/doi/10.1002/pen.10511/full> [Accessed June 22, 2014].
- Potente, H., 1984. Ultrasonic welding—Principles & theory. *Materials & Design*, 5(November), pp.228–234. Available at: <http://www.sciencedirect.com/science/article/pii/0261306984900323> [Accessed April 2, 2014].
- Prager, S. & Tirrell, M., 1981. The healing process at polymer–polymer interfaces. *The Journal of Chemical Physics*, 75(10), pp.5194–5198.
- Rinco Ultrasonics AG, 2008. *Dynamic 3000 with Generator ACU - Operating Instructions*,
- Romero, M.B., Villegas, I.F. & Bersee, H., 2012. Optimizing ultrasonic welding of carbon-fibre-reinforced polyetherimide. *JEC Composites Magazine No 70*, (February), pp.54–58. Available at: <http://cat.inist.fr/?aModele=afficheN&cpsidt=25493878> [Accessed April 2, 2014].
- Silverman, E. & Griese, R., 1989. Joining methods for graphite/PEEK thermoplastic composites. *Sampe Journal*, 25(5), pp.34–38. Available at: <http://scholar.google.nl/scholar?hl=nl&q=silverman+griese+joining+methods&btnG=&lr=#0> [Accessed April 18, 2014].
- Tolunay, M.N., Dawson, P.R. & Wang, K.K., 1983. Heating and bonding mechanisms in ultrasonic welding of thermoplastics. *Polymer Engineering and Science*, 23(13), pp.726–733. Available at: <http://doi.wiley.com/10.1002/pen.760231307>.
- Troughton, M., 2008. Ultrasonic Welding. In *Handbook of plastics joining: a practical guide*. Norwich: William Andrew Inc., pp. 15–35.
- Tsujino, J. et al., 2002. Ultrasonic plastic welding using fundamental and higher resonance frequencies. , 40, pp.375–378.
- Villegas, I., 2013a. In situ monitoring of ultrasonic welding of thermoplastic composites through power and displacement data. *Journal of Thermoplastic Composite Materials*. Available at: <http://jtc.sagepub.com/cgi/doi/10.1177/0892705712475015> [Accessed April 2, 2014].
- Villegas, I., 2013b. Optimum Processing Conditions For Ultrasonic Welding Of Thermoplastic Composites. In *The 19th International Conference on Composite Materials*. Montreal, pp. 1–8. Available at: <http://confsys.ensc.concordia.ca/ICCM19/AllPapers/FinalVersion/FER80442.pdf> [Accessed April 2, 2014].

- Villegas, I. & Bersee, H., 2010. Ultrasonic welding of advanced thermoplastic composites: An investigation on energy-directing surfaces. *Advances in Polymer Technology*, 29(2), pp.112–121. Available at: <http://onlinelibrary.wiley.com/doi/10.1002/adv.20178/full> [Accessed April 2, 2014].
- Villegas, I.F. et al., 2014. A comparative evaluation between flat and traditional energy directors for ultrasonic welding of thermoplastic composites. In *16th European Conference on Composite Materials*. Seville, pp. 22–26.
- Villegas, I.F. et al., 2013. Process and performance evaluation of ultrasonic, induction and resistance welding of advanced thermoplastic composites. *Journal of Thermoplastic Composite Materials*, 26(8), pp.1007–1024. Available at: <http://jtc.sagepub.com/content/26/8/1007.short> [Accessed April 2, 2014].
- Yousefpour, A., Hojjati, M. & Immarigeon, J.-P., 2004. Fusion Bonding/Welding of Thermoplastic Composites. *Journal of Thermoplastic Composite Materials*, 17(4), pp.303–341. Available at: <http://jtc.sagepub.com/cgi/doi/10.1177/0892705704045187> [Accessed April 2, 2014].
- Zhang, Z. et al., 2010. Study on Heating Process of Ultrasonic Welding for Thermoplastics. *Journal of Thermoplastic Composite Materials*, 23(5), pp.647–664. Available at: <http://jtc.sagepub.com/cgi/doi/10.1177/0892705709356493> [Accessed April 2, 2014].

Appendices

Appendix A. Squeeze Flow &

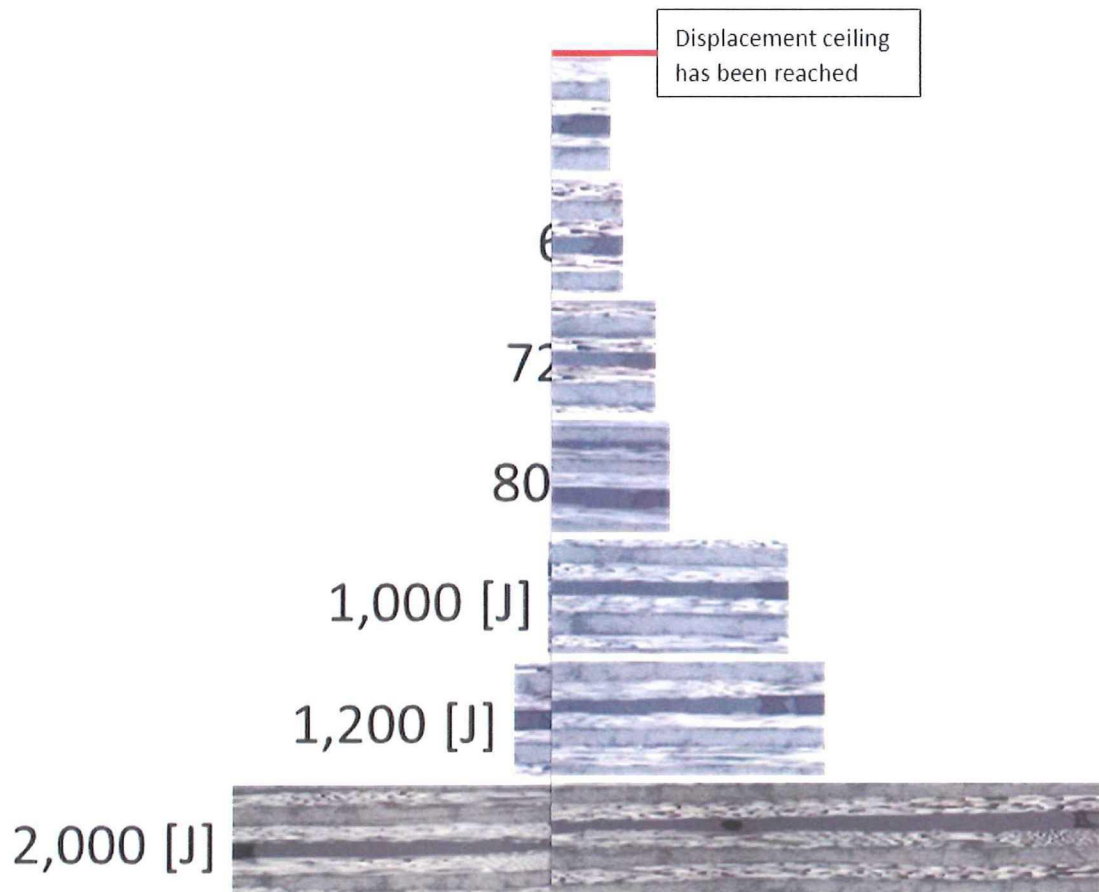


Figure A-1: Overview of cross-section microscopy panoramas and the dashed blue lines indicate the initial size and

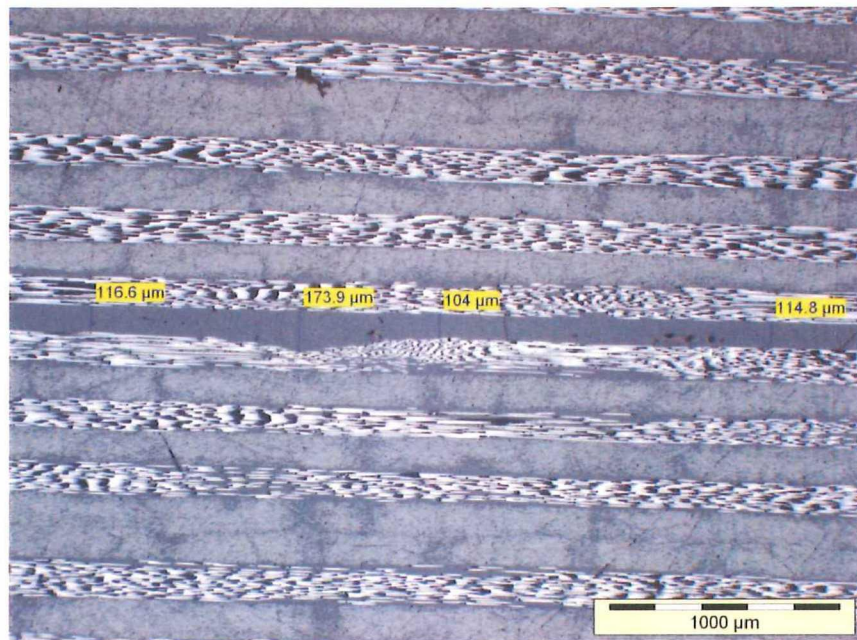


Figure A-2: Squeeze flow of ED at the welding interface of a sample clip welded with 800 [J]. The deformation of the first ply indicates that the substrate material started to melt.

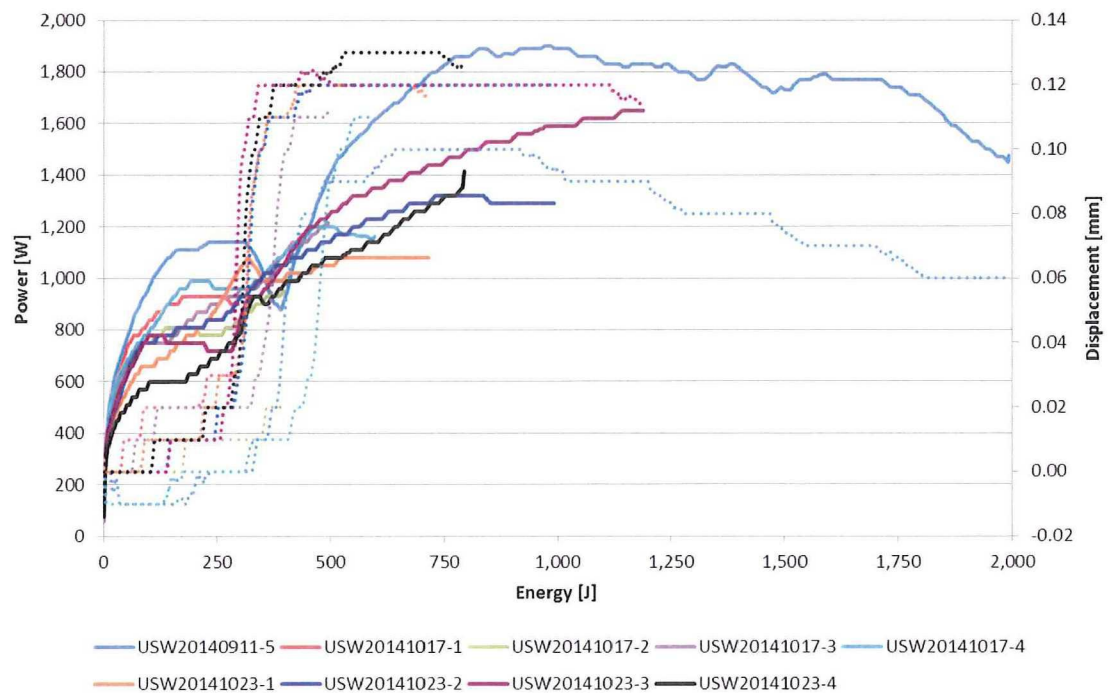


Figure A-3: Power (solid) and displacement (dots) plots of sample clips used for optical microscopy. Welding settings: 51.8 [μm]; 1,500 [N].

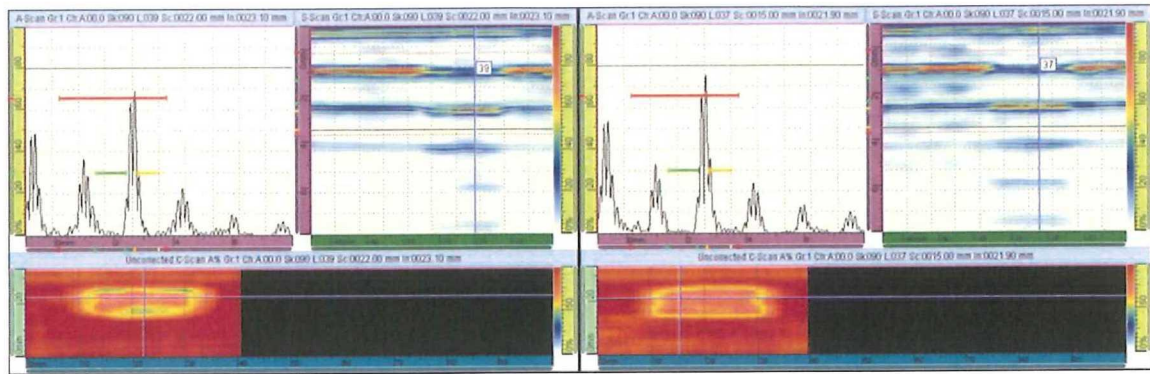


Figure A-4: PA Scan of USW141001-01 which is welded with 720 [J].

Figure A-5: PA Scan of USW141001-02 which is welded with 720 [J].

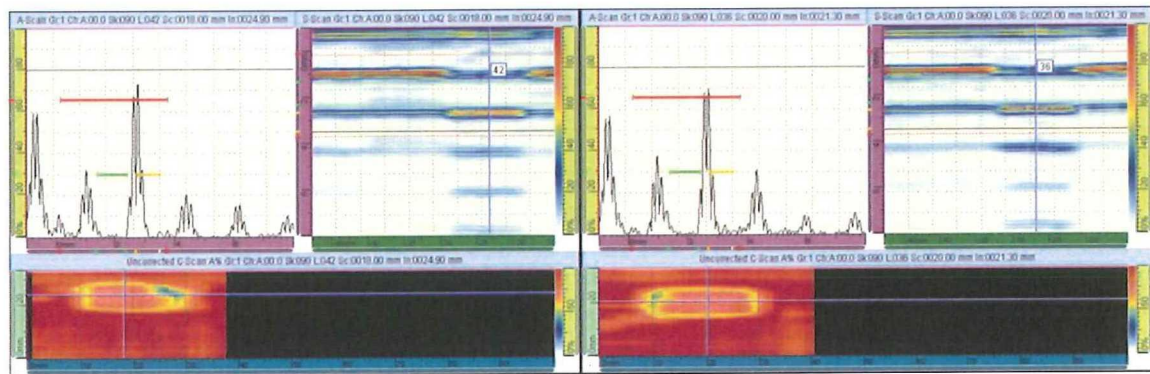


Figure A-6: PA Scan of USW141001-03 which is welded with 720 [J].

Figure A-7: PA Scan of USW141001-04 which is welded with 720 [J].

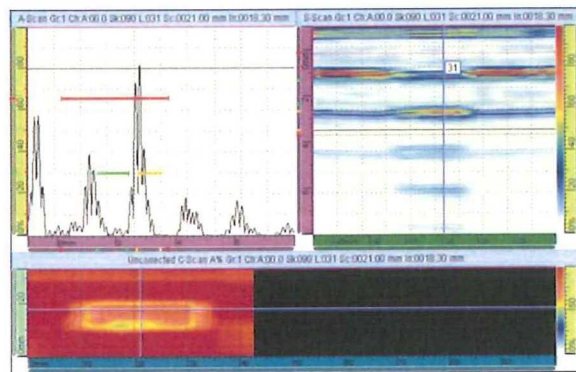


Figure A-8: PA Scan of USW141001-05 which is welded with 720 [J].

Appendix B. CAD Drawings

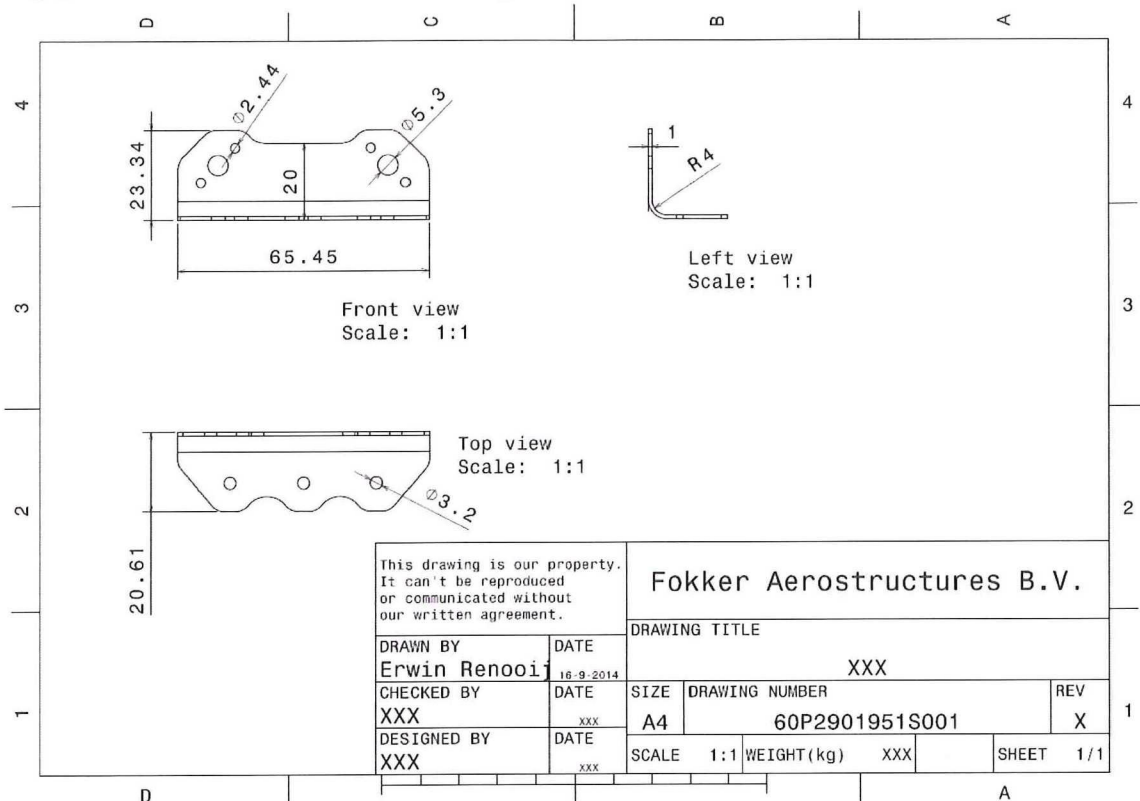


Figure B-1: Aluminum clip

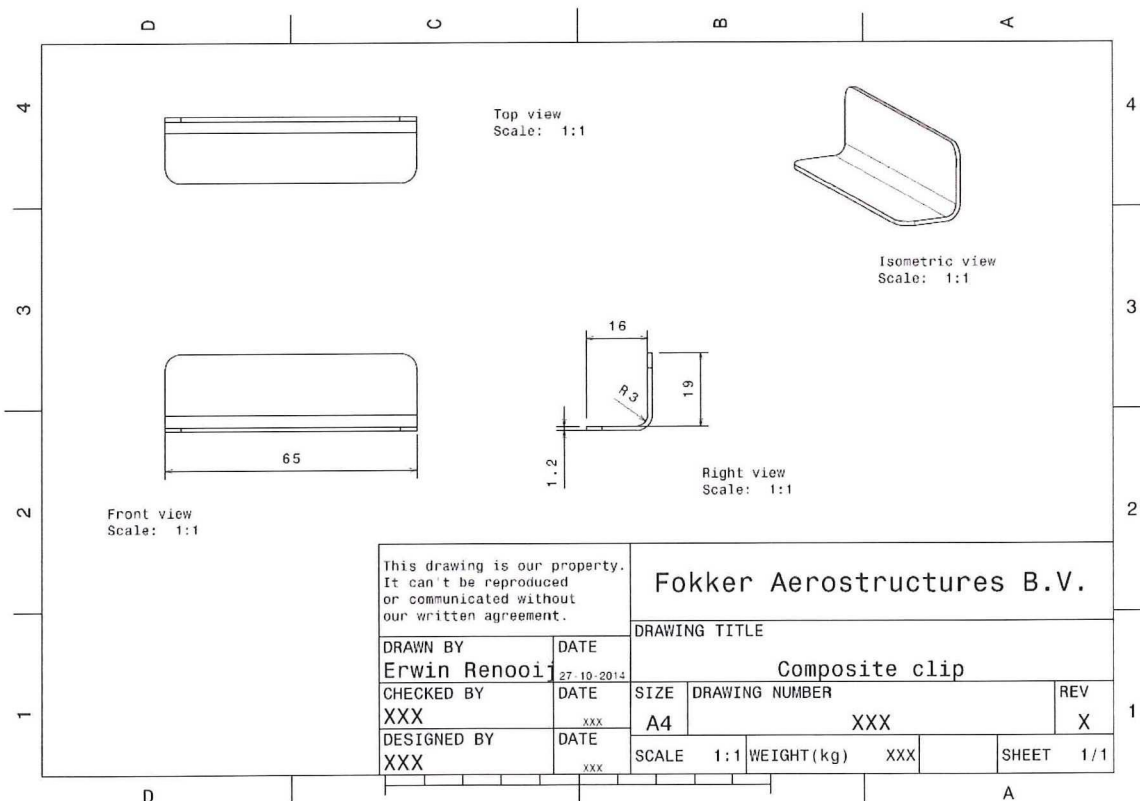


Figure B-2: Composite clip

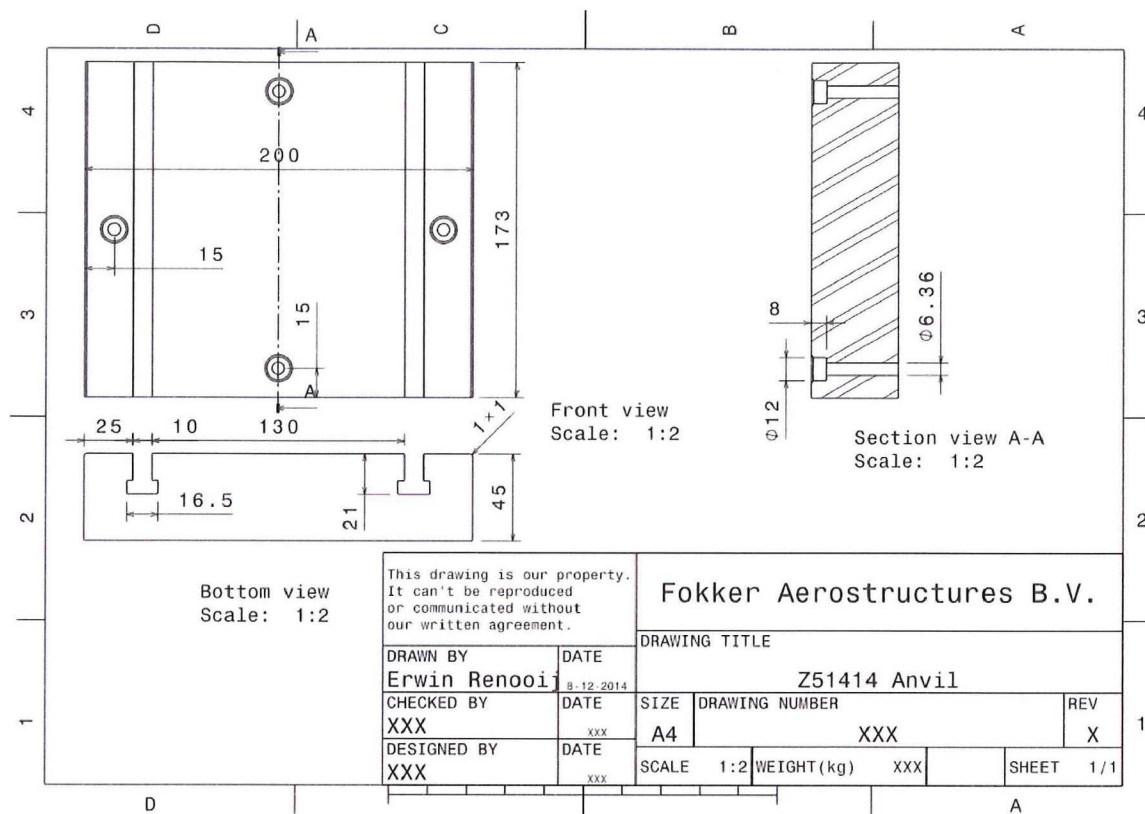


Figure B-3: Z51414 Anvil

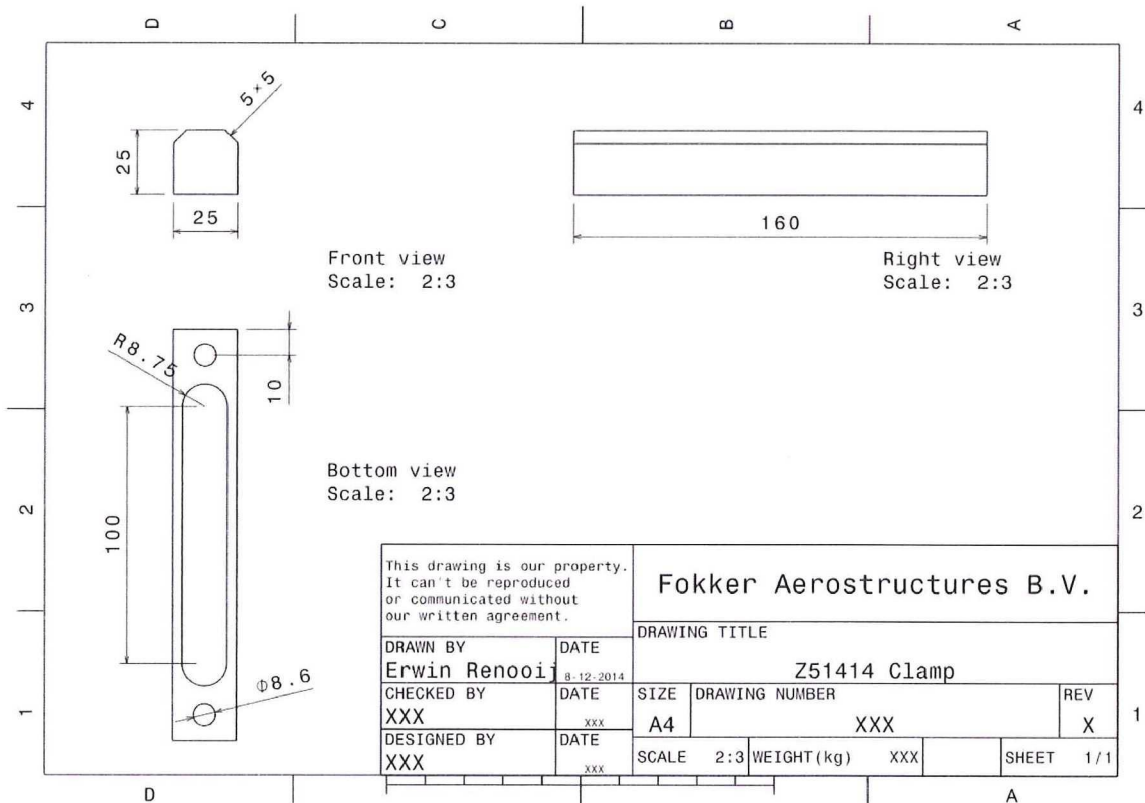


Figure B-4: Z51414 Clamp

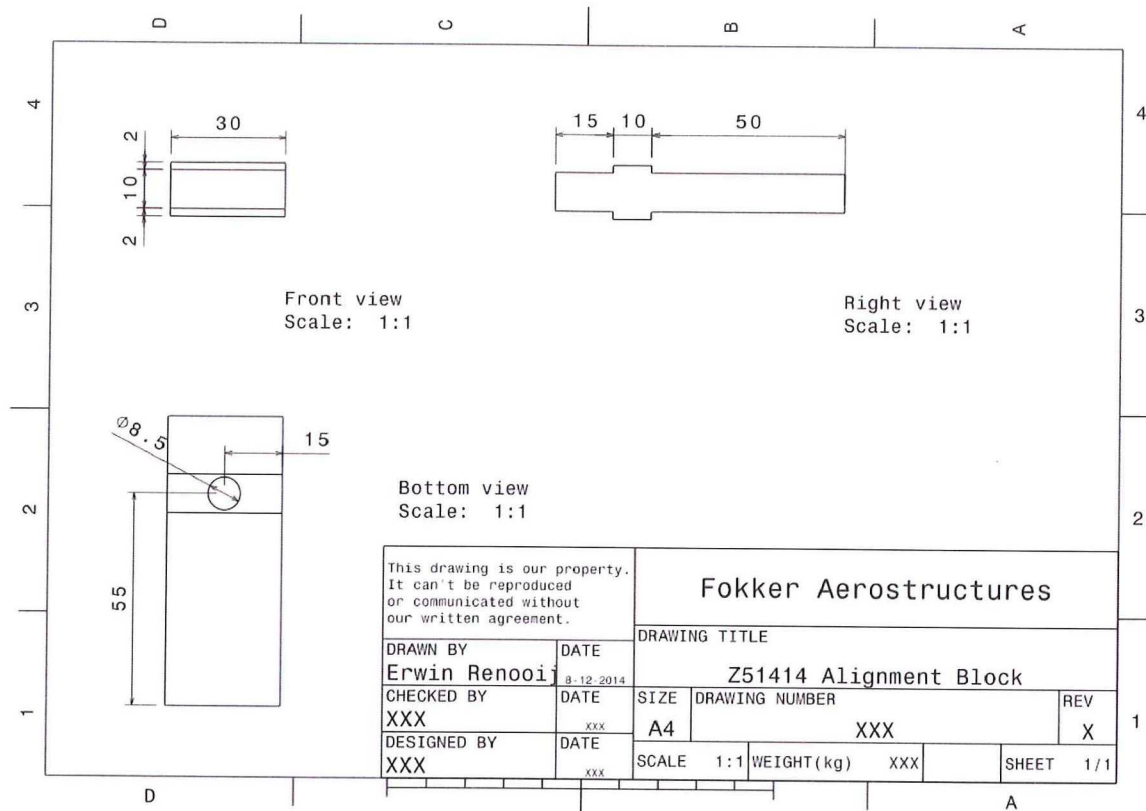


Figure B-5: Z51414 Alignment Block

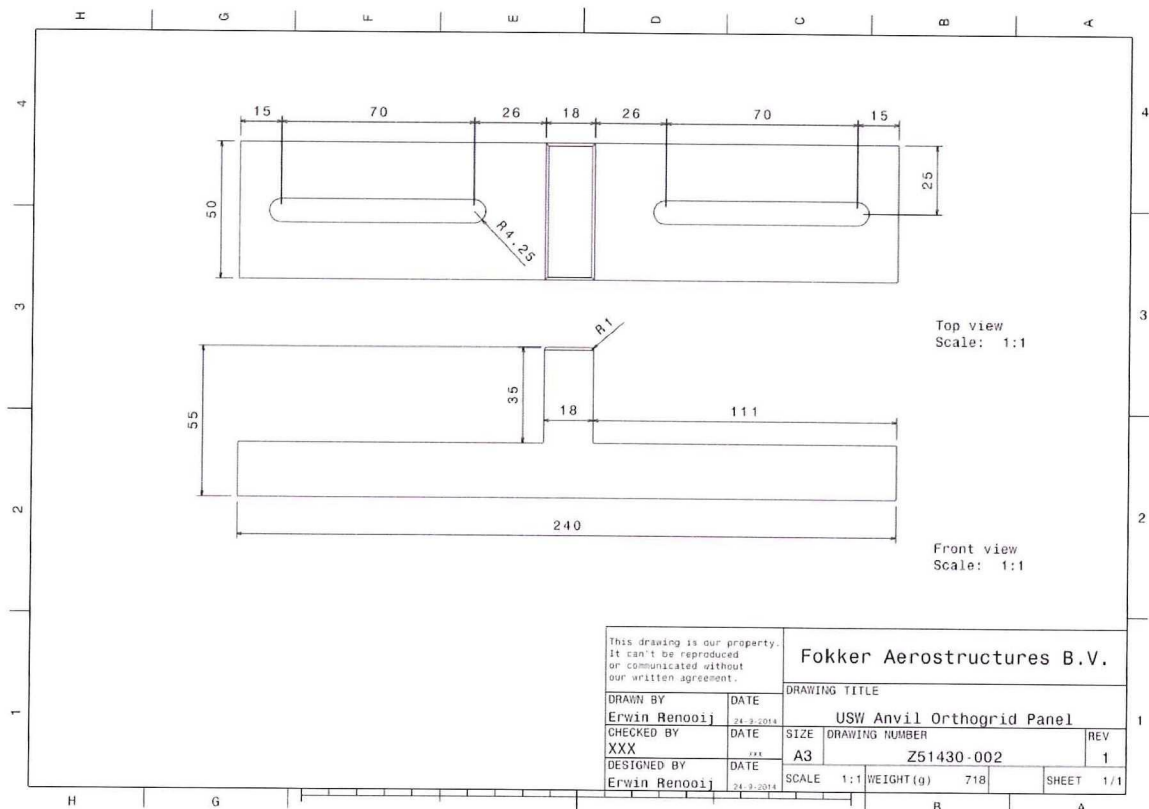


Figure B-6: Z51430 Anvil

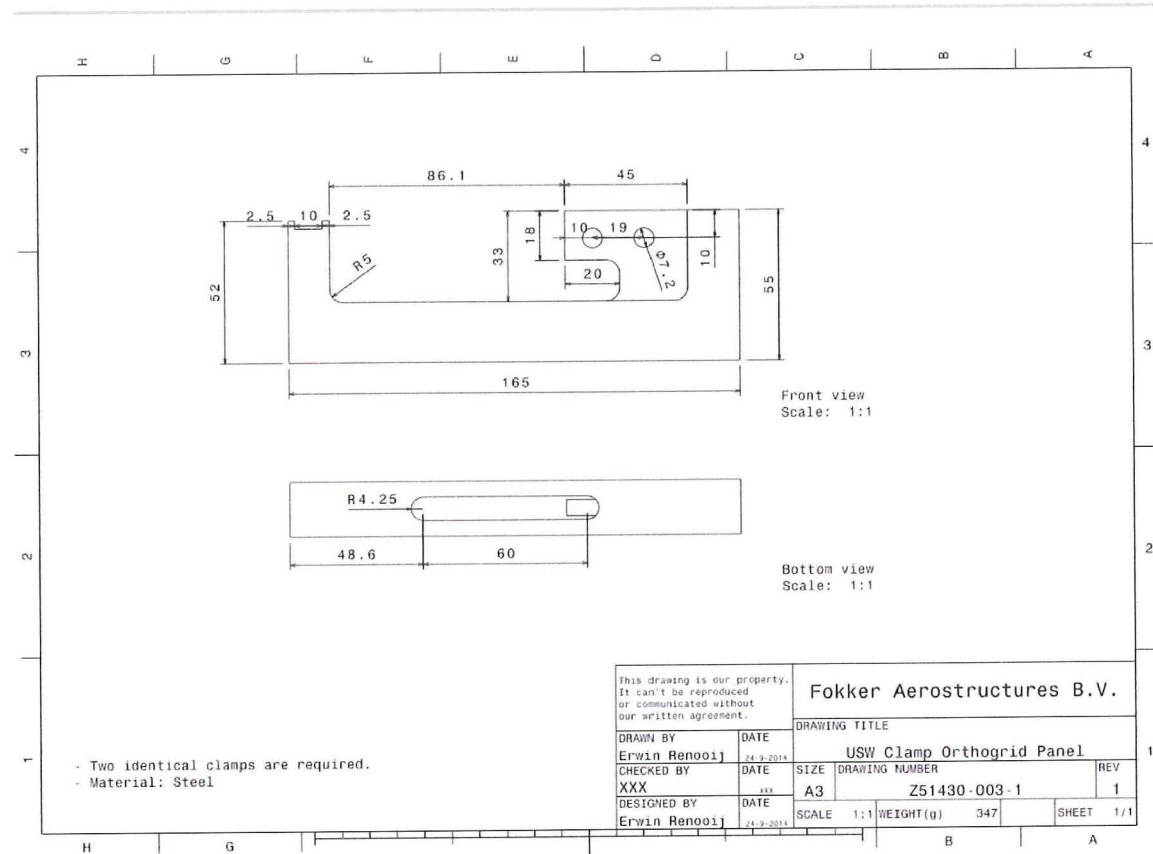


Figure B-7: Z51430 Clamp

Appendix C. Materials & Manufacturing

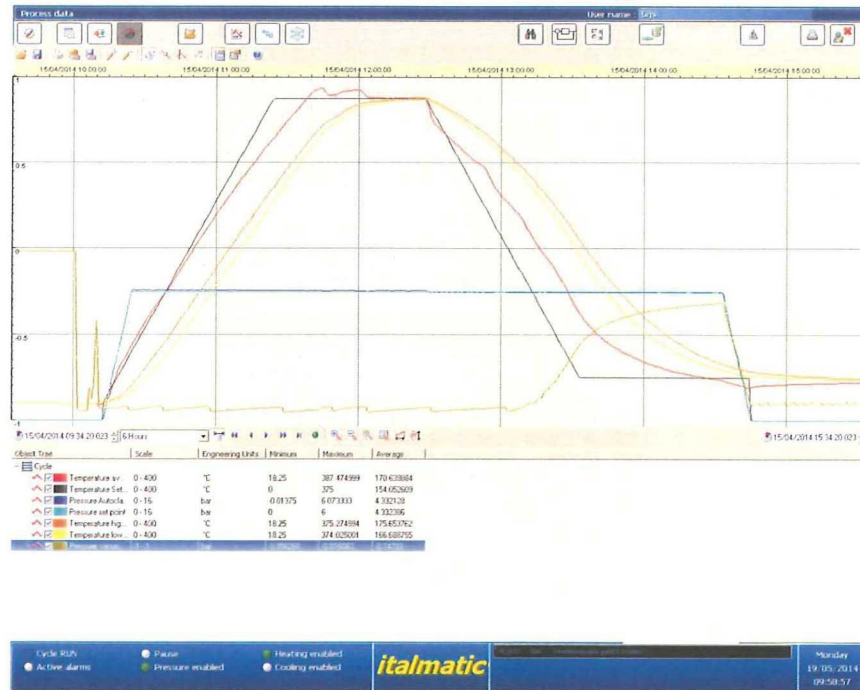


Figure C-1: Example of autoclave cycle in which the CF/ PEKK laminates are consolidated.



Figure C-2: Autoclave cycle in which the PEKK ED is consolidated.

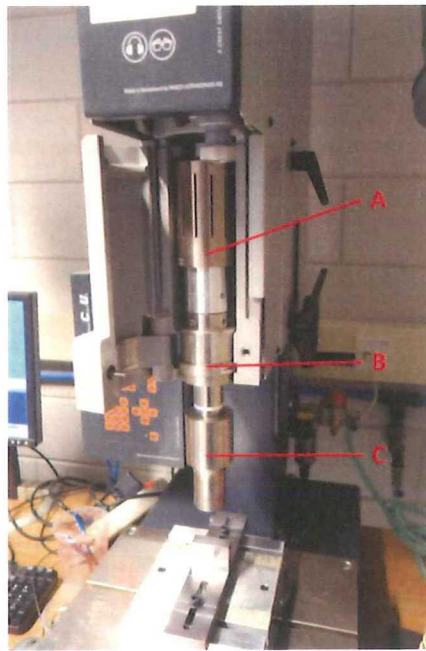


Figure C-3: Welding stack of the Rinco Dynamic 3000. A: Piezoelectric converter, B: Booster, and C: Sonotrode.

Appendix D. Integrated Triangular Energy Directors

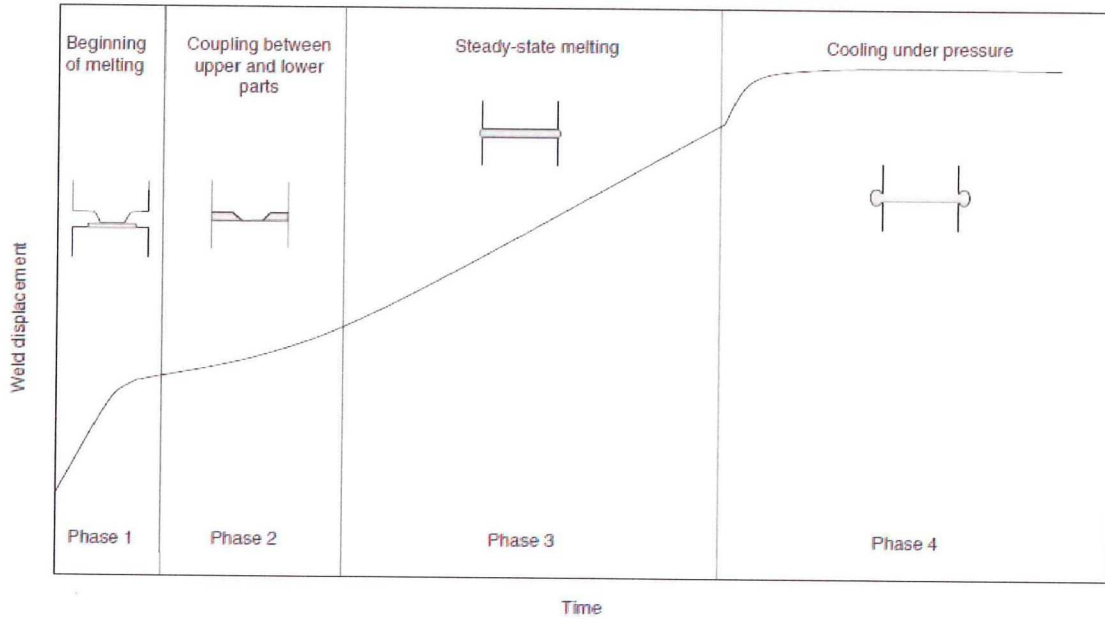


Figure D-1: Ultrasonic welding stages for plastics with integrated triangular EDs (Troughton, 2008)

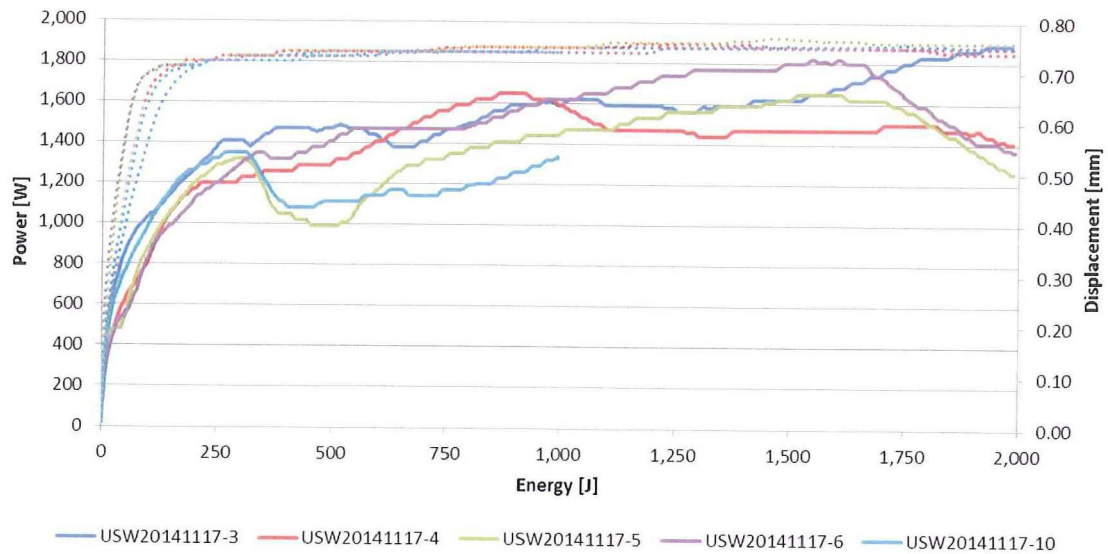


Figure D-2: Power (solid) and displacement (dotted) curves of five samples with integrated triangular ED ribs. Welding settings: 51.8 μm ; 1,500 [N]; 2,000 [J].

Appendix E. Single-Side Clamping

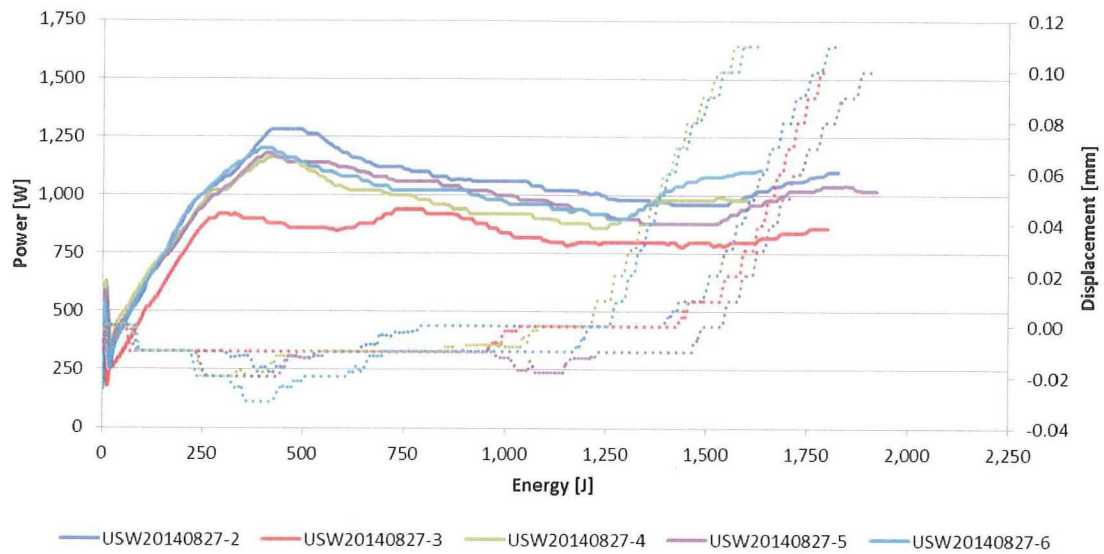


Figure E-1: Power (solid) and displacement (dotted) plots of single-side clamped ASTM D1002 samples clamped at 6 [cm] from the centerline with rubber pads and a torque of 2.5 [Nm] per bolt. Welding settings: 70.4 [μm]; 500 [N]; 0.11 [mm].

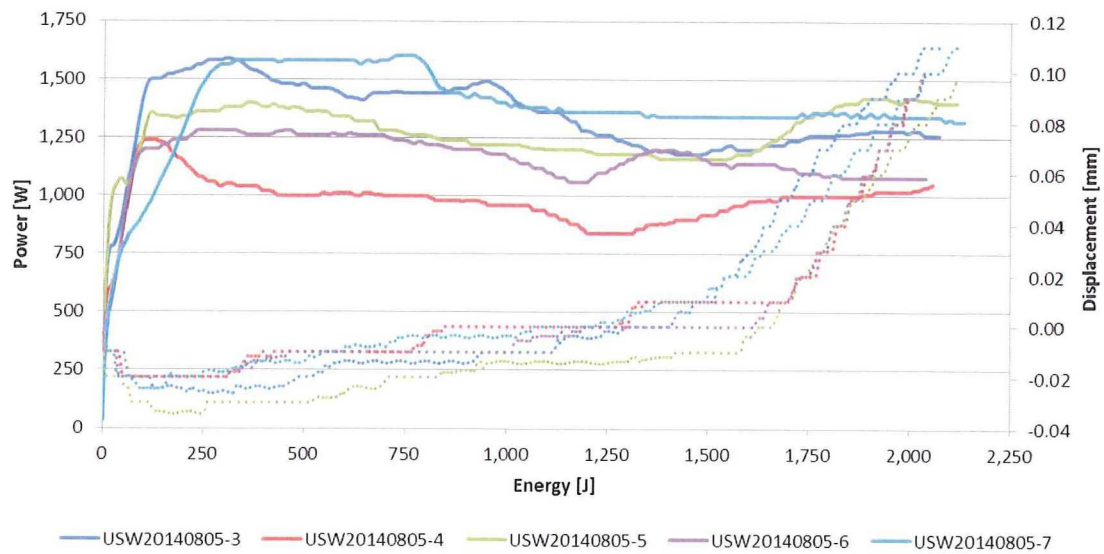


Figure E-2: Power (solid) and displacement (dotted) plots of single-side clamped ASTM D1002 samples clamped at 3.5 [cm] from the centerline with rubber pads and a torque of 2.5 [Nm] per bolt. Welding settings: 70.4 [μm]; 500 [N]; 0.11 [mm].

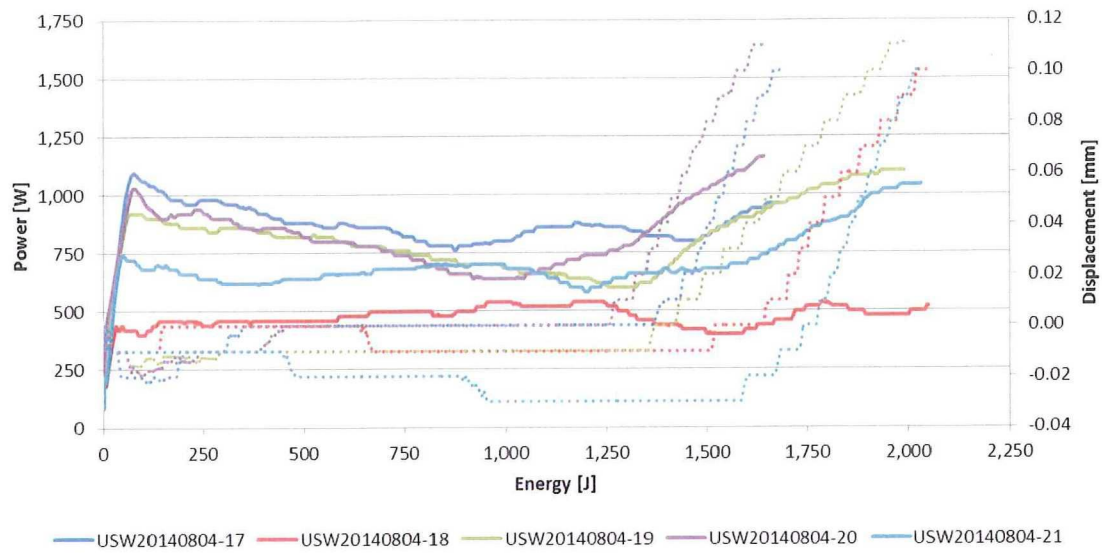


Figure E-3: Power (solid) and displacement (dotted) plots of single-side clamped ASTM D1002 samples clamped at 1.5 [cm] from the centerline with rubber pads and a torque of 2.5 [Nm] per bolt. Welding settings: 70.4 [μm]; 500 [N]; 0.11 [mm].

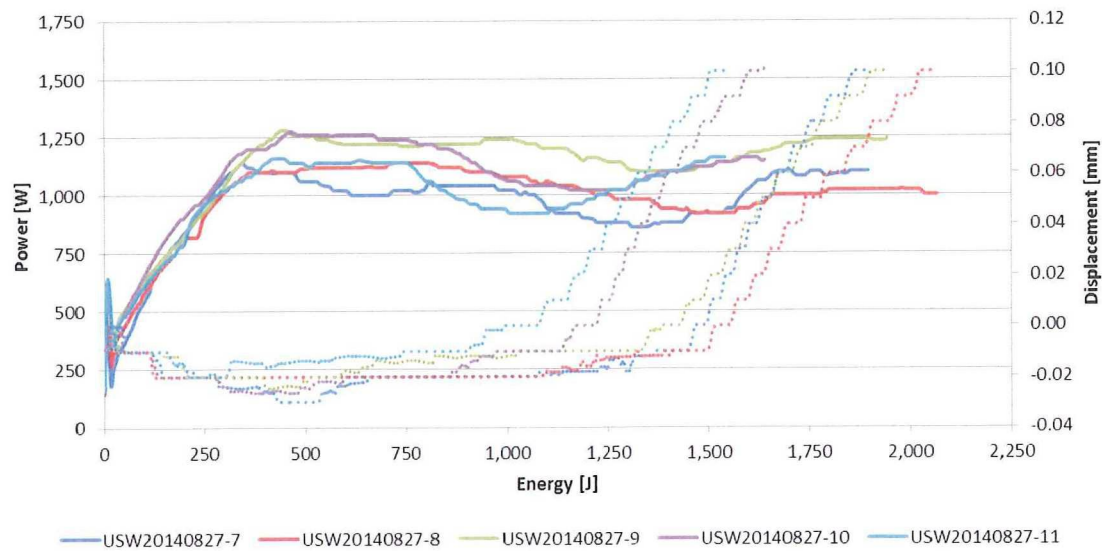


Figure E-4: Power (solid) and displacement (dotted) plots of single-side clamped ASTM D1002 samples clamped at 6 [cm] from the centerline with rubber pads and a torque of 7.5 [Nm] per bolt. Welding settings: 70.4 [μm]; 500 [N]; 0.11 [mm].

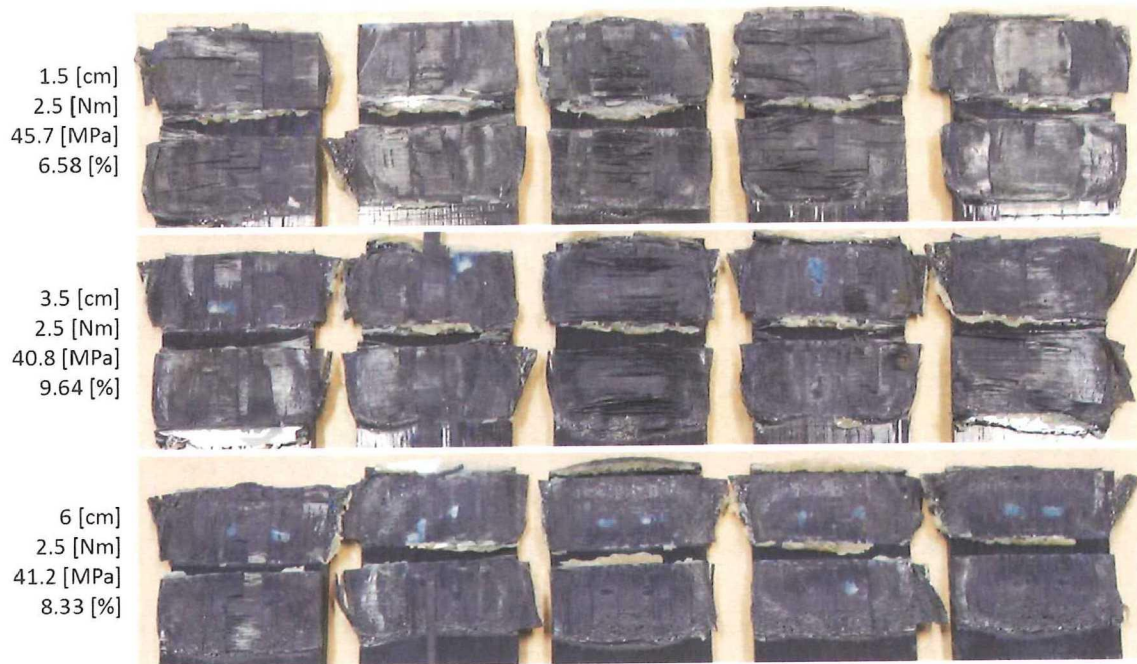


Figure E-7: Fracture surfaces of single-side clamped ASTM D1002 samples clamped with rubber pads at the distances: 1.5 [cm], 3.5 [cm], and 6 [cm]. The bolts of the clamp are tightened with 2.5 [Nm]. Welding settings: 70.4 [μ m]; 500 [N]; 0.11 [mm]. The third value given is the LSS and the fourth is the CoV of the LSS.

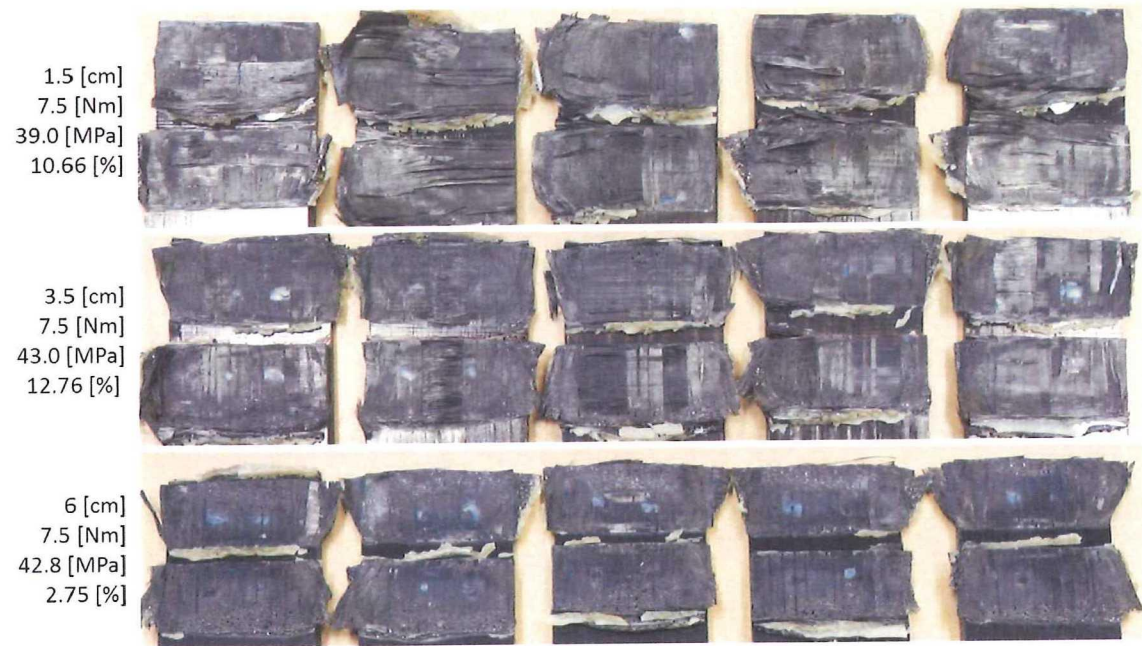


Figure E-8: Fracture surfaces of single-side clamped ASTM D1002 samples clamped with rubber pads at the distances: 1.5 [cm], 3.5 [cm], and 6 [cm]. The bolts of the clamp are tightened with 7.5 [Nm]. Welding settings: 70.4 [μ m]; 500 [N]; 0.11 [mm]. The third value given is the LSS and the fourth is the CoV of the LSS.

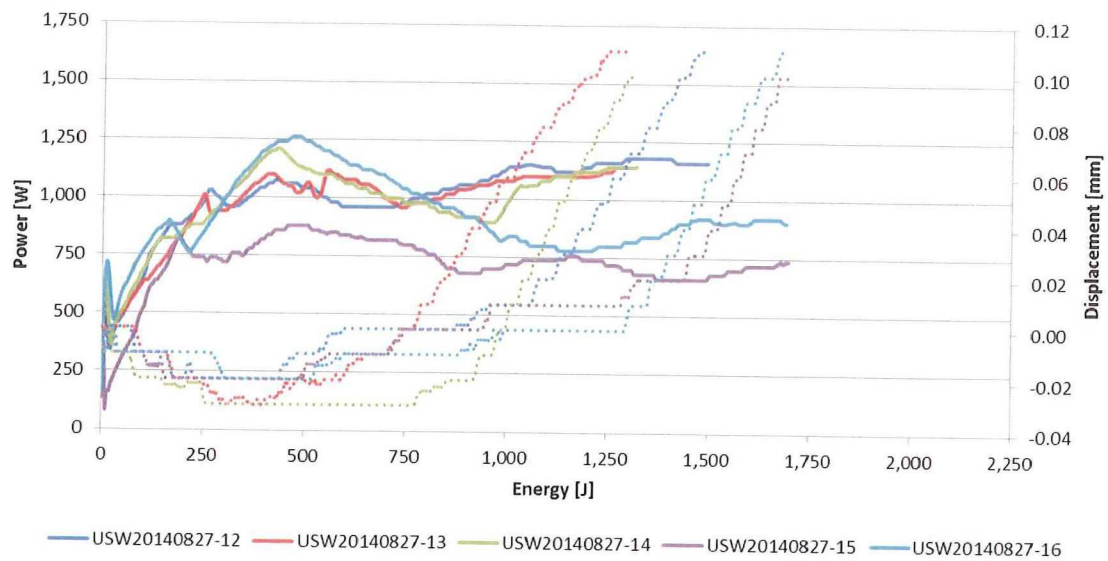


Figure E-5: Power (solid) and displacement (dotted) plots of single-side clamped ASTM D1002 samples clamped at 3.5 [cm] from the centerline with rubber pads and a torque of 7.5 [Nm] per bolt. Welding settings: 70.4 [μ m]; 500 [N]; 0.11 [mm].

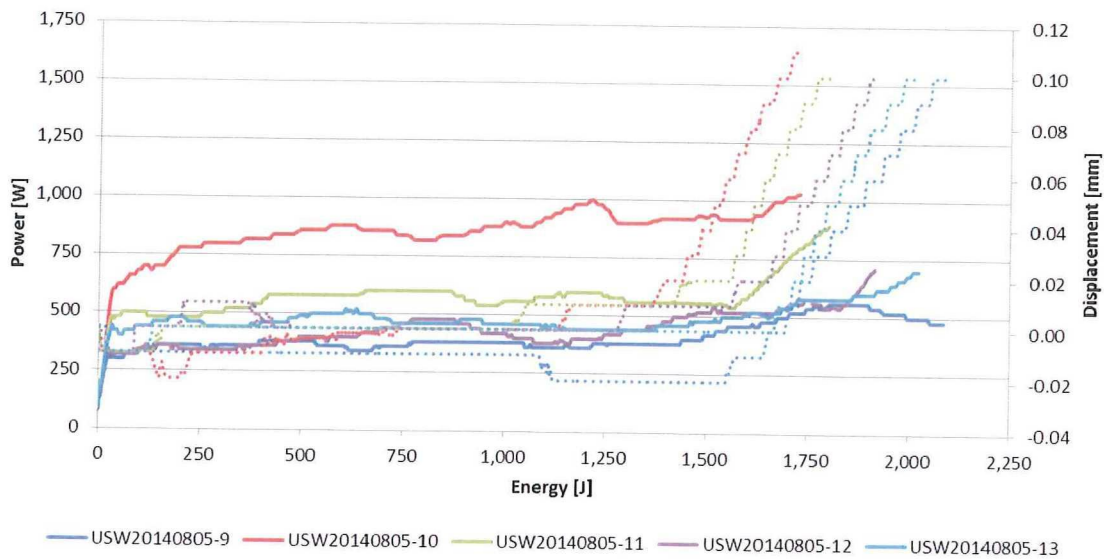


Figure E-6: Power (solid) and displacement (dotted) plots of single-side clamped ASTM D1002 samples clamped at 1.5 [cm] from the centerline with rubber pads and a torque of 7.5 [Nm] per bolt. Welding settings: 70.4 [μ m]; 500 [N]; 0.11 [mm].

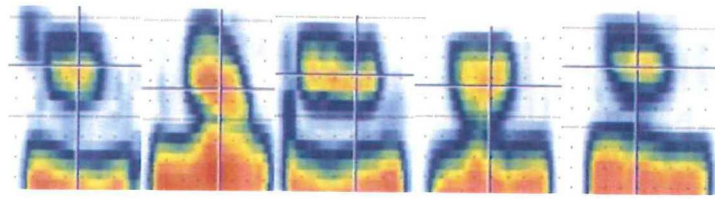


Figure E-9: The C-scans of samples clamped at 3.5 [cm] and with a torque of 2.5 [Nm].

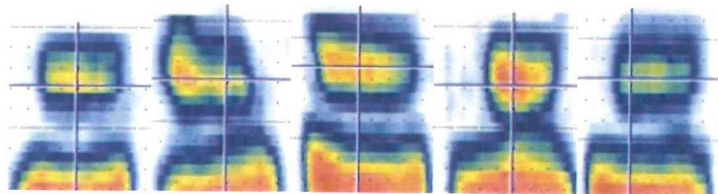


Figure E-10: The C-scans of samples clamped at 3.5 [cm] and with a torque of 7.5 [Nm].

Appendix F. System Clips



Figure F-1: Horizontal stabilizer of the Gulfstream G650 being assembled at Fokker Aerostructures in Papendrecht. Various clips are riveted on the ribs.

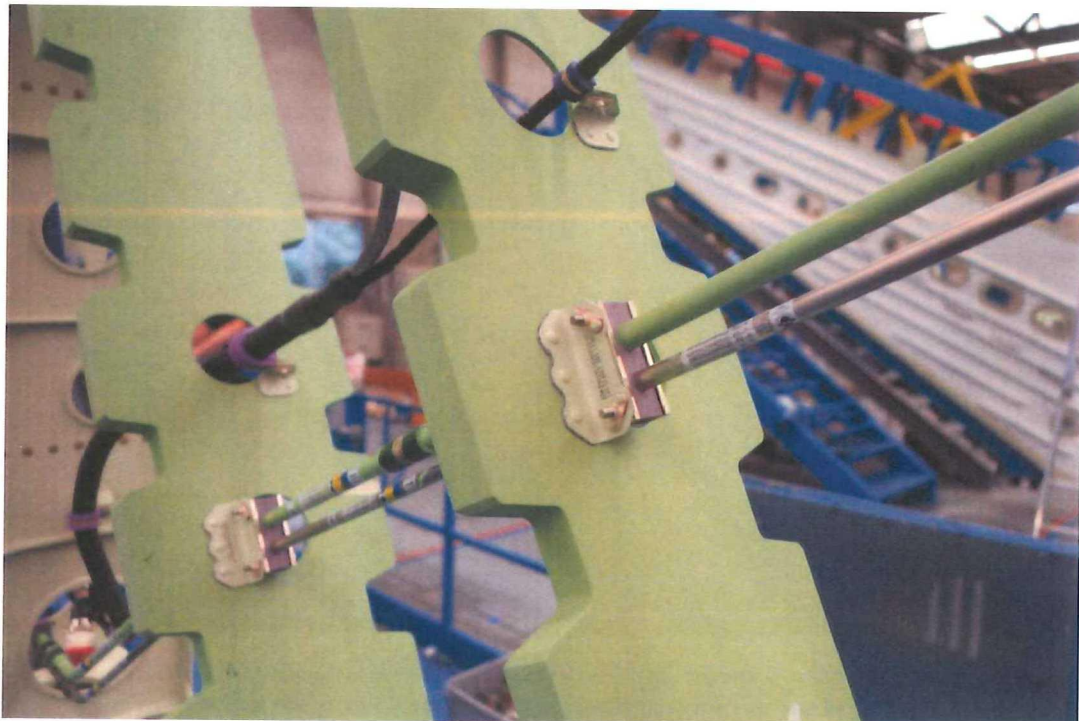


Figure F-2: System clip on which the composite clip, welded in this thesis, is based.



Figure F-3: Cargo hold of Boeing 737-800 being maintained by KLM Engineering & Maintenance. Numerous system clips can be seen that could possibly be welded in case the load carrying beams of the cargo floor were made of CFRTPCs.



Figure F-4: Floor panel of Boeing 737-800 seen from the cargo hold which is being maintained by KLM Engineering & Maintenance. Numerous system clips can be seen that could possibly be welded in case the load carrying beams of the cargo floor were made of CFRTPCs.

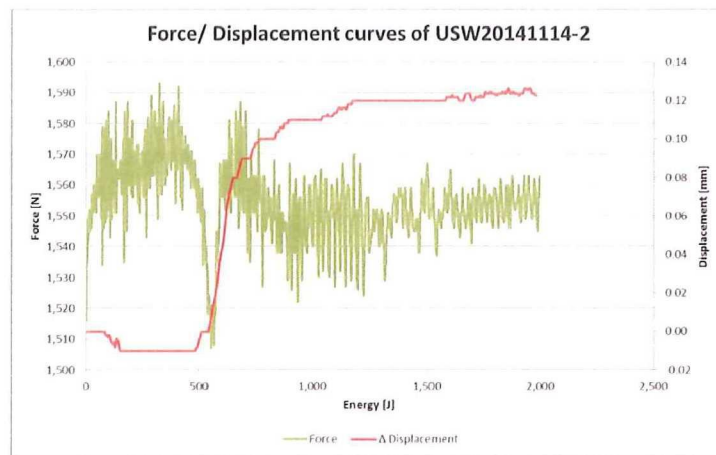


Figure F-5: Force and displacement curves of system clip welded with 2,000 [J].

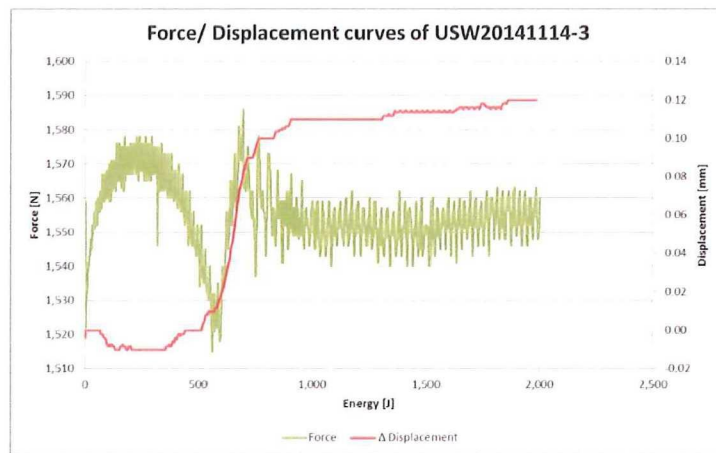


Figure F-6: Force and displacement curves of system clip welded with 2,000 [J].

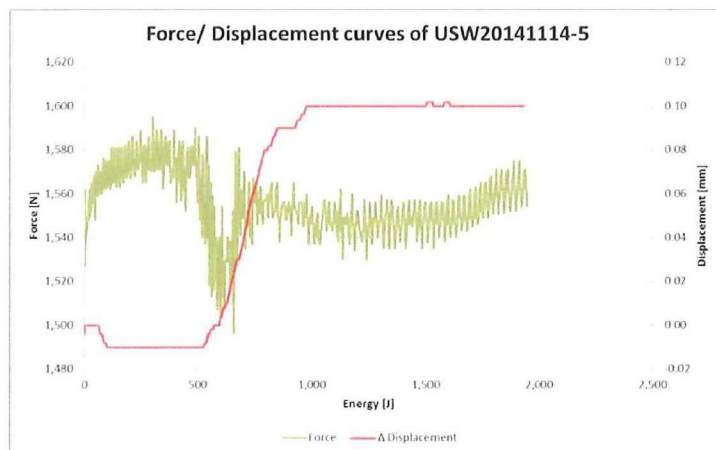


Figure F-7: Force and displacement curves of system clip welded with 2,000 [J].

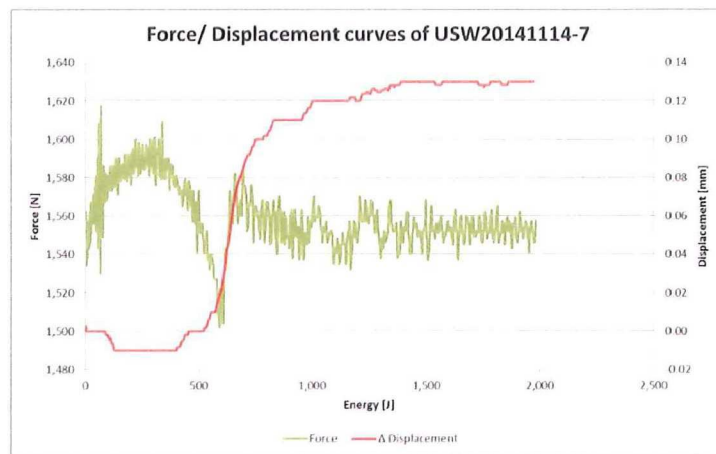


Figure F-8: Force and displacement curves of system clip welded with 2,000 [J].

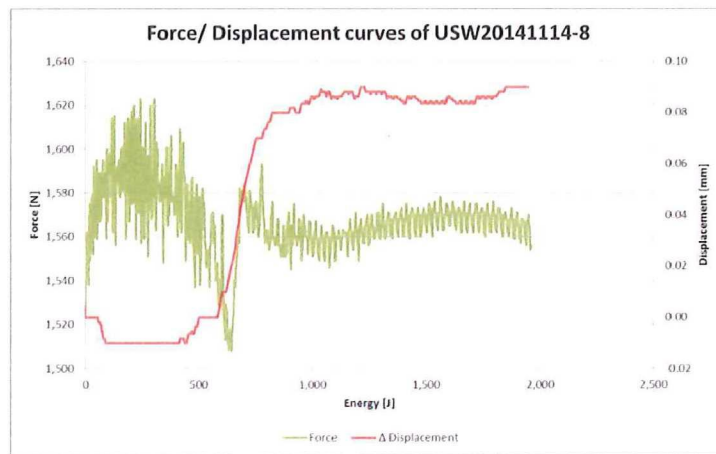


Figure F-9: Force and displacement curves of system clip welded with 2,000 [J].

Appendix G. Fuselage Frame



Figure G-1: A fuselage frame ultrasonically welded to a section of the orthogrid panel. Left: bottom view; right: top view.

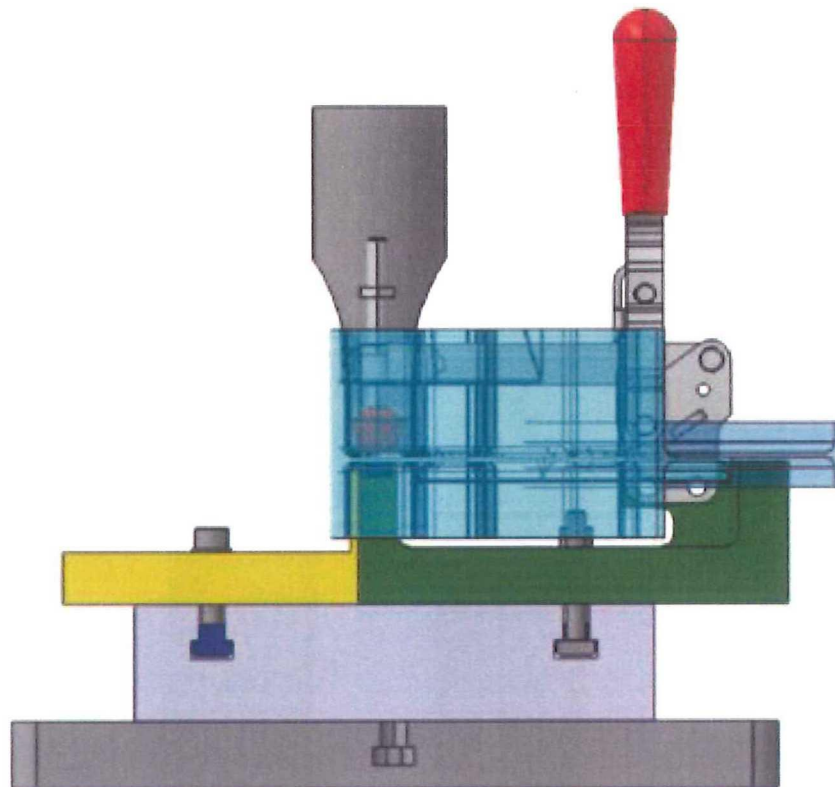


Figure G-2: Side-view of the Z51430 fixture to weld the fuselage frame to the orthogrid panel.

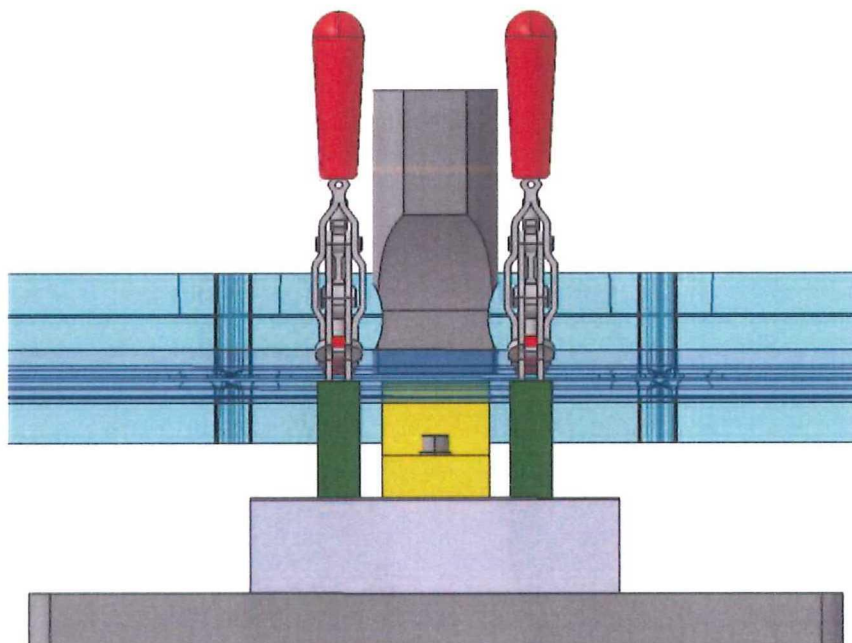


Figure G-3: Front-view of the Z51430 fixture to weld the fuselage frame to the orthogrid panel.



Figure G-4: The fuselage frame and the orthogrid panel clamped in the Z51430 fixture.

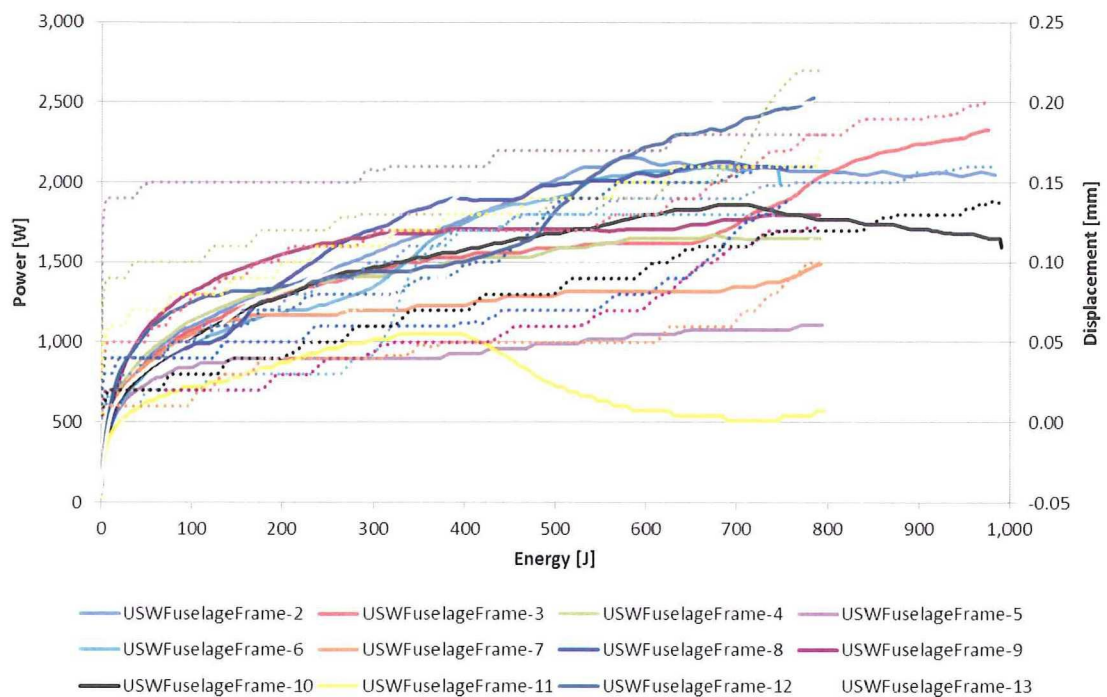


Figure G-5: Power (solid) and displacement (dotted) plots of the fuselage frame welded to the orthogrid panel. Welding settings: 52.8 [μ m]; 1,500 [N]. (No data was stored for the first weld).

Appendix H. Outlook

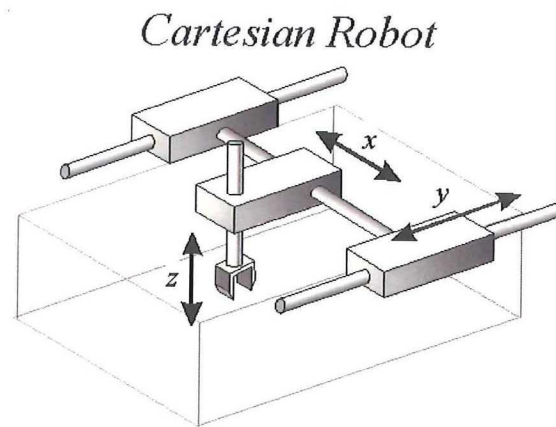


Figure H-1: Schematic drawing of a Cartesian robot.

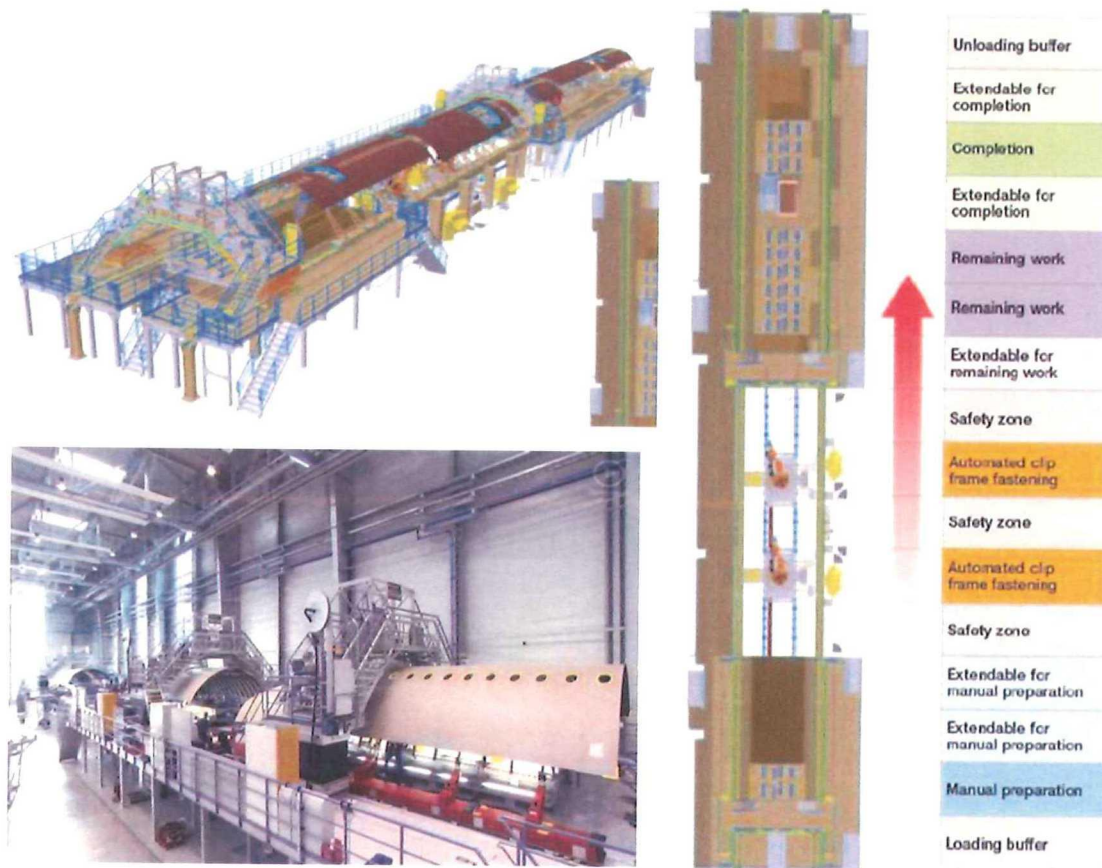


Figure H-2: A350 fuselage panel assembly line. Frames are fastened to clips on the skin panels. The same line can be envisioned for welding of CFRTPC frames and skin panels (van Ingen, 2014).

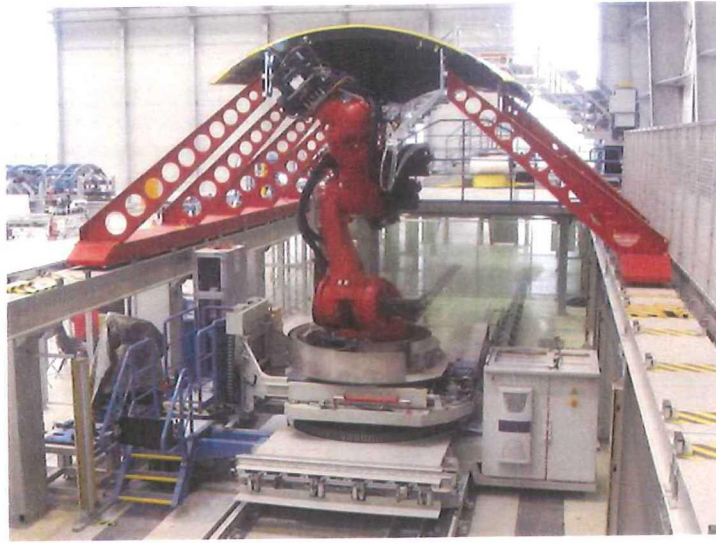


Figure H-3: Automated riveting in preliminary fuselage assembly line using a robot arm on rails (Broetje-Automation, 2014).